A FEASIBILITY STUDY OF INTERNAL EVAPORATIVE COOLING FOR PROTON EXCHANGE MEMBRANE FUEL CELLS

A Thesis

by

LOREN E. SNYDER

Submitted to the Office of Graduate Studies of
Texas A&M University
in partial fulfillment of the requirements for the degree of

MASTER OF SCIENCE

December 2004

Major Subject: Mechanical Engineering

A FEASIBILITY STUDY OF INTERNAL EVAPORATIVE COOLING FOR PROTON EXCHANGE MEMBRANE FUEL CELLS

A Thesis

by

LOREN E. SNYDER

Submitted to the Office of Graduate Studies of
Texas A&M University
in partial fulfillment of the requirements for the degree of

MASTER OF SCIENCE

Approved as to style and content by:

Thomas R. Lalk (Chair of Committee)	A. J. Appleby (Member)
D. O'Neal (Member)	D. O'Neal (Head of Department)

December 2004

Major Subject: Mechanical Engineering

ABSTRACT

A Feasibility Study of Internal Evaporative Cooling for Proton Exchange Membrane Fuel Cells.

(December 2004)

Loren E. Snyder, B.S., Colorado State University

Chair of Advisory Committee: Dr. Thomas R. Lalk

An investigation was conducted to determine the feasibility of using the technique of ultrasonic nebulization of water into the anode gas stream for evaporative cooling of a Proton Exchange Membrane (PEM) fuel cell. The basic concept of this form of internal evaporative cooling of the PEM fuel cell is to introduce finely atomized liquid water into the anode gas stream, so that the finely atomized liquid water adsorbs onto the anode and then moves to the cathode via electro-osmotic drag, where this water then evaporates into the relatively dry cathode gas stream, carrying with it the waste thermal energy generated within the fuel cell. The thermal and electrical performance of a 50 cm^2 PEM fuel cell utilizing this technique was compared to the performance obtained with conventional water management. Both techniques were compared over a range of humidification chamber temperatures for both the anode and cathode gas streams so as to determine the robustness of the proposed method. The proposed method produced only meager levels of evaporative cooling (at best 2 watts, for which a minimum of 30 watts was required for adequate cooling), but the average cell voltage increased considerably (as much as a 10% gain), and the technique increased the fault tolerance of the fuel cell (the Nafion™ membrane did not dry out even if cell temperature went well in excess of 70° C despite both anode and cathode humidification temperatures of 55° C). An interesting phenomena was also observed wherein the fuel cell voltage oscillated regularly with a period of tens of seconds, and that the amplitude of this oscillation corresponded inversely with the level of humidification received by the fuel cell.

DEDICATION

I dedicate this thesis to those lovely people closest to me. These important people are my family: mother Trudy, my sister Cara, my father Loren, my stepmother Deborah, and my stepfather Peter. Of course, my family includes my doggies: Thoreau (a.k.a. Big Boy, Hog Dog), Holly, Lexi (a.k.a. Schnortimer, Little Taliban, Yipers, Dr. Destructo), Sally (a.k.a Bandito) and the posthumous hounds Ladybug, Brandy, Athena, Hera, and Blaze.

The person I most wish to dedicate this thesis to is a rather exceptional person I've known since August 11 of 1999, my best friend, my Booboo, Hiam Nawas. Thanks for all of your support Booboo.

ACKNOWLEDGEMENTS

I would like to take this opportunity to thank my adviser Dr. Lalk for all of his advice, interesting conversation, and help wrangling with the local bureaucracy. Here's to Glen finishing his transmission before his thesis.

I would like to thank Dr. Appleby for his support and technical advice. It has been a pleasure working for you, and I hope CESHR can continue to push the envelope of direct electrochemical energy conversion. I must also say that I wish more world renowned experts were as humble and endearingly eccentric as Dr. Appleby.

I'd also like to thank Betty Mahan for all of her help. Without her help, nothing would have ever been accomplished at CESHR by ANYONE. Mrs. Mahan is a case study of a one-woman management team. If every administrator at A&M had her same friendly personality and solid work-ethic, well…let's just say it would improve things considerably.

Last but not least I'd like to say thanks to Arthur Thomason, Prasanth (Paul), Dr. Chunsheng Wang, Dr. Arnaldo Visitin, and Glen Wilcher. You were all fun to hang around with, and you all helped me out at some point, so thanks guys.

TABLE OF CONTENTS

Page

LIST OF FIGURES

Page

Page

Page

LIST OF TABLES

Page

1. INTRODUCTION

Proton Exchange Membrane fuel cells (PEMFCs) have, within the past decade, become the focus of much interest in engineering because of their potential to make electrical power production more "green": that is, environmentally responsible. Because of the commercial availability of mass-produced fuel cell components, the concept of using fuel cells on a large scale to help supply grid electrical power, or for use in automobiles, is becoming closer to a reality every day. However, because of the rather high specific capital cost of fuel cells in their present limited production (that is, cost per unit of generating capacity, usually measured in dollars per kilowatt), fuel cells have not yet made significant inroads into commercial power generation or as automotive powerplants. These high specific capital costs for PEMFC based systems are due to several intrinsic factors: one, the platinum and other precious metals used as catalysts; two, the high cost of the Proton Exchange Membrane(PEM) material, Nafion™; three, the Hydrogen gas storage and/or generating equipment; four, the rather extensive Balance of Plant equipment (gas handling equipment, water management equipment, control system, etc.); and most of all, the fuel cell systems are hand-made in limited production and are not mass-produced.

In order to make fuel cells more attractive, much effort has been made to either increase the performance of PEMFC components, or to decrease their costs, or both.
Much of the work during the mid- to late- 1990's on PEM fuel cells was aimed at reducing the cost of the electrocatalysts used in the MEAs. Most of the work during this period focused on reducing the amount of platinum and other precious metals used as the electrocatalysts. In fact, this work succeeded in reducing the platinum loading of the MEAs from approximately 4 mg/cm^2 to the current 0.4 mg/cm^2, a 10 fold reduction in platinum loading, and therefore resulted in a significant cost reduction [1]. Further reduction in platinum catalyst loading, however, does not seem possible without

---

This thesis follows the style of the *Journal of Power Sources.*

significant deterioration of performance. There have been efforts to utilize other metals or metal oxides as less expensive electrocatalyst materials, but these also suffer from poor performance, or require operational temperatures higher than those tolerable for the Proton Exchange Membrane. Therefore, it does not appear that further specific cost savings will be derived from work related to the electrocatalysts without a major breakthrough.

One area that does promise to yield some further improvement in terms of performance and/or cost reduction is that of the balance of plant equipment. In particular, the water and thermal management subsystems of a PEM fuel cell system could be significantly simplified and abbreviated if internal evaporative cooling could be successfully utilized instead of the present method of thermal management, which is the use of a circulated coolant fluid.

The concept of evaporative cooling of the PEM fuel cell is very simple: admit a modest quantity of liquid water into the anode side of a PEM fuel cell, and allow electroosmotic drag to carry this water to the cathode side, where it evaporates into the relatively dry cathode gas stream. When the water evaporates from the cathode, it absorbs the very large enthalpy of vaporization in doing so, thus cooling the fuel cell with a relatively small amount of liquid water and directly removing the waste thermal energy produced by the fuel cell at its source. In contrast, the present method of cooling, which is the circulation of dielectric coolant, relies on conductive and then convective heat transfer in order to move the waste thermal energy to the coolant. Thus the present cooling method is indirect in the removal of the waste thermal energy from the fuel cell, leading to possible hot spots within the fuel cell due to low local heat transfer flux. Another advantage of evaporative cooling is that, because water is needed to humidify the membrane of the PEM fuel cell, one is in effect “killing two birds with one stone” when using evaporative cooling as a water and thermal management technique.

The use of evaporative cooling as a thermal management technique in PEM fuel cells has been proposed in patents [2], but it has never been used in a commercial PEM

fuel cell design, nor has the experimental performance of such a system been demonstrated in the literature to the author's knowledge.

A simple, lightweight, and inexpensive method of introducing finely dispersed water into a gas stream is the use of an ultrasonic fountain nebulizer. Ultrasonic nebulizers are currently in widespread consumer, medical, and commercial use as humidifiers, and respiratory therapy/drug delivery systems.

Because evaporative cooling has not been explored to any depth in the literature, and because ultrasonic nebulization is a simple, mature and inexpensive technology to adopt, it is justifiable to pursue an investigation into the use of ultrasonic nebulization

1.1 Objective

The objective of this investigation is to determine the feasibility of using ultrasonic nebulization as a water and thermal management technique for PEM fuel cells.

1.2 Scope of research and organization of thesis

In order to satisfy the objective, questions were first devised that, when answered, could determine the feasibility of the proposed water and thermal management method. These questions consisted of:

1. "What is the maximum cooling capacity of the proposed method, and how does this compare to the conventional cooling method?"
2. "What happens to the electrical performance of the fuel cell when the proposed method of water and thermal management is used, and how does this compare to the performance obtained with the conventional method of water management?"
3. "What is the response time of the proposed cooling method? Again, how does this compare to the conventional cooling method?"
4. "How stable is the proposed water and thermal management method to perturbation? How does this stability compare to the stability of the conventional methods of water and thermal management?"

Experiments were then devised and conducted to answer these questions quantitatively as well as qualitatively. The resulting data from these experiments was analyzed, and the author frequently used this data to intelligently direct further experimentation to obtain a better understanding of the behavior of the proposed method of water and thermal management. Finally, once enough data was collected to unambiguously determine an answer the question of feasibility, the data was analyzed and presented herein.

This thesis is organized into seven sections including this introduction. Section 2, Background, is intended to give the reader a background in the basic electrochemistry, thermodynamics, and transport phenomena of PEM fuel cells, as well as a systems level explanation of the functions performed by the equipment in a fuel cell system. If the reader is familiar with the fundamentals of fuel cell operation, then it is recommended that they omit section two. Section 3, Techniques of Water and Thermal Management of Fuel Cells, discusses the conventional water and thermal management of PEM fuel cells, as well as the proposed method using evaporative cooling. The justification for using ultrasonic nebulization humidification as technique to effect evaporative cooling within a PEM fuel cell is also discussed within this section, as well as an explanation of the underlying physics of ultrasonic nebulization. Section 4, Experimental Setup and Procedures discusses the physical set up of the apparatus used to conduct the experiments, as well as the experimental procedures used to conduct the experiments. Section 5, Results and Discussion, gives the results of the investigation that pertain to the objective, as well as unexpected results that point to the use of ultrasonic nebulization of water for electrical performance enhancement. Section 6 contains the conclusions obtained in this investigation. Finally, section 7 lists the recommendations of the author regarding future experimental work towards the development of evaporative cooling for PEM fuel cells. **It is important for the reader to note that all figures and tables referred to in the body of the thesis are contained immediately after the Bibliography in Appendix A.**

2. BACKGROUND

2.1 PEM fuel cell basics

In order to fully appreciate and understand this thesis and the supporting research, it is necessary that the reader have at minimum a basic understanding of the fundamental physics and electrochemistry of PEM fuel cells. The following section is intended to address this need, should the reader not happen to be well-versed in the science of PEM fuel cells. To follow are four subsections devoted to the basic electrochemistry and thermodynamics, thermal management, transport processes, and water management of PEM fuel cells.

2.1.1 Basic electrochemistry and thermodynamics of PEM fuel cells

A chemical reaction is, by definition, a movement or rearrangement of chemical species and outer shell (usually valence shell) electrons. This movement of electrons is, at the atomic/molecular level, a transition from an energetically unstable quantum state to a more stable state, or vice versa. In the former case, the movement of electrons is accompanied by a release of energy, in the latter case, energy is absorbed. In either case, this energy can be absorbed or supplied by an external electric field, and this provides the theoretical basis for an electrochemical energy conversion device.

When a chemical reaction occurs, it often involves one or more redox couple(s). That is, many chemical reactions can be described as a reaction between a reducing agent and an oxidizing agent, which are commonly known as redox reactions. In a redox reaction, the reducing agent loses one or more electrons to the oxidizing agent. In reality, the redox reaction never occurs in a single step- there are often a myriad of intermediate steps consisting of the interactions between reactive intermediaries (radicals), neutral molecules, electrons, and other charged species. A redox reaction can be described in terms of two half-reactions – one half reaction for the reducing agent, and one for the oxidizing agent. Although these two half-reactions do not reveal anything about the

various intermediate reaction steps, it does enable one to understand the transfer of electrons from the reducing agent to the oxidizing agent.

All electrochemical energy conversion devices work by coupling reduction and oxidation half-reactions to an external electric circuit in a controlled manner. In order to do this, it is necessary to control the movement of electrons such that reduction or oxidation can only proceed with an accompanying external electrical current. In other words, every electron that is stripped from a reducing agent and donated to an oxidizing agent inside of the device must also be made to flow in an external electrical circuit. Without this control of electrons, useful direct electrical work cannot be performed, and the device simply acts as a regular chemical reactor, and the only possible by-product of the electrochemical reaction is a transfer of less exergetically valuable thermal energy. The control exercised over the transfer and flow of electrons is done by allowing the oxidation and reduction half-reactions to occur at two different electrode/reactant interfaces – the anode and the cathode. The anode is where the oxidation half-reaction occurs, whereas the cathode is where the reduction half-reaction occurs.

In order to prevent short-circuiting of the electrochemical reaction in an electrochemical energy conversion device, the anode and cathode reactions must be isolated from one another. There are two ways to accomplish this isolation: one, use an ion-selective membrane to physically separate the two reactions; or two, use an enzyme or other highly selective catalyst at the anode and cathode (used in biological fuel cells). Because enzyme-based electrocatalysts are expensive, perform poorly (only very low current densities are possible), and have a very short lifetime, the use of selective anode/cathode electrocatalysts is not in widespread use. Therefore, many but not all electrochemical energy conversion devices utilize a membrane in order to separate the anode and cathode reactions.

In a PEM fuel cell, the anode and cathode are separated by an electrically nonconductive, relatively impervious membrane with a highly selective ionic conductivity. That is, for all practical purposes, the membrane is conductive for only a select few ions. The membrane must also be highly impervious to the reactants,

meaning that the membrane slows diffusion of electrically neutral species to an extremely low rate. However, for those ions which are mobile in the membrane, the membrane is highly conductive. This selective ionic conductivity prevents reactive neutral and charged chemical species from migrating across the membrane and short circuiting the electrochemical reaction, while still allowing the intended charged reactive species to migrate through the membrane relatively unimpeded.

As the reader may well be aware, a fuel cell is essentially a battery, the difference being that for a fuel cell, the reactants are not self-contained as in a battery, they are instead continuously fed into the fuel cell as needed. In a PEM fuel cell, a reducing agent (fuel), such as hydrogen, is oxidized at the anode, and the freed electrons are sent out from the anode to the bipolar plate current collector where they eventually travel out of the fuel cell by the anode electrical connection, and a charged ionic species (hydronium ion or H_3O^+) moves through an ionically conductive/electrically nonconductive electrolyte to the cathode (see red arrows in Figure 1). It is important to note that this hydronium ion is formed by the combination of a proton donated by the hydrogen fuel and water present at the catalyst site. Once outside of the fuel cell, the electrons travel through the electrical leads to the load where they perform electrical work at a rate given by Ohm's Law:

$$P_{electrical} = I^2R \tag{1}$$

or

$$P_{electrical} = V*I \tag{2}$$

(where I is the current in Amperes, V the voltage in Volts, and R the resistance in Ohms). Once the ionic species from the anode has reached the cathode, it reacts with the oxidizer (oxygen in air) and the electrons (generated at the anode) returning through the cathode electrical connection and cathode bipolar plate, thereby reducing the oxidizer (oxygen from the air) to the reaction product, water. See Figure 2 for an illustration of the internal anatomy of a PEM Fuel Cell.

In a PEM fuel cell, the anode and cathode are both electrically conductive and porous; this allows the reactant gases to flow in a direction perpendicular to the direction of ionic/electrical current and still be able to reach the active sites of the catalyst/membrane matrix. The membrane is composed of a proton-conducting polymer electrolyte, perfluorosulfonate terminated- polytetrafluoroethylene (Nafion). The half-cell reactions that take place at the electrodes are as follows [3]:

Net Anode Reaction: $H_2 \rightleftharpoons 2H^+ + 2e^-$ (3)

Net Cathode Reaction: $\frac{1}{2} O_2 + 2H^+ + 2e^- \rightleftharpoons H_2O$ (4)

Overall Reaction: $H_2 + \frac{1}{2} O_2 \rightleftharpoons H_2O$ (5)

At 25 °C this reaction of hydrogen with oxygen has an enthalpy of reaction of –286.2 kJ/mol (for liquid water as the product) and -241.9 kJ/mol (for gaseous water as the product) [4].

It is important to note that the half reactions never occur in a single step, and that free protons are never produced. In an aqueous medium, the anode half reaction occurs in two steps as follows:

$$H_2 \rightleftharpoons 2\dot{H} \quad (6)$$

$$2\dot{H} + 2H_2O \rightleftharpoons 2H_3O^+ + 2e^- \quad (7)$$

The first step (equation 6) is dissociation of the diatomic hydrogen molecule into two hydrogen radicals by severing the hydrogen-hydrogen covalent bond. The second step is the ionization or charge separation step wherein the two electrons separate from the two hydrogen radicals. This second step results in the formation of two hydronium ions, because the charge separation proceeds in coordination with a neighboring, highly polar water molecule which is attracted by the densely charged hydrogen nucleus.

From thermodynamics, we can determine the maximum amount of reversible electrical work done by this chemical reaction. To begin, recall that the Gibbs free energy is defined as:

$$G = H - TS \tag{8}$$

In differential form this gives:

$$dG = dH - TdS - SdT \tag{9}$$

Substituting the definition of enthalpy gives:

$$dG = d(U + PV) - Tds - SdT \tag{10}$$

or

$$dG = dU + PdV + VdP - TdS - SdT \tag{11}$$

recalling from the first law of thermodynamics for a closed system:

$$dE = \delta Q - \delta W = dU \tag{12}$$

substituting this into equation 11 gives:

$$dG = \delta Q - \delta W + PdV + VdP - TdS - SdT \tag{13}$$

For a reversible process:

$$\delta Q = TdS \tag{14}$$

For a fuel cell operating at constant temperature and pressure this gives:

$$dG = -\delta W + PdV \tag{15}$$

To find maximum electrical work, we impose the condition that no expansion work be done:

$$PdV = 0 \tag{16}$$

Therefore:

$$dG = -\delta W_{electrical} \tag{17}$$

In other words, the maximum electrical work that can be done by a chemical reaction is given by the change in Gibbs Free Energy, ΔG, of the reaction.

This electrical work can be expressed in terms of a charge Q moved through a potential V:

$$W_{electrical} = QV \tag{18}$$

or

$$W_{electrical} = nFV \tag{19}$$

where n is the number of moles reacted, F faraday's constant (96,487 coulombs/mol).

From this last equation, we can calculate the reversible voltage for the hydrogen/oxygen reaction used in the fuel cell, which corresponds to 1.229 volts at 25 °C (for gaseous reaction product). *This is the maximum voltage possible given consideration of the second law of thermodynamics*.

If one were to substitute the enthalpy of reaction for hydrogen/oxygen instead of the gibbs free energy of reaction as the maximum electrical work in equation 19, one would arrive at values of 1.48 and 1.25 volts (for liquid and gaseous reaction products, respectively). *That is, these voltages correspond to the maximum voltage possible from a first law of thermodynamics point of view, but which are physically impossible as a result of the second law of thermodynamics*. In order to achieve these voltages, the total entropy of the universe would have to decrease, as the reaction product has less entropy than the sum of entropies of the two reactants. These first law maximum voltages are of interest when calculating the waste thermal energy generation rate, which will be discussed shortly.

To predict the maximum conversion efficiency of the fuel cell, one can express the ratio of the maximum reversible work to the chemical reaction to the enthalpy of the reaction. That is, the maximum efficiency can be expressed as the ratio of the gibbs free energy of the reaction to the enthalpy of the reaction, thus:

$$\eta_{\text{maximum}} = \frac{\Delta G_{\text{reaction}}}{\Delta H_{\text{reaction}}} \tag{20}$$

It is important to note that for reactions which produce water (or any other condensable reaction products), there are two enthalpy values or fuel energy content values of interest: the higher heating value (HHV) and the lower heating value (LHV). The higher heating value gives the total enthalpy of reaction (combustion) of a fuel at a given temperature, and it includes the enthalpy contribution from the condensation of any reaction products (in this case, water). The lower heating value gives the enthalpy of reaction for a fuel without the contribution of condensation of reaction product(s). The higher heating value is the true thermodynamic equilibrium enthalpy of a reaction at a constant temperature, but it is not necessarily the appropriate enthalpy value to consider.

This is because, from an engineering design standpoint, nearly all combustion reactions encountered in practice do not result in the condensation of reaction products. For a fuel cell, it is appropriate to consider the lower heating value, as no additional work can be recovered from the condensation of the products. From equation 20 we find that the maximum conversion efficiency of a hydrogen/oxygen fuel cell is approximately 83% efficient at 25 °C.

In actual operation, the reversible potential is never reached (even at infinitesimal current density), and is in fact substantially less, often in the range of 0.8 to 0.6 volts. The reason that this potential is not achieved is due to irreversibilities associated with the operation of the fuel cell. There are three contributors to the irreversibility of energy conversion in a fuel cell, and they are ohmic losses (I^2R losses), mass transport losses (starving for reactant), and limitations in the kinetics of the reaction or activation losses (the rate of electrocatalysis is finite, which is especially true at the cathode in a PEM fuel cell). These irreversibilities cause the fuel cell to be substantially less efficient than the efficiency predicted by equation 20.

The effect of the irreversibilities on the electrical performance of a fuel cell can be demonstrated by a *polarization curve*, which is depicted in Figure 3. A polarization curve is a plot of the fuel cell voltage as a function of the cell current or, more frequently, the current density. From left to right, one can see first a very sharp drop in cell voltage, then a transition to a relatively gentle slope, and finally a "knee" at about 1.2 A/cm^2 (the "knee" does not necessarily occur at this current density for all PEM fuel cells, but it is a typical value). The first or leftmost sudden drop in voltage is due to activation (or reaction kinetics) losses. The activation loss is not strongly a function of the current beyond a few mA/cm^2, and is therefore regarded as a constant voltage drop, that is:

$$V_{loss(activation)} = V_{(open\ circuit)} - V_{(infinitessimal\ current)} = \text{Constant} \qquad (21)$$

The ohmic losses are responsible for the steady decline in cell voltage in the gentle slope region. That is, the ohmic losses are directly proportional to the current or current density, and are given by ohm's law:

$$V_{loss(ohmic)} = I * R_{internal} \quad (22)$$

where I is the cell current, and $R_{internal}$ is the internal electrical resistance of the fuel cell. The sudden drop in voltage starting at the "knee" is due to mass transport losses. The mass transport losses are caused by the mass transport limitation imposed by the finite rate of reactant diffusion.

The overall fuel cell voltage can be described as the sum of the voltage produced by the anode relative to a reference, and the voltage of the cathode relative to this same reference, that is:

$$V_{cell} = (V_{anode} - V_{reference}) + (V_{cathode} - V_{reference}) \quad (23)$$

The reference voltage used most often in fuel cell work is the reduction potential of hydrogen, and is arbitrarily assigned a voltage of zero. Thus, all reduction (cathode) and oxidation (anode) potentials are referenced relative to that of hydrogen. This concept of describing fuel cell voltage output as the sum of the anode and cathode potentials is of use in understanding the concept of *overpotential*. The difference in voltage between the reversible voltage and the actual or irreversible voltage is referred to as the sum of the anode and cathode overpotentials. That is:

$$V_{actual} = (V_{reversible(anode)} - V_{overpotential(anode)}) + (V_{reversible(cathode)} - V_{overpotential(cathode)}) \quad (24)$$

This difference in voltages is referred to as an overpotential is because it represents the hypothetical potential applied to the electrode to overcome the irreversibilities and drive the reaction. This overpotential is actually supplied by the reaction, and is therefore subtracted from the voltage produced at the given electrode.

Because of irreversibilities, considerable waste thermal energy is produced during operation. This waste thermal energy must therefore be removed from the PEM fuel cell, as otherwise the waste thermal energy would cause the internal temperature to rise uncontrollably beyond the maximum safe operation temperature of approximately 80 °C.

The amount of waste thermal energy produced during the operation of the fuel cell can be given in terms of the actual operating potential or irreversible potential, the first law maximum voltage, and the current:

$$\frac{dq}{dt} = I\left(V_{first\_law} - V_{irreversible}\right) \quad (25)$$

This equation can also be used with the current density to give the heat flux produced within the fuel cell:

$$q'' = J(V_{first\_law} - V_{irreversible}) \quad (26)$$

Typical current densities of operation are 0.4 to 0.8 amps/cm^2, giving a typical heat flux in the range of 0.15 to 0.48 W/cm^2.

The surfaces of the anode and cathode in a PEM fuel cell consist of a dispersion of an extremely fine noble metal catalyst powder (Platinum or Platinum\Ruthenium) in contact with the membrane. The catalysts are used because of the relatively low operating temperature of PEM fuel cells. At the relatively low operating temperature of PEM fuel cells, the rates of reaction (at both anode and cathode) without catalysts are extremely low. The catalysts allow reaction rates which are orders of magnitude higher than that possible with a bare electrode.

As was mentioned previously, the hydronium ion is formed at the anode by combining a proton from the hydrogen fuel and water that is present at the anode catalyst site. Thus, water must be supplied in some fashion to the anode of a PEM fuel cell. The water that is required to form the hydronium ion can come from two sources – diffusion from the cathode, where it is produced as the overall reaction product, and the hydrogen gas stream itself. Because the diffusion of water though the Nafion membrane is rather slow, it is necessary to humidify the anode (hydrogen) gas stream. It is important to note, also, that because this hydronium ion moves from the anode to the cathode, there is a net flux of water from the anode to the cathode side. This flux is commonly known as electroosmotic drag, as it is driven by the migration of a charge carrying species (hydronium ion). Electroosmotic drag has been studied extensively, and the consensus is that for a well hydrated membrane, on average 2.5 water molecules are dragged from anode to cathode per every hydronium formed, and this ratio can be as high as 2.9 for a saturated membrane [5].

The ionic conductivity of the Nafion membrane is strongly a function of its moisture content. The ideal moisture content of a Nafion membrane is 20% by weight [3]. In order to accomplish this, both the anode and cathode gas streams are humidified. Because water is transported via electroosmotic drag from the anode to the cathode, and because most of the product water does not back-diffuse, the cathode stream need not be humidified to the same level needed at the anode. However, the cathode gas stream is humidified in an attempt to keep the vapor pressure high enough to prevent excessive evaporation. If excessive evaporation occurs on the cathode side, the local ionic conductivity of the MEA is reduced near the cathode electrocatalyst sites, resulting in an increase in ohmic losses and a corresponding decrease in the cell voltage.

2.1.2 Construction of a typical PEM fuel cell stack

By now, the reader has learned some of the fundamental aspects of PEM fuel cell operation, and it is appropriate to describe the construction of a generic PEM fuel cell stack. A fuel cell stack is simply a collection of individual fuel cells electrically connected together in a series or series-parallel arrangement to give the desired voltage and current needed for a particular application. Because each cell produces between 0.6 to 0.8 volts at typical current densities of 0.4 - 0.8 amps/cm^2, and because most switching power supplies or inverters require several tens of volts to achieve practical power densities and efficiency, most stacks consist of at least 20 cells in series.

Grouping these fuel cells together as a stack in a manner that meets the competing objectives of high conversion efficiency, power density, and low cost, is not a trivial matter, but neither is it an insurmountable task. The approach that has gained by far the most widespread adoption is a sandwich type arrangement of bipolar plates (called “bipolar” because one side of the plate is in contact with the anode of one cell and the cathode of the adjacent cell), Membrane Electrode Assemblies (MEAs), flow fields, gaskets, and end plates. See Figure 4 for a photograph of a PEM stack. In Figure

4, one can see that the stack is comprised of repeating elements of a bipolar plate, MEA, gasket, and flow fields.

The heart of every fuel cell stack are the membrane electrode assemblies (MEAs) which are the product of several decades of PEM fuel cell evolution. Figure 5 is a photograph of the commercially produced (3M Corp.) MEA used in this research. An MEA is comprised of a Nafion ion exchange membrane, an anode catalyst layer, a cathode catalyst layer, and two carbon cloth gas diffusion layers (one for the anode and one for the cathode). One can clearly see the carbon cloth which is used as the gas diffusion layer (GDL). The gas diffusion layer performs two functions: one, it allows the passage of reactants and products through its fine pores while allowing electrical current to pass perpendicular to its surface to the flow field and/or bipolar plate. To form the MEA, the carbon cloth gas diffusion layer is first soaked in a Teflon™/carbon black suspension, and then heated in an oven to melt the Teflon™ and wick it into the carbon fiber pores. This Teflon™ pore filling gives the carbon cloth the property of being hydrophobic (which helps prevent waterlogging of the electrocatalyst active sites). Next the carbon cloth is coated on one side with an "ink" of platinum black nanoparticles (supported on somewhat larger carbon black particles) suspended in a low-molecular weight (~1100 molecular weight) Nafion™ solution. The loading of electrocatalyst used is approximately 0.4 mg/cm^2 [6]. The carbon cloth is then given a final, light coating (on the same side) with a Nafion™ solution. Finally, both carbon cloth gas diffusion layers are bonded catalyst side facing inward to the Nafion™ membrane by hot pressing for several minutes at ~150 °C and 150 psi [6]. This hot pressing performs two important functions: one, it mechanically bonds the carbon cloth gas diffusion layer (GDL) to the Nafion™ membrane; and second, it forces the catalyst particles into intimate contact with the Nafion™ membrane.

For the MEA to function, reactant gas must be delivered to the surfaces of the anode and cathode, product water must be removed from the cathode, and the electrical current must be conducted normal to the surface of the MEA. The flow field concept was the solution to the design problem of needing to move reactant gases and water in a

direction tangent to the surface, whilst conducting an electrical current in the normal direction.

There are several types of flow field used in modern PEM fuel cells; however, two designs are by far the most commonly encountered: serpentine flow fields and metal foam flow fields. See Figure 6 for an illustration of each type of flow field. Serpentine flow fields are most commonly constructed of graphite or a graphite/polymer composite, although they are occasionally made from a corrosion-resistant metal (such as stainless steel or titanium). Metal foam flow fields are almost exclusively made from nickel foam, although titanium has been used. Nickel is the preferred metal of choice for metal foam flow fields because of its low cost, ease of manufacture, oxidation stability in moderately acidic conditions (pH ~5), and the insolubility and relatively high electrical conductance of the trivalent oxide formed only slowly by corrosion.

With a serpentine flow field, reactant gas, water vapor, and water droplets move through a set of circuitous passages which are machined, stamped, or cast into the surface of the bipolar plate, and electrical current is conducted by those parts of the flow field in contact with the MEA. The surface of the MEA which is below the serpentine passages has easy access to reactants, but no direct electrical connection to the bipolar plate – the current must flow laterally first in order to then flow out normal to the MEA surface. Conversely, for those parts of the MEA in direct contact with the flow field/bipolar plate, the reactant gases and moisture must move laterally through the gas diffusion layer before being able to advect into or out of the gas stream. It is because of these two conditions that the passage spacing and wall thickness of the serpentine flow field is kept small (on the order of 0.020 - 0.050 inches). Smaller spacing cannot be used because of increasingly high pressure drop losses, poor water transport characteristics, and fragility [7]. The concept of the serpentine flow field is not new; it is, in fact the first method used, and has remained popular due to its simplicity, and ease of incorporation into mass-production designs. Despite its simplicity, the serpentine flow field concept does suffer from the fact that it only offers mediocre electrical and reactant/product transport performance.

There are three difficulties encountered with serpentine flow fields. One problem is the uneven distribution of gas, especially near the end of the serpentine path. Another difficulty is (for the cathode) blockage of the passages near the end of the serpentine path due to water build-up. Both of these conditions cause significant mass transport losses, and are most marked at high current density. The third problem is the very high pressure drop experienced moving the gas through the long, narrow serpentine channel, which amounts to an increase in parasitic loss from extra compressor work [7].

To overcome the transport difficulties encountered with serpentine flow fields, the metal foam flow field concept was developed. A metal foam flow field is simply a piece of high porosity metal foam inserted between the bipolar plate and the MEA. The metal itself is usually Nickel or a Tin-plated Nickel with an average porosity of approximately 95% and an average pore size of 100 p.p.i. (pores per lineal inch). The metal foam allows much better transport characteristics without sacrificing electrical conductivity. This is because the metal foam allows for an effective "channel" spacing of 0.010 inches or less without suffering from the problems of fragility, high pressure drop of the reactant gas, or having aggregate plug flow at moderate levels of water entrainment. Because of this increased performance, and the relatively low cost of incorporating metal flow fields into a design, they are becoming more widely used. The sole disadvantage of metal foam flow fields is the problem of long-term corrosion, which causes a gradual decrease in electrical conductivity at the MEA/metal foam interface, and a decrease in the ionic conductivity of the Nafion due to incorporation of solvated (aqueous) metal ions. In this research, a Nickel metal foam flow field was used due to the increased performance it offered.

In the stack, the MEAs are sandwiched between bipolar plates with a silicone rubber or Teflon gasket to maintain a gas tight seal. See Figure 7 for a photograph of a gasket, MEA, flow field and bipolar plate used in this research. These bipolar plate/gasket/MEA sandwiches are stacked as units as needed to form the fuel cell stack, and are capped on the end by end plates. The entire stack is held together in compression by rather long tie rods or studs. The stack is held in compression for three reasons: one,

to ensure that the gaskets have seated properly and to provide a preloading to prevent gasket blow-out; two, to ensure good mechanical contact between the MEAs and flow fields so as to minimize electrical contact resistance; and three, to provide the stack with mechanical structure that is capable of supporting itself from the loads induced by gravity and to any other reactions that the stack may be subjected. See Figure 4 for a photograph of a preprototype commercial fuel cell stack.

2.1.3 Transport processes

Because a fuel cell is an electrochemical device that converts chemical potential energy to electrical energy, it is necessary to continually input reactants and remove product(s) so long as the fuel cell is operating. Furthermore, the performance of the fuel cell is heavily dependent upon the ability of reactants to migrate swiftly to the catalyst/membrane matrix reaction sites. Thus, it is important to understand the physical processes by which the reactants and products are transported within an actual fuel cell.

With conventional gas distribution, the transport of reactant gases to the catalytically active sites from the gas streams in the flow field occurs in two steps. Figure 8 illustrates these two steps. The first step is advection from the moving gas stream in the flowfield to the surface of the gas diffusion layer. The second step is diffusion of the gas through the pores of the gas diffusion layer to the active sites of the catalyst. The second step, diffusion, forms the mass-flow bottleneck of the fuel cell, as it is several of orders of magnitude slower than advection.

With the use of the rather novel interdigitated flowfields, transport of gas and liquids is accomplished entirely by advection. See Figure 9 for an illustration of an interdigitated flow field. With interdigitated flow fields, reactant gas is forced by differential pressure from one channel down through the gas diffusion layer into the adjacent channel. Interdigitated flowfields have significant performance advantages over serpentine or metal foam flow fields, especially for the cathode, where the overpotential is inversely proportional to the oxygen concentration [8]. However, the significant

pressure differential required for operation imposes a very hefty penalty in terms of parasitic power losses for the compressor, and these parasitic losses negate any efficiency gains in the fuel cell itself [7]. Because of this parasitic loss, the use of interdigitated flowfields is not popular; because of these parasitic losses and difficulty of manufacture, interdigitated flowfields were not used in this investigation.

At the anode, hydrogen, water vapor, and water droplets are transported to the catalyst sites where they react and are consumed. At the cathode, oxygen is transported from the gas stream to the catalyst active sites, and the water vapor and water droplets experience a net transport away from the catalyst sites.

Transport of both reactant(s) and product(s) in a fuel cell can be improved by the use of high reactant flow rates, far in excess of the rates needed to feed the electrochemical reaction occurring within the fuel cell. In any electrochemical conversion device, the reactant delivery flow rate associated with delivering exactly the reactant needed by the electrochemical reaction taking place is called the stoichiometric flow rate. The minimum stoichiometric flow rate used in PEM fuel cells is approximately1.25 for the anode and 1.6 for the cathode. The use of these higher-than-stoichiometric flow rates not only improves transport, but it also helps to ensure that no portion of the fuel cell is ever starved for reactant(s). The reason that the minimum cathode stoichiometric flow rate is so high is because the partial pressure of oxygen in the air becomes very low near the end of the fuel cell stack if a stoichiometric flow ratio of less than 1.6 is used; because the overpotential (or efficiency loss) of the cathode is inversely a function of oxygen concentration, it is necessary to maintain as high of an oxygen partial pressure as feasible.

2.1.4 Reactant gas delivery schemes–deadending, recirculation, and feed-through

There exist three distinct strategies of delivering the reactant gases to a PEM fuel cell system: deadending, recirculation, and feed-through. One method, deadending is to simply force the reactant gases into the fuel cell under pressure. That is, deadending can

be viewed analogous to keeping a leaky balloon inflated, in that reactant gases are forced in under pressure to the fuel cell, but have nowhere to go other than to feed the "leak" which is the electrochemical reaction. In deadending, flow only occurs as the reactant gases are consumed. With recirculation, reactant gases are circulated through the fuel cell, but only a fraction of the reactant gases inputted to the fuel cell are consumed. The excess reactant gases are allowed to exit the fuel cell, where they are recompressed and mixed with make-up reactant gas. In flow through, more reactant gas flows into the fuel cell than is needed, but is not recompressed, but is instead simply vented to the atmosphere.

The advantage of deadending is that it is the most energy efficient way of providing the reactant gases to the fuel cell system. With deadending, however, it is impossible to use air as a reactant gas, as the oxygen would quickly be consumed out of the initial charge, and any additional oxygen would have to travel via diffusion from the compressor/tank to the fuel cell – an impossible arrangement for to use for any type of practical device. This problem, that is the build up of inert gases as the reactants are consumed, is the major drawback of deadending. Deadending, therefore, is only used with highly pure hydrogen and oxygen, as is the case with the fuel cell that was used on the Apollo missions. Deadending also results in the transport of reactants at the "end of the line" to be poor, and can lead to significant starvation at high current densities and consequent low conversion efficiency/voltage.

Recirculation is a balance of the deadending and feed-through strategies. Recirculation ensures that adequate reactants are delivered to the fuel cell even when operating at high current densities, without the waste of reactant gases that results from venting them to atmosphere (which occurs in feed-through). Recompression of the excess gases consumes more power than deadending as the ratio of total moles of gases inputted to moles of gas consumed. That is, if 200% of theoretically required (2.0 stoichiometric flow rate) hydrogen is circulated in a recirculation scheme, it would require twice as much anode gas compressor power as a deadending scheme. Because of this extra power requirement for the compressor, the recirculation ratio in practical

systems is limited. The power required to run the compressor is a parasitic loss for the overall fuel cell energy conversion system. Recirculation in PEM systems is used for the anode hydrogen gas stream, but is only used for the cathode gas stream if pure oxygen is used. If air is used for the cathode feed gas, there is no incentive to use recirculation, as it is not a valuable reactant.

Feed-through is also an energy intensive strategy, and like recirculation, consumes more power than deadending, and this compressor power requirement is the ratio of total moles of gases inputted to moles of gas consumed, with the consequent parasitic power/efficiency loss. Again, as in recirculation, feed-through ensures that adequate reactants are delivered to the fuel cell even at high current densities. Another advantage of feed-though is that, for the cathode gas stream, the excess air very effectively carries the product water out of the fuel cell, where it is simply vented/drained or collected in a simple catch basin. For this research, the feed-through strategy was adopted for both the anode and cathode gas streams because it was the simplest scheme to implement. In a commercial PEM fuel cell system, recirculation would be used instead because of its performance advantages.

2.1.5 Water management

As previously mentioned, PEM fuel cells require that both gas streams be humidified in order to maintain the moisture content of the Nafion membrane. It is also necessary to remove the product water from the fuel cell, and then either reuse it for humidification and/or dispose of the excess product water. The performance of these two tasks comprises water management of PEM fuel cells.

2.1.6 Thermal management

As mentioned previously, the PEM fuel cell, like any other practical energy conversion device, is not 100% efficient in performing energy conversion, and therefore waste heat is produced during operation. This waste heat must be removed in some fashion, as it will otherwise cause the stack to reach temperatures high enough to melt or severely weaken the Nafion membranes, resulting in the complete destruction of the rather expensive fuel cell stack. For PEM fuel cells in automotive applications, it may also prove necessary to warm them up on cold days, as PEM fuel cells will not work at all in temperatures below 0 °C. Thus, thermal management of the PEM fuel cell system is of vital importance.

3. WATER AND THERMAL MANAGEMENT TECHNIQUES

This section concerns the techniques used to perform the tasks of water and thermal management for PEM fuel cells. The first section describes the presently used methods of cooling, reactant gas humidification, and product (waste) water removal. The second section discusses evaporative cooling, and how this technique would be implemented for a PEM fuel cell system. The third section describes how an ultrasonic nebulizer works, and the engineering design advantages that make it attractive to use as part of an evaporative cooling system.

3.1 Conventional water and thermal management

The following subsection describes the present techniques used to solve the issues of water and thermal management in PEM fuel cells. While these solutions are sound, they require the use of additional balance-of-plant equipment in a PEM fuel cell system. This additional equipment occupies space, adds considerable mass to the system, and in the case of the thermal management system, can utilize a significant amount of electrical power in order to operate. Furthermore, although the present methods of water and thermal management are robust, the additional equipment can fail (especially rotating machinery such as pumps and fans).

3.1.1 Conventional water management

The conventional method of humidifying the reactant gas streams is to bubble each of them separately through a column of water at a temperature slightly below or at the operating temperature of the fuel cell. If the water temperature in the bubbler is too cold, insufficient water vapor is present in the gas stream to provide enough humidification, whereas if the water temperature is too high, the water vapor will

condense on the cooler MEA and possibly cause waterlogging of the active sites of the electrocatalyst (especially on the cathode).

The removal of the water from the PEM fuel cell can be accomplished in a number of ways. One way is to build a wick like structure into the bipolar plate to wick the product water away from the cathode by capillary action. Such a wick structure will work even in zero g environments, but has the distinct disadvantage of making the design of the bipolar plate and stack much more complicated, and it decreases the effective active area of the cathode. Another way to remove water is to simply run the fuel cell with no humidification of the reactant gases, and to allow any excess product water to evaporate into the rather dry cathode gas stream. Using no reactant gas humidification causes the Nafion membrane to have a rather low moisture content, and consequently, such an arrangement forces the fuel cell to be operated at very low current densities due to the poor ionic conductivity of the partially dehydrated Nafion membrane. This method essentially sacrifices power density and conversion efficiency for the convenience of being able to dispose of the product water as a gas that is vented with the cathode exhaust stream. However, the majority of PEM fuel cell systems remove the product water as mix of vapor and liquid phase water in the cathode gas stream exhaust. This two phase mixture of water, water vapor, and air can also be vented to atmosphere, although care must be taken to not allow too much water to be entrained into the cathode gas stream before it exits the fuel cell, as waterlogging of parts of the cathode can otherwise result.

The most common method of water removal from the PEM fuel cell is thus simply to vent it to atmosphere and/or allow it to drain as it exits the fuel cell along with the cathode exhaust gas. In most all cases of terrestrial PEM fuel cells, the feed-through reactant gas supply scheme is used on the cathode side to facilitate this very simple and inexpensive product water management technique.

3.1.2 Conventional thermal management

The fuel cell stack in terrestrial applications is in contact with the ambient air, but the surface area available for external cooling is much too small to afford any type of meaningful external convective cooling. Thus, it is necessary to remove the waste thermal energy generated internally by circulating a coolant within the stack structure, or to use the reactant gases themselves as gas coolants. The latter concept, of using the reactant gases as coolants, has proven much too energetically costly for most terrestrial applications, as these considerable volumes of these gases would have to be compressed relative to the amount consumed in the fuel cell itself.

The conventional method of thermal management in PEM fuel cell stacks is to circulate a suitable cooling fluid through cooling passages within the fuel cell stack structure. These passages are machined, stamped, or cast into the bipolar plates, and allow this dielectric cooling fluid to circulate directly beneath the active area of each MEA. See Figure 10 for an illustration. The dielectric fluid used is usually air or a water/glycol mixture. The cooling fluid must be a dielectric (insulator) as it would otherwise short out each fuel cell. However, because almost fuel cell stacks produce relatively low voltage (220 volts or less), it is not necessary that this dielectric fluid have a high breakdown voltage.

There are two paradigms of operation for the circulation of a dielectric coolant inside the fuel cell stack: closed loop, and open loop. See Figure 11 illustrating both methods. Closed loop operation is reserved almost exclusively for use with a liquid, and open-loop is always used with air as the coolant. The closed loop system can be used with a gas coolant, but in practice rarely if ever is because of the significant disadvantages that the use of a compressible coolant poses, to say nothing of increased likelihood of coolant leakage. The closed loop system is virtually identical to the used in modern automobiles: a centrifugal pump circulates the coolant within the coolant passages in the bipolar plates of the fuel cell stack, and then through a radiator (liquid-to-air heat exchanger) which may or may not be thermostatically controlled. At the

radiator, a fan is used in order to promote enough convection with the ambient air. For the open loop system, ambient air is simply forced through the coolant passages and then vented to the atmosphere.

For nearly all commercial PEM fuel cell systems, closed-loop liquid cooling is used. This method is very robust and reliable, but adds considerably to the cost, complexity, and weight of the overall PEM fuel cell system. The main contributors to the cost and weight of the system are the pump, liquid-to-air heat exchanger, and heat exchanger fan. While it is possible to use a thermosiphon system to possibly reduce cost, minimize parasitic losses, and increase reliability, this forces the usage of a much larger liquid-to-air heat exchanger, thus imposing a major weight and system volume penalty.

In small systems (<1 kW), open-loop air cooling is often used because it is simple and inexpensive to implement [7]. The main disadvantage of this technique is that the blower consumes a disproportionately high level of power to operate compared to the pump used in a liquid cooled system. This excessive power consumption is due to the fact that air is a compressible fluid, meaning that to generate a given pressure drop, the specific volume of the air changes enormously when compared to an almost incompressible liquid. Furthermore, because of the low density, conductivity, and heat capacity of air, a much larger volumetric rate of flow is required as compared to a liquid for the same amount of cooling. Again, as with the closed loop liquid system it is possible to use a thermosiphon (convection cooled) design, but this is largely impractical for any system more than a few hundred watts electrical in size.

For both methods of conventional cooling, one is paying a price in terms of parasitic power losses, volume, mass, and cost in order to have a PEM fuel cell stack with any economically reasonable power density. To give the reader an idea of the power consumed for cooling, the very well engineered 2.0 kW PEM demonstrator produced by the Paul Scherr Institute used 70 W alone just to power the cooling blower [7].

3.2 Evaporative cooling

Now that the reader is familiar with the advantages and disadvantages posed by the conventional methods of water and thermal management in PEM fuel cell systems, the method of evaporative cooling can be discussed. Evaporative cooling is a process intimately familiar to anyone who has ever exerted themselves in the heat of day- and sweated. Phase changes are often accompanied by a large amount of heat transfer per unit mass and per unit area, and in the case of water, this is especially true.

The concept of the "swamp cooler" can be extended to a PEM fuel cell stack. If it were possible to evaporate product and cooling water from the surface of the MEA into a relatively drier gas stream, one could put evaporative cooling to work within the fuel cell. Such an arrangement would have the benefit of eliminating the need for external circulation pumps, fans, heat exchangers, etc., and in turn, bipolar plates could be constructed in a much lighter and inexpensive fashion. In fact, such an idea is in theory quite feasible, as water evaporation already takes place within the fuel cell at a considerable rate. The question, then, becomes how one goes about using this concept of evaporative cooling in a way that does not degrade the electrical performance of the PEM fuel cell whilst providing an adequate method of removing waste heat. The following section discusses how coolant water can be delivered to the fuel cell via the anode gas stream, transported through the membrane, and then evaporated into the cathode gas stream, and in doing so, cool the PEM fuel cell without adversely affecting its conversion efficiency/electrical performance.

3.2.1 Putting electroosmotic drag to work for evaporative cooling

The reader may recall that the process of electroosmotic drag was first introduced and discussed in section 2.1.1, where it was mentioned that the hydronium ion was formed by electrocatalysis at the anode and that this hydronium ion then proceeded to move through the membrane to the cathode. Because on average 2.5 water molecules are

pulled across per hydronium ion, one could potentially be able to use the latent heat of vaporization of 5 moles of water molecules for every one molecule of hydrogen consumed. The evaporation of these 5 moles of water per every mole of hydrogen would provide more than adequate cooling for a fuel cell operating at normal efficiencies.

Because on average 2.5 water molecules are moved from anode to cathode by electroosmotic drag for every hydrogen molecule consumed, it would seem necessary to supply this same water-to-hydrogen ratio in the anode feed gas. However, this is not the case because in the PEM fuel cell, neutral water is able to back-diffuse from the cathode, where the water concentration is the greatest. This back-diffusion of neutral water from the cathode to the anode is what allows the fuel cell to operate at reasonable current densities, since typically the molar ratio of water to hydrogen in the anode feed gas is much less than 2.5:1; it is in fact closer to 0.4:1 ! As an example, consider the case of conventional humidification, which delivers saturated hydrogen gas at 70 °C to the PEM fuel cell at a total pressure of 1 atmosphere. Assuming ideal gas behavior of the hydrogen gas and water vapor mixture, application of Dalton's Law of Additive Pressures gives a molar ratio of:

$$\frac{P_{sat}}{P_{hydrogen}} = \frac{P_{sat}}{P_{total} - P_{sat}} = .445 \tag{27}$$

With conventional humidification, it is obvious that not enough water is entering through the hydrogen gas feed to completely supply the hydronium production, and therefore this water must be present at the anode catalyst site due to back-diffusion from the cathode.

In order to provide evaporative cooling, the concentration of *liquid* water in the anode gas stream must be increased substantially, and the cathode gas stream made less humid to accommodate evaporation. Liquid water must be present in the anode gas stream in order to benefit from the very large latent enthalpy of vaporization of water (2333.8 kJ/kg at 70 °C [9]). If the water arrives at the anode as a gas and condenses, then the membrane absorbs this latent enthalpy of vaporization, and no net cooling takes place after the water evaporates at the cathode(unless there is a large temperature

gradient across the very thin membrane, a scenario that is both extremely unlikely and undesirable).

3.2.2 Getting the liquid water to the anode-water atomization

In order to deliver liquid water to the anode via the anode gas stream, one is faced with a choice: to either suspend liquid water particles into the gas stream, or to simply inject water into the gas stream. If one injects water into the gas stream, the mixture will almost certainly be nonhomogenous spatially. That is, with injection, one will most likely find that the water to hydrogen ratio will vary widely in both space and time, even during steady state operation. Thus, with this type of flow regime, one would expect that the distribution of water within the anode compartment to be very uneven, leading to waterlogging of some portions the electrocatalyst sites and starvation of others.

In contrast to injection, an anode gas stream consisting of fine, suspended particles of water would be a more ideal delivery method because the water and hydrogen could be distributed evenly, and the likelihood of uneven water distribution would be much lower. One reason suspended water would be distributed more evenly is because the coalescence rate of a fine water suspension is slow enough to prevent it from "dropping out" en masse before moving through most of the fuel cell. Also, with a fine water suspension, it is possible for the water droplets to move through the gas diffusion layer without impeding the flow of hydrogen gas, as the fine droplets can pass through the Gas Diffusion Layer (GDL) pores without clogging them.

The question thus becomes how one produces this fine suspension of water particles in the anode feed gas, that is, atomize the water. Atomization can be accomplished with several different processes driven by liquid energy (spraying), gas energy (pneumatically), mechanical energy (rotary atomizers), mechanical vibration energy (acoustic or ultrasonic), or electrical energy (electrostatic atomizer) [10]. Each method is characterized also by the distribution of particle sizes produced, mass flow

rates of liquid and gas, and power consumption. On the basis of gross power consumption, only spraying and mechanical vibration are suited for use with a small fuel cell system, as the other methods require at minimum hundreds of watts to operate [10]. Unfortunately, all atomization processes are energy intensive in that the ratio of necessary work input to that required to perform the necessary work (against surface tension) is rather high. In other words, the mechanical efficiency of all forms of atomization is very low, being less than 0.1% [10]!

Thus, the choice is whether to use spraying or mechanical vibration to atomize the water. For relatively low flow rates of gas and water, a form of mechanical vibration atomization, ultrasonic fountain nebulization, has several advantages over using spray atomization. Nebulization is the term used to describe any atomization process that uses acoustic or ultrasonic energy to perform the atomization. The principal advantage of ultrasonic fountain nebulization is that the particle size distribution is extremely fine (1-5 um) [10], and ***independent of water or gas mass flow rate*** [11]. With spraying, the droplet size distribution is directly dependent on the water mass flow, as this influences the characteristics of the disintegration of the jet into particles. Therefore, the best choice of nebulizer for the low flow rates used in a single 50 cm^2 cell (~0.3-0.4 standard liters per minute, slm) is the ultrasonic fountain nebulizer.

Whether one elects to use injection or nebulization to deliver the water to the anode compartment, it is important that the flowfield and bipolar plate be designed to distribute both the gas and the water as evenly as possible, and to allow the excess water at the cathode to evaporate or advect away quickly and with minimal backpressure.

3.3 The ultrasonic nebulizer

In section 3.2.2 it was established that the preferred method of delivering finely suspended water particles to the anode gas stream was through the use of an ultrasonic nebulizer. To follow is a discussion of how ultrasonic nebulizers work, and how the nebulizer was used in this investigation.

An ultrasonic fountain nebulizer consists of a piezoelectric transducer with a narrow (highly directional) acoustic radiation pattern placed face up at the bottom of a shallow (1”-2” depth) pool of water. The ultrasonic beam is focused at the surface of the water, and because of the tight radiation pattern and relatively high transducer power, acoustic streaming results, forming a fountain with an inverted paraboloid shape. Near the top of the surface of the fountain, a dense fog of very fine water droplets in formed. The exact mechanism of droplet formation is the focus of an unresolved controversy. One school of thought is that the droplets are formed by a cavitation driven process, where the intense jets formed by the collapse of the cavitation bubbles literally blast the water into droplets. The other school of thought is that the droplets are formed by the breakdown of surface capillary waves [12, 13].

The frequency of oscillation of most ultrasonic fountain nebulizers is in the range of 700 kHz to 6 MHz. An empirical relation has been developed to predict the mean size of the particles produced by ultrasonic nebulization [12]:

$$D_{mean} = \left(\frac{\sigma}{\rho \omega^2} \right)^{1/3} \tag{28}$$

where σ is the surface tension, ρ the liquid density, and ω the frequency of transducer oscillation. From this equation, the mean particle size produced by the nebulizer used in this investigation (1.7 MHz) at 70 °C is 2.8 μm.

Ultrasonic fountain nebulizers are in widespread commercial, medical and consumer appliance use for humidification and respiratory therapy. Because of the low cost and availability of these nebulizer units, the use of ultrasonic fountain nebulization as a thermal and water management technique could be readily accomplished. In fact, the transducer and oscillator unit used for this investigation was purchased for ~30 dollars at a local retail store.

4. EXPERIMENTAL SETUP AND PROCEDURES

The objective of this investigation was to evaluate the feasibility of using anode gas stream ultrahumidification via ultrasonic nebulization as a water and thermal management technique for PEM fuel cells. In order to accomplish this evaluation, one first has to determine what the metrics of performance will be, and then design the experiments in a way that will give a definitive answer based on these metrics of performance.

Therefore, the first step in performing this investigation was to determine the metrics of performance to be used. There are of course dozens of possible choices for performance metrics, but the information most important from a design perspective is the maximum amount of heat that can be removed with this method, the electrical performance/conversion efficiency encountered, and the response time of the proposed method.

To obtain this performance information, it was necessary to operate a thermally well-insulated PEM fuel cell with the proposed method of water management, and with the conventional method of water management. The fuel cell current and temperature would be recorded chronologically, so as to investigate both stability of the system, as well as to determine transient behavior. Both methods of water/thermal management would be operated under various scenarios in order to explore the performance and robustness of both methods. Once this data was collected, an objective comparison of the electrical and thermal performance of both methods of water management was possible.

Although the primary experimental work in this investigation focuses on determining the performance effects of the proposed method of water/thermal management on PEM fuel cell operation, there were two other considerations which had to be addressed in order to adequately address the question of feasibility. The first consideration was that the maximum rate of evaporative cooling would be limited by the input mass flow rate of liquid water on the anode side of the fuel cell. The second consideration was that it was impossible to directly measure the rate of evaporative cooling as other heat transfer

mechanisms were simultaneously present within the fuel cell. These two considerations required additional experimentation to be performed.

Because the maximum rate of evaporative cooling would be limited by the input mass flow rate of liquid water on the anode side of the fuel cell, it was necessary to measure the liquid water output mass flow rate of the nebulizer as a function of both the water bath temperature and the hydrogen mass flow rate. With this information, it was possible to quantify the maximum expected evaporative cooling available for a given humidification scenario, as well as understand the limitations of the nebulizer itself. The methods used to determine the liquid water mass flow rate are discussed in section 4.2.2.

As was mentioned previously it was not possible to directly measure the rate of evaporative cooling in the PEM fuel cell as other heat transfer mechanisms were simultaneously present within the fuel cell. These other internal heat transfer mechanisms are conduction (through the insulation to the environment) and internal advection (to excess reactant gases). Thus, the author first had to experimentally determine the magnitude of these heat transfer mechanisms. The methods used to determine the heat transfer rate due to conduction and advection are discussed in section 4.2.3. Once an accounting of the conduction and advection heat transfer rates was found, their contribution to the total amount of cooling could be subtracted to give the contribution by evaporative cooling as follows:

$$\dot{q}_{evaporation} = \dot{q}_{total} - \dot{q}_{internal\ advection} - \dot{q}_{conduction} \tag{29}$$

This remainder of this section is divided into 2 main subsections, Experimental Setup and Experimental Procedure. The experimental setup subsection gives a general description of the experimental set up used in the 3 sets of experiments including a listing of the apparatus used in each of the experiments, as well as detailed information on the PEM fuel cell, anode gas humidification chamber/nebulizer, and computer based data acquisition system used in this investigation. Detailed information on the other apparatus used in this investigation is included in Appendix B. The experimental

procedure subsection discusses the procedures used to acquire the data for the 3 sets of experiments performed for this investigation.

4.1 Experimental setup

To follow are general descriptions of the experimental setup of the experiments conducted in this investigation, including a listing of the apparatus used in each experiment set.

4.1.1 General description of the experimental setup to determine performance of PEM fuel cell operating with and without nebulized water in the anode gas stream

Figure 12 is a schematic of the general experimental set up used to determine the performance of the PEM fuel cell using both conventional water management and ultrasonic nebulization water/thermal management. The set up is comprised of the following apparatus:

PEM fuel cell, housing, and insulation

Cathode gas humidification bottle

Anode gas nebulizer/humidification chamber

Lambda 5Volt/100 Amp (max) Switching Power Supply

Omega CN9000A Temperature Controllers

MKS 1159b reactant gas mass flow controllers

Type T Thermocouple

HP 6050A Load Controller

Backbias watchdog contactor

MCS 32 channel 12 bit Analog to Digital data acquisition system

Polyethylene Tubing (for gas delivery)

As one can see from the experiment schematic (Figure 12), the fuel cell was connected in series with the watchdog, 5V switching power supply, and the HP 6050A load controller. During each of the trials, the HP (now Agilent Corp. Palo Alto, CA) load controller was used to operate the fuel cell at a constant current (40 amps during the data collection period). A current measuring shunt was used to verify the calibration of the load controller before the trails were conducted. A voltmeter was used to monitor the fuel cell voltage independently of the data acquisition system, so as to corroborate readings with said system and to enable the author to monitor the fuel cell behavior when not in close proximity to the computer monitor. The fuel cell temperature was measured by use of the Type T thermocouple, and was monitored by the data acquisition system. The uncertainty of temperature measurement was +/- 1 °C.

The mass flow rate of the hydrogen gas and air was controlled by use of MKS (MKS, Inc.Wilmington, MA) mass flow controllers. The actual mass flow set points used in the investigation were 0.86 standard liters per minute (slm) for the hydrogen and 1.63 slm for the air.

The fuel cell was operated under various humidification conditions, and this was accomplished by manipulation of the temperature set points of the anode and cathode humidification chambers for a given experiment. The uncertainty of both the anode and cathode humidification temperature was +/- 2 °C.

The temperature in the water bath was held constant during the trials by use of the Omega Temperature Controller. A Type J thermocouple and three electric heaters were built into the nebulizer/humidifier unit for use with this closed-loop temperature (heater) controller.

4.1.2 General description of experimental setup to determine average water mass flow output from anode gas nebulizer/humidifier

For experiments to determine the water mass flow rate output from the nebulizer/humidification chamber, the following equipment was used:

Nebulizer/humidification chamber

Omega Temperature Controller

Type J Thermocouple

Desiccator Water collector

Fisher Electronic Analytical Balance

Polyethylene Tubing (for gas delivery)

To measure the average water mass flow rate, the desiccator collector was employed to trap both the water vapor and droplets present in the exiting hydrogen gas. The desiccator collector was connected to the nebulizer/humidifier by the same tubing that was used to connect to the fuel cell. The mass of the water thus collected was determined by measuring the final mass of the collector and subtracting the dry weight. The mass of the collector was determined (and rounded to 4 significant figures) by use of the Fisher Electronic Analytical Balance.

As was discussed in section 3.1.1, the temperature in the water bath was held constant during the trials by use of the Omega Temperature Controller. A Type J thermocouple and three electric heaters are built into the nebulizer/humidifier unit to be used with this closed-loop temperature (heater) controller.

Experiments were conducted with and without the nebulizer energized, in order to determine the amount of additional water added by the nebulizer to the gas stream, and to ascertain the average relative humidity of the non-nebulized gas stream.

4.1.3 General description of experimental setup to determine insulation heat loss rate and internal convection heat transfer rate

For experiments to determine the rate of heat loss due to external conduction/convection/radiation and internal convection, the following equipment was used:

Type – T thermocouples

Fuel cell, housing, and insulation

Data acquisition system

GW Digital Multimeter

Electrical cables

Omega SRFG 203 Silicone rubber, metal foil element sheet heater

0-120 volt, 1500 watt variac (autotransformer)

These experiments were very simple in nature, and were performed to determine the amount of heat loss (cooling) that the fuel cell experienced due to heat loss through the insulation, and heat loss due to internal convection of the excess reactant gases. In order to do so, varying amounts electrical power was applied to the heater, and the steady state temperature of the fuel cell was measured. The fuel cell itself was not operated; that is, no electric current passed through it during these experiments.

A general schematic of the experimental setup is given in Figure 13. The Omega SRFG 302 silicone rubberized heater was used to generate the heat at the fuel cell. The temperature of the fuel cell was measured with the 30 gauge type-T thermocouple which was epoxied to the top of the anode bipolar plate. The electric power applied to the heater was determined by measuring the voltage and current applied to the heater. The variac was used in order to make it easy to vary the heater power, although the logarithmic nature of the control made fine-tuning difficult at the higher power levels.

It is important to note that the fuel cell was never removed from the insulated box prior to or during these experiments. The fuel cell was not removed from this insulated

cradle so that the heat losses through the insulation present during the primary experiments could be determined with some level of confidence. Had the fuel cell been removed from the cradle, the subsequent experiments would have at best yielded results which were only representative (order of magnitude correct) of the heat losses occurring through the insulation.

4.1.4 Apparatus

The remainder of this section contains in-depth description of the components/apparatus used in the three sets of experiments.

4.1.4.1 Fuel cell

The single cell fuel cell used in this investigation was comprised of a Membrane Electrode Assembly (MEA) manufactured by 3-M, Centerpoint Energy (formerly Reliant Energy) Fuel Cell Housing and Bipolar plates, ERG Aerospace Nickel foam flowfields, and silicone rubber closed cell foam gaskets. The Centerpoint Energy Fuel Cell housing and bipolar plates were designed and manufactured by Stren Mechatronics of Houston, Texas.

The Membrane Electrode Assembly (MEA) used in this investigation is a proprietary design of 3-M Corporation (St. Paul, MN), and so exact specifications are not known. However, a general description of its construction is possible. The MEA is a 50 cm^2 five layer design- that is, it is composed of a Nafion 115 membrane, a Pt/C cathode catalyst layer, a Pt/C anode catalyst layer, and the two hydrophobic carbon cloth gas diffusion layers. See Figure 5 for a photograph of the MEA. As one can see, the gas diffusion layer is bonded not only on its face, but also around the edges by a cast Nafion "picture frame", greatly improving its durability. The 3-m MEA offers exceptional performance – it has routinely given >0.5 volts at 1 A/cm^2 and 0.3 volts at 1.4 A/cm^2; by

comparison, most PEM fuel cells are not capable of producing any net voltage at 1.4 A/cm^2!

The bipolar plates are shown in Figure 14 and are composed of high conductivity pyrolytic graphite. From Figure 14 one can see the gas ports and the recess for the metal foam flow field. One can see that the gas enters through a port on the upper left corner, moves through the flow field, and then exits through the low right corner. The ports were enlarged to 0.128" diameter (from 0.020") in order to decrease pressure drop at high flow rates, and to allow water to flow out of the bipolar plate without puddling along the header. Thin wall Teflon tubing is inserted into the ports on the side facing the end plates for location purposes. The end plates were machined from aluminum alloy and hard anodized, and have two passages drilled for reactant gases, one passage drilled for a thermocouple well, and one passage drilled for a cartridge heater. A cartridge heater was not used in this investigation because previous experience has shown that cartridge heaters often develop shorts from the heater winding to the case, resulting in a dangerous and destructive situation where the end plate becomes energized with approximately 120 volts a.c. Instead of a cartridge heater, a silicon rubber pad heater was glued onto the exterior of both end plates.

The flowfield used was uncoated nickel foam made by ERG Aerospace. The Nickel foam had a porosity of approximately 95%, and a pore density of 100 pores per lineal inch. Hard gold plated nickel foam was tried at the beginning of the investigation, but it was found that the plating was quickly destroyed on the anode by galvanic corrosion, resulting in membrane failure.

A 30-gauge type-T (Copper/Constantan) thermocouple was epoxy bonded to the top of the anode bipolar plate in order to measure the "cell" temperature. Because of conduction losses, the temperature of the actual membrane was somewhat higher (on the order of perhaps 5 °C). Although this situation was not ideal, it was not feasible to install the thermocouple closer to the actual membrane because it would have involved accurately drilling a small diameter hole in the brittle graphite bipolar plate – a job better suited to an electric discharge machining center (edm) machine. Because an edm

machine was not readily available, and because of the long wait and great expense of having such work performed by a job shop, it was decided to forego this procedure.

The fuel cell was wrapped in two directions with expanded polyethylene foam insulation, and placed in a cardboard box –see Figure 17. A strip of the expanded foam insulation was also placed in the gap between the current collector plates immediately above the bonded thermocouple. The unoccupied space within the cardboard box was stuffed with additional insulation. It was believed that such an arrangement would provide very effective insulation. However, it was later discovered that the cell was not as thermally insulated as initially believed – at 70 °C, the cell loses 27 watts to the environment through the insulation.

4.1.4.2 The anode gas humidification unit – ultrasonic nebulizer/humidification bath

The anode gas humidification unit was designed to allow the hydrogen to be humidified via bubbling through the temperature-controlled bath, while simultaneously allowing additional humidification by ultrasonic fountain nebulization. The unit can be seen in Figures 18 and 19. The gas bubbles up from behind the three heater tubes, which has the benefit of improving heat transfer from the heaters to the water (due to the rather turbulent forced convection induced). The gas then passes through the humidification chamber out through the outlet at the side of the cylindrical body, which is located approximately ¾" above the water level. The top plate has port which acts as a feedthrough for the type-J bath thermocouple, a refill port for bath make-up water, and a chamber pressure test port (which was used to measure backpressure at the fuel cell anode inlet). The make-up water was admitted from a gravity-pressurized reservoir via a small needle valve in-line with the make-up water tube. The nebulizer was activated by simply plugging into the 120 v a.c. receptacle.

The nebulizer transducer and electronics package is a "clone" of the TDK NB-59S. This transducer operates at approximately 1.7 MHz and has a maximum transducer

power of 40 watts. The transducer itself is a metallized disc, and is believed to be composed of barium titanate.

The nebulizer/humidifier housing was machined entirely from Plexiglas (polymethylmethacrylate) 1" plate and ¼" wall tube. The three 20 watt Omega CSS 10120 electric cartridge heaters were housed in three 304 stainless steel sheaths (one per sheath), with the sheaths making an interference fit (~.002" over) with the Plexiglas bottom and top plates. The nebulizer transducer came stock with an aluminum housing which was bolted to the underside of the bottom plate with four stainless 8-32 Allen head capscrews. Silicone rubber face gaskets were hand cut from the same gasket stock used in the fuel cell (0.032" medium durometer) to seal the bottom and top of the body tube. Four ¼" –20 all thread tie rods were used to compress the housing to provide a gas-tight seal and were torqued to 20 inch-pounds. All Plexiglas parts were heated overnight in an oven at ~80 °C prior to machining to avoid shrinkage and subsequent misalignment during use (Plexiglas shrinks ~4 % upon heating above 70 °C for the first time).

The electronics and transducer for the nebulizer were salvaged from a consumer ultrasonic humidifier (ReliOn H-0565-0). The electronics were encapsulated in polyethylene (hot glue) and then housed in an open top aluminum electronics box. The common collector bipolar power output transistor was mounted on an aluminum spacer and then bolted to the aluminum box so as to serve as both a heat sink and groundplane for the ultrasonic oscillator/amplifier. The transmission line between the transducer and amplifier was lengthened by the addition of approximately 10 inches of 53-ohm thin gauge coaxial cable.

When the nebulizer transducer is energized, a dense cloud of water is formed throughout the entire humidification chamber, and the nebulized water is advected out with the hydrogen gas. The nebulized water cloud formed is so dense as to render the normally transparent humidification chamber totally opaque (due to Mie scattering in the mist).

All components of the nebulizer/humidifier in contact with water were made from either Plexiglas or stainless steel because of corrosion issues experienced with

other materials. The nebulizer/humidification unit base was originally machined from aluminum, but the galvanic action of dissimilar metals and the unusually low pH of the water supply conspired to cause many difficulties with corrosion. Because the fuel cell membrane is exceptionally sensitive to contamination of the coolant water with metallic ions, it was decided to pursue a design which eliminated the possibility of corrosion.

4.1.4.3 P.C. based data acquisition system

Early in this investigation, it was decided that the best method to obtain data for the experiments involving the operation of the PEM fuel cell was to use a p.c. based data acquisition system, as this would allow the collection of a vast quantity of data, without requiring much operator intervention. In doing so, transient effects could be observed, as well as making the performance of the experiment easier and more repeatable. This decision to utilize a computer based data acquisition system was later found to be very fortuitous, as unexpected phenomena was observed and recorded with the system, allowing for additional findings unrelated to the objective of the investigation.

The method used to collect the lion's share of the data collected in this investigation was done with a modern, p.c.-based digital to analog data acquisition system. The use of such a data acquisition system ensured that the data would be recorded at regular intervals, and also made it possible to conduct the investigation with minimal intervention by the investigator. To follow is a description of the hardware and software used, and the implications that the use of such hardware had on the experimental uncertainty.

4.14.3.1 Data acquisition system - hardware

The data acquisition hardware consisted of a 32 channel multiplexer and an 8 channel, 12 bit analog-to-digital converter, both manufactured by Measurement Computing Systems, Inc. (Middleboro, Massachusetts). The multiplexer expansion board (EXP-32) was fully differential, with DIP-switch selectable preamplifier gain and a semiconductor cold-junction reference (for use with thermocouples). The analog-to-digital converter (PCI DAS08) was a pci bus based expansion card inserted into the backplane of the host computer. The analog-to-digital converter (A/D) had a maximum sample rate of 100 ksamples/sec; however, when used with the multiplexer expansion board, the maximum sample rate is much slower (perhaps 1 ksamples/sec). For this investigation, a fast sampling speed was not necessary, and so this was not an issue.

The multiplexer and A/D were calibrated by using the interactive Instacal software. Calibration of the expansion multiplexer consisted of shunt-jumpering the high low, and ground inputs together on junctions 0 and 16 and then adjusting the appropriate 10-turn potentiometers located on the expansion board until the software indicated that a zero-volt condition was met.

The 12 bit analog-to-digital converter has a bias limit of +/- ½ of the least significant bit. One bit is used to specify polarity (sign), and with the range being –5 to 5 volts, this gives a bias limit of:

$$\frac{5}{2^{12}} = .00122\,volts \tag{30}$$

The random noise present due to EMI, Johnson noise, etc. was found empirically by running the data acquisition system with the thermocouple(s) at a known temperature or with the differential voltage input shorted (0 d.c. volts).

4.1.4.3.2 Data acquisition system – Labview 6.1 ,Universal Library, and Instacal software

The software used for this investigation allowed the author to acquire large quantities (15,000 data points typical) of floating point data acquired over a period of hours to be stored as ASCII text files on the local hard disk drive. The software used in this investigation was Instacal, Universal Library, and Labview 6.1. The Instacal software (produced by Measurement Computing Systems, Inc.) was used to install and manually calibrate both the A/D converter and the expansion board multiplexer. Labview 6.1, produced by National Instruments Inc. (Austin, TX), was used as the graphical programming interface with the data acquisition equipment. Universal library provided a library of "virtual instrument" driver files for use with Labview.

Labview was chosen for the programming interface because of its ease of use (for both the end-user and program developer), low-cost, and most importantly, because it minimized the development time for the data acquisition programming. Although the data acquisition program could have been made far smaller in size, and made to execute much more rapidly if programmed in C or C++, the extra development time and lack of debugging support makes such an option very unattractive. The additional benefit of Labview is that, because it is such a user-friendly, portable and simple interface, the programs are useful to future users, who can upgrade/modify them as needed, even with newer versions of Labview (it is mostly reverse compatible).

The Labview program used for this investigation cycles through 6 different voltage and 6 different temperature channels per acquisition cycle. The user specifies the number of total acquisition cycles desired prior to the start of the program. At run time, two arrays are allocated in memory to hold the data, one for voltage values and one for temperature values (both are arrays of single-precision/16 bit floats). A for-loop is used to index through the arrays as they are loaded with data. Channel numbers are "managed" by the use of shift registers. Acquisition occurs through the use of the Universal Library "virtual instrument" driver files. Once the arrays are filled at the end

of an acquisition run, the two arrays are concatenated, and stored in an ASCII text file with a file handle specified by the user.

4.2 Experimental procedure

In this subsection, the author will discuss how the experiments were organized and conducted. The first subsection of experimental procedure will discuss the experiments conducted to determine the performance of the PEM fuel cell operated with conventional water management and with the method of nebulization. The second subsection of experimental procedure will discuss the experiments performed to determine the output water mass flow rate from the anode nebulizer/humidification chamber. The third subsection of experimental procedure will discuss the experiments performed to determine the external heat losses and internal heat transfer rates.

4.2.1 Study of PEM fuel cell performance with conventional and proposed water management techniques

The objective of this investigation was to determine the feasibility of using ultrasonic nebulization as a water and thermal management technique for PEM fuel cells. To make this determination, it was necessary first to decide what criteria or performance variables would be used to judge the performance of the technique. It was decided that these performance variables were fuel cell output voltage, maximum heat transfer rate, sensitivity to perturbation, and response time.

4.2.1.1 Motivation for parametric study

In order for any water and thermal management technique to prove useful for use with a PEM fuel cell, it must be able to perform well under a wide range of fuel cell electrical current densities and reactant gas flow rates, while maintaining the cell temperature between 40 °C to 70 °C. In addition, the technique must be able to maintain the hydration of the ionomer membrane without waterlogging the active sites of the electrocatalyst. The technique must also be able to operate properly within a wide range of coolant water temperatures. Therefore, it was necessary to test the performance of the technique under a variety of conditions to determine its robustness. However, as desirable as it would be to test the proposed technique through the full range of current densities, gas flow rates, coolant water temperatures, and fuel cell temperatures, this task is far too time prohibitive to realistically perform. Therefore, it was decided to operate the PEM fuel cell at one current density (0.8 A/cm^2), one set of reactant gas flow rates, and perform a parametric study in which the water temperature was the independent variable.

4.2.1.2 Selection of parameter ranges

The current density selected to use in this investigation corresponds to that typically experienced at, or very close to, the maximum electrical power density for a PEM fuel cell. The practical importance of operating a PEM fuel cell at maximum power density is somewhat obvious: operating a PEM fuel cell at maximum power density allows one to minimize the size, weight, and cost of a PEM fuel cell sized for a given electrical load. Therefore, the justification for selecting this current density is that it corresponds to the electrical loading that is of particular interest to the design of a PEM fuel cell system for automotive, aerospace, or distributed generation applications. Thus,

in order for this water/thermal management technique to be successful, it most certainly must perform well at this current density.

The maximum fuel cell temperature to be used in this investigation was selected to be 70 °C, in order to ensure the longevity of the rather expensive (and difficult to replace) MEA. Although it is possible to operate the PEM fuel cell at temperatures up to 140 °C, doing so dramatically reduces the operating lifetime of the membrane. The customary upper limit of operation found in literature is approximately 80 °C because of the difficulty of ensuring adequate humidification above this temperature, and because the concerns of reducing the mechanical fatigue lifetime of the membrane.

The range for the temperature of the anode and cathode humidification water was selected to be 50 °C to 65 °C. This temperature range was selected on the basis of the author's experience. The minimum bound was selected to be 50 °C because prior experimentation had shown that below this temperature, the membrane dried out and the cell voltage decreased dramatically as a result. The upper bound was selected to be 65 °C because it was desired to use a coolant water/gas temperature that provided some added margin of safety in terms of cooling via sensible ($c_p\Delta T$) heat transfer while the fuel cell was at the maximum operating temperature.

The gas flow rate used for this study was selected as a compromise between using a high reactant gas flow rate to ensure very high water delivery rate (anode) and evaporation rate (cathode), and the need to minimize compressor power consumption in a realistic system. In other words, using a high hydrogen gas flow rate ensures sufficient water delivery, and using a high cathode gas (air) flow rate ensures efficient evaporation/water advection, but the use of such high flow rates would increase parasitic power losses in a real system, in addition to requiring a larger compressor. The stoichiometric flow rates selected were 3.0 for hydrogen, and 2.5 for air. The actual flow rates were 0.857 and 1.63 standard liters per minute for hydrogen and air, respectively These actual flow rates corresponded to stoichiometric gas flow rates of 3.08 and 2.46 for hydrogen and air, respectively.

A listing of the values of the experimental parameters used in the investigation is presented in table 1 (in Appendix A).

4.2.1.3 How the parametric study was conducted

The parametric study was used to affect an understanding of both the performance of the ultrasonic nebulizer water/thermal management system, as well as the sensitivity of such a system to perturbation. Prior experience had given the author knowledge of the parameter ranges useful for this investigation as well as an intuition for whether a system was malfunctioning due to problems unrelated to the water management system. Because the PEM fuel cell is extremely sensitive to so many different parameters, it requires a fair amount of hands-on experience with the assembly and operation of PEM fuel cells to be able to conduct meaningful experiments.

To follow is a general description of the procedures used in this investigation to operate the nebulizer water/thermal management system, and PEM fuel cell.

4.2.1.3.1 Start up/warm up of fuel cell system

The fuel cell and instrumentation start up consisted of first turning on the electrical power to all of the instrumentation. The temperature set point of the humidification chambers was then set to the appropriate values for the first experiment. Next, the fuel cell anode was purged with nitrogen for 10 minutes to remove any traces of adsorbed oxygen from the anode electrocatalysts. After purging, the anode gas was switched to hydrogen. Once the open-circuit voltage was observed to reach 0.8 volts, the load controller was programmed to give load of 10, then 20, then 40 amps, all the while ensuring that the output voltage never went below 0.2 volts. The anode was humidified by use of the nebulizer throughout the purging and warm-up process. Once the voltage of the fuel cell exceeded 0.52 volts, the fuel cell was deemed ready for experiment. The entire purge/warm up process required approximately 45 minutes to complete.

4.2.1.3.2 Experimental run of fuel cell system

Once the fuel cell was ready for an experimental run, the data acquisition system was programmed to acquire data for the appropriate time-period (approximately 3 hours), and data acquisition commenced. Should the experiment have required that additional data be acquired, the author simply programmed the data acquisition system to run for an additional 30 minutes, and this was repeated as needed. During the experiment, the fuel cell voltage and temperature was monitored. If the temperature went beyond 70 °C or if the voltage dropped below 0.2 volts, the experiment was terminated, and the cell was cooled down/hydrated as needed to prepare it for the next experiment, or the system was shut down as necessary.

4.2.1.3.3 Transition to next experimental run of fuel cell system

After completion of an experiment, the fuel cell was cooled down below 60 °C and simultaneously hydrated as well as possible by operation of the nebulizer (if not already in use). The cell was cooled down by operating at 10 amps (0.2 A/cm^2), until such time that the temperature had dropped below 60 °C. While the cell was cooling, the temperature set-point(s) would be adjusted for the next experiment as needed. Once the cell had cooled down and the appropriate set-point temperatures had been reached, the next experiment would commence.

4.2.1.3.4 Shutdown of fuel cell system

Shut down consisted of a simultaneous anode gas purge, nebulizer humidification, and cell cool-down period. First, the anode gas was switched from hydrogen to nitrogen. Immediately upon switching the anode feed gas, the current was reduced to 20 amps. The author then monitored the cell voltage, and reduced the current

as needed (usually by increments of ½ present value, i.e. the pattern would be 20-10-5-2-1, etc.) to maintain the cell voltage above 0.1 volts until virtually all of the adsorbed hydrogen within the cell had been consumed, at which point the cell current was 0.01 amps. This process of removing the adsorbed hydrogen required approximately 10 minutes to perform. Once the hydrogen had been purged/consumed, the cell was allowed to cool down under nitrogen purge until it reached 50 °C, at which point the gases were switched off, and all instruments turned off.

The hydrogen was purged and or consumed from the anode chamber because it was deemed a prudent practice by the author. If the hydrogen were not purged/consumed, the cell would continue to operate at an extremely low current (the leakage current), and this leakage current would slowly consume the hydrogen present in the anode chamber, and eventually create a partial vacuum. This partial vacuum could cause collapse of the humidification chamber, or at the very least, cause air or water to be drawn into the anode chamber, thereby increasing the risk of damage to the fuel cell. Another risk was that an unattended cell with hydrogen left in it has the potential to be dangerous to those unfamiliar with or unwilling to acknowledge the risks of low impedance electrochemical devices. A “primed” fuel cell, much like a charged capacitor, can store a considerable amount of electrical potential energy that can unleash itself in the form of an accidental arc welding of the stray screwdriver or misplaced wrench.

4.2.2 Nebulizer/humidification chamber output water mass flow rate measurement

In order to understand the performance limitations of the ultrasonic nebulizer humidification system, it was necessary to determine the actual water mass flow rate produced by the nebulizer. By knowing the total water output mass flow rate of the nebulizer and the temperature, one is able to determine the maximum possible cooling available. A question that arises is how one determines the amount of water present in vapor and liquid form; this is easily resolved by considering the fact that the water vapor

will always be fully saturated when the nebulizer is in use – so much water is in fine suspension that extremely rapid saturation is guaranteed. Therefore, if one measures the total water mass flow rate of the nebulizer, one can then subtract the vapor fraction from this to obtain the liquid fraction. The vapor fraction mass flow rate can be predicted by Dalton's Law of additive partial pressures by knowing the total pressure (atmosphere pressure), the hydrogen mass flow rate and the water vapor pressure at the temperature of interest (readily obtained in any steam table found in an undergraduate thermodynamics textbook). This predicted vapor mass flow rate can then be compared against data from experiments conducted with the nebulizer inactive in order to determine whether the gas is truly saturated when the gas is simply bubbled through the water.

To follow is a description of the procedures used to measure the output water mass flow rate of the anode gas nebulizer/humidification chamber.

4.2.2.1 Measurement of nebulizer output water mass flow rate

The measurement of water mass flow rate was relatively simple. A sorption/desiccant collector was connected to the end of the output tube of the anode nebulizer and allowed to collect water during timed collection trials. Each experimental condition (bath temperature and hydrogen mass flow rate) was repeated at least four times in order to provide data that was statistically meaningful. This repetition of each experimental condition proved very important, as random noise was found to be quite significant in all of the trials conducted.

4.2.2.1.1 Start up procedure to measure nebulizer output water mass flow rate

Prior to commencing any measurements, the mass flow controller was allowed to warm up for at least 30 minutes at the desired flow rate while using hydrogen. This was done to ensure stability of the mass flow rate, as the MKS mass flow controllers are known to be inaccurate and somewhat unstable prior to this warm up period. During this same period, the nebulizer was started if needed, and the bath temperature was adjusted as necessary. Once the bath temperature and hydrogen mass flow rates were sufficiently stable, the system was ready for experimentation.

It is important to note that hydrogen was used at all times in these water mass flow experiments. This is because one desires to know the water loading condition of the hydrogen gas stream as it is used in a running fuel cell. Undoubtedly, somewhat different water loading conditions would exist for other gases, but that is of little relevance to this investigation. It was also essential to always use hydrogen because the anode gas mass flow controller was factory calibrated for hydrogen gas – while it is possible to use other gases, the mass flow controller is not as accurate at controlling the mass flow rate other gases.

4.2.2.1.2 Experimental procedure to measure nebulizer output water mass flow rate

Once the nebulizer and gas handling systems were ready, the experimental runs were begun. At the beginning of each trial, the mass of the desiccant collector was measured with the electronic balance and recorded. Thereafter, an electronic countdown timer was programmed for a 15 minute interval. The timer was started, and immediately the collector was connected to the output tube of the nebulizer. The collector was placed at the same elevation as the output connector on the nebulizer, so as to minimize collection errors due to puddling or back-drainage. The collector was also placed as level as possible to minimize experimental variability. Once the trail was over, the collector

was disconnected from the output tube and the mass of the collector was immediately measured with the electronic balance and recorded.

After two trials, both the desiccant and the cotton sorption plug were removed and replaced. The used Drierite™ desiccant was collected in an aluminum pan and regenerated in an electric muffle furnace at 300 °C for six hours once enough of the used desiccant had accumulated to warrant the regeneration procedure. Ample quantities of active desiccant were always available, so that at no time was it necessary to forgo experimentation for lack of desiccant.

The experiments were normally conducted back to back, and in most cases, the water mass flow experiments were done for a long period throughout a day. This was done to minimize any temporal effects, such as changes in room humidity or temperature, as well as any long term drift manifested in the electronic balance.

4.2.3 Measurement of internal and external heat transfer rates for fuel cell assembly

The accurate measurement of both the internal and external heat transfer rates was of critical importance to the investigation as the amount of experimentally determined evaporative cooling would directly depend on these measurements.

Normally, a single PEM fuel cell (as opposed to a stack) is able to remain sufficiently cool during operation without an external cooling system because the conduction heat transfer path from the membrane to the outside surfaces is relatively short and occurs through highly conductive material. The steady state heat transfer due to conduction can be suppressed to a large extent by insulating the outer surfaces of the fuel cell housing, and this was done for this investigation. It was not possible, however, to suppress internal advection heat transfer.

4.2.3.1 Experimental determination of external heat transfer rate for the PEM fuel cell assembly

The experiments to determine external heat transfer rate as a function of temperature were quite simple though extremely time consuming. An electric heater, glued to one side of the fuel cell, was administered electrical power via a variable autotransformer (variac) connected to the 120 volt (a.c. rms voltage) mains line. The voltage and current applied to the heater were monitored by a digital voltmeter and digital ammeter, respectively. The voltage and current was recorded and monitored, as well as the fuel cell temperature, which was provided by the type-T thermocouple that was epoxied to the top of the anode bipolar plate. For any given power level applied, the system was given at least 8 hours to reach thermal equilibrium. The final cell temperature was recorded once the author was satisfied that it did not make a net change in a 30 minute period. A series of these experiments was conducted in order to generate an external heat loss versus cell temperature curve.

4.2.3.2 Experimental determination of internal heat transfer rate to excess reactant gas for the PEM fuel cell

The internal heat transfer rate was not measured directly. Instead, the total heat transfer rate was measured for a given condition of gas mass flow, gas temperature, and heat power. The least-squares curve fit of the external heat transfer rate was used to generate a curve whose value at a given temperature could be subtracted from this total heat transfer rate to give the internal heat transfer rate to the circulating excess reactant gases.

As with the external heat transfer rate measurements, the heater power and cell temperature were monitored and then recorded once both had taken a considerable amount of time to reach pseudo-equilibrium.

The dependent variables for these experiments were heater power, anode gas temperature, and cathode gas temperature. It was later discovered that the total heat transfer rate was virtually unaffected by reactant gas temperature, and so a complete parametric study involving all three of these variables was not attempted.

5. RESULTS

The experiments were organized by investigating different humidification scenarios or cases. This organization was such that the experimental variables (anode and cathode humidification chamber temperature, use of nebulizer) were changed at the beginning of an individual experiment, but were not varied during a given experiment, and each experiment was thus regarded as a case. This allowed observation of a given case while operating over a fairly wide cell temperature range (while it warmed up), and while operating over a relatively long time span (around 4 hours per case for those cases where the nebulizer was in use).

For the sake of brevity, the experiment cases will be referred to by the temperature of the anode and cathode gas humidification chamber temperature respectively. For example, the 65/55 case label would refer to a case wherein the anode gas humidification temperature was 65 °C and a cathode gas humidification temperature was 55 °C. A listing of the values of the parameters used in the investigation of the electrical and thermal performance of the PEM fuel cell system is presented in table 1.

The results section is divided into two subsections. The first section concerns the results of the investigation of thermal management, and the second section concerns the results of the investigation of electrical performance. The first results subsection thus is provided to fulfill the portion of the investigational objective concerned with determining whether the use of ultrasonic nebulization of water is an effective thermal management technique. The second subsection also helps to fulfill the investigational objective, but also includes data which proved totally unexpected. Several phenomena regarding the electrical performance of the fuel cell were discovered that were directly related to the use of the ultrasonic nebulizer, and these data suggest that further investigation is warranted regarding the use of the use of ultrasonic nebulization of water for anode gas humidification.

5.1 Thermal management

The suitability of the technique of using ultrahumidification of anode feed gas via ultrasonic nebulization as an evaporative cooling technique would largely be determined by the maximum rate of cooling possible with this technique. Thus it was important to experimentally determine this maximum rate of evaporative cooling. Recall that:

$$\dot{q}_{\text{evaporation}} = \dot{q}_{\text{total}} - \dot{q}_{\text{internal advection}} - \dot{q}_{\text{conduction}} \tag{31}$$

It is important to note that the heat transfer rate of both conduction and internal advection are strongly dependent on the fuel cell temperature and the temperature of the surroundings. For internal advection, the heat transfer rate is also strongly dependent on the temperature of the reactant gases. Expressed mathematically this is:

$$\dot{q}_{\text{conduction}} = f(T_{\text{cell}}, T_{\text{surroundings}}) \tag{32}$$

$$\dot{q}_{\text{internal advection}} = f(T_{\text{cell}}, T_{\text{surroundings}}, T_{\text{air}}, T_{\text{hydrogen}}) \tag{33}$$

The surroundings (room) temperature remained constant throughout this investigation at 24 °C with an uncertainty of +/- 2 °C. Therefore, it was reasonable to determine conduction heat transfer solely as a function of the cell temperature, and to determine advection heat transfer as a function of the cell temperature and the two reactant gas temperatures. Therefore, for this investigation:

$$\dot{q}_{\text{conduction}} = f(T_{\text{cell}}) \tag{34}$$

$$\dot{q}_{\text{internal advection}} = f(T_{\text{cell}}, T_{\text{air}}, T_{\text{hydrogen}}) \tag{35}$$

Figure 19 illustrates the functional relationship between conduction heat transfer rate, and advection plus conduction heat transfer rate (for reactant gas temperatures of 65/65) with cell temperature. That is, the set of curves to the left in Figure 19 shows the steady state cell temperature as a function of heater power when no gases flowed through it, and the rightmost set of curves shows the cell temperature as a function of heater power when reactant gases (air and hydrogen) at 65 °C were passed through it. As one can see,

the cell temperature increases with increasing heat dissipation rate for both sets of curves. It appears that the two sets of curves run more or less parallel until just above the last grouping of experimental data points, whereupon it appears that the two sets of curves would eventually intersect at higher heat dissipation rates. However, this is an artifact of the choice of curves fitted to the limited experimental data, as there is no physical reason that the internal advection heat transfer rate would decrease with increasing cell temperature. The difference between the two curves would give the advection contribution, which is approximately 20% of the total.

For the cases where the fuel cell was operated without the nebulizer, no average evaporative cooling rate could be calculated because there was no steady state cell temperature below the maximum safe operating temperature of 70 °C. That is, for those cases where the nebulizer was not used, the fuel cell temperature steadily increased, never reaching a plateau before exceeding the maximum safe operating temperature of 70 °C (see Figure 20 for an example). These cases were therefore assumed to have an average evaporative cooling rate of zero.

The amount of total heat transfer for the cases where the fuel cell was operated with the nebulizer is compared graphically in Figures 21 through 23. Figure 21 compares the cases of 65/65 and 65/60 nebulizer cases against the total heat transfer curve fit set for 65/65. Figure 22 compares the nebulizer cases of 60/60, 65/55, and 60/65 against the total heat transfer curve fit set for 60/60 reactant gas inlet temperatures. Figure 23 compares the nebulizer cases of 55/55 and 50/65 against the total heat transfer curve fit set for 55/55 inlet temperature. A tabulation of the determined evaporative cooling rate for all of the cases can be found in Table 2. The average temperature of the fuel cell operating under the various cases of anode and cathode humidification chamber temperature was determined by taking the arithmetic mean of the cell temperature over 1000 seconds of operation after the fuel cell had reached equilibrium. This average temperature has an uncertainty of +/- 1 °C. The heat dissipation rate was calculated from the cell voltage and current (40 amps) and had an uncertainty of +/-.23 watts.

The calculated evaporative cooling rate for the cases of 65/65 and 65/60 (hydrogen/air temperature) were found to be effectively zero. In fact, as one can see from Figure 21, the cell temperature was *higher* than that for a cell cooled solely by conduction and internal advection. It is believed that this anomalous result is due to the fact that the experiments conducted to determine advection heat transfer used an air mass flow rate that was about 10% too high. However, because of the relatively small magnitude of the error, this anomaly does not detract from the conclusion that little or no evaporative cooling occurred for these cases. The case of 50/65 was also found to be effectively zero because, while the fuel cell did run slightly cooler than predicted, this difference was less than the uncertainty associated with the temperature measurement. For the case of 60/65, the fuel cell was found to run at a temperature within the uncertainty bounds for the curve fit data, thus giving a determined evaporative cooling rate of zero.

The evaporative cooling rate for the remaining cases were found to be nonzero, but were very small in relation to the overall heat transfer rate. For the case with the largest amount of evaporative cooling (55/55), this represented only about 7% of the total amount of heat transfer occurring. **Therefore, no significant evaporative cooling occurred with the use of the ultrasonic nebulizer used in this investigation.**

The conclusion that no significant evaporative cooling of the PEM fuel cell occurred is further borne out by the results from another set of experiments conducted to measure the output water mass flow rate of the ultrasonic nebulizer anode gas humidification unit. Figure 24 graphically illustrates the calculated liquid output water mass flow rate of the anode gas humidification unit while using the ultrasonic nebulizer as a function of bath temperature. As one can see, the liquid water mass flow rate is *not* strongly a function of temperature in this range of temperatures. While the liquid water flow rate from the nebulizer is impressive given the rather small hydraulic diameter of the tubing used for gas delivery (~0.10” i.d.), it is still insufficient to meet the required minimum to deliver sufficient cooling. **If one assumes an evaporation temperature of 70 °C, and a cooling load of 30 watts, this would require a *minimum* liquid water**

delivery rate of 0.013 g/s, which is approximately *7 times* the rate of delivery provided by the anode gas nebulizer operating under the most favorable conditions.

Another set of experiments were performed to determine whether the mass flow of liquid water from the nebulizer was a function of gas mass flow rate. Figure 25 demonstrates that this is indeed the case. In Figure 26, the ratio of liquid water mass flow between the high anode gas mass flow rate case(0.86 slm) and the low anode gas mass flow rate case (0.43 slm) is plotted as a function of temperature. As one can see, the temperature has little effect on this ratio, and that this ratio is very close to 2.0. This ratio of water mass flow rates corresponds directly to the ratio of the hydrogen gas mass flow rates between the high and low gas flow rate cases, which is also 2.0. **From this, we can reasonably conclude that the liquid water mass flow rate is directly proportional to the anode gas mass flow rate, and furthermore that the density of the water particles delivered to the fuel cell remained constant. This indicates that the limiting factor in liquid water delivery from the nebulizer is the water particle density**. This limitation in particle density may very well be a constraint imposed by the tubing and fittings used for the anode gas delivery system, and it may very well be the case that the nebulizer is capable of delivering sufficient water to the fuel cell with a gas handling system specifically designed to distribute hydrogen with a high density of fine suspended water particles. Therefore, a question that needs to be addressed is whether or not the water particle density can be increased within the hydrogen gas stream, and whether it is the nebulizer that is the limiting factor, or if it is the gas delivery system. It is the author's speculation that the main limitation of using ultrasonic nebulization lies in the gas delivery system, and that it may prove very difficult or impossible to design a system that will work well for a large stack.

Another consideration in the use of ultrasonic nebulization as an ultrahumidification technique is the very large expenditure of energy to atomize the water, owing to the extremely poor mechanical efficiency of the atomization process. The input electrical power to the nebulizer was measured to be 19.3 Watts; for an average flow rate of $1.8 * 10^{-3}$ grams per second of liquid water, this corresponds to an

energy expenditure of 10.7 kJ/g! By contrast, given a surface tension of $6.62*10^{-2}$ N/m (at 60 °C) and a particle size of 2.8 um, the minimum energy expenditure is only 0.142 J/g, giving a mechanical efficiency of only 0.0013% [14]. However, the nebulizer used in this investigation could be used to supply more than one fuel cell at a time. According to the specifications of a major manufacturer (TDK Inc.), a consumer appliance ultrasonic nebulizer is capable of delivering 575 ml/hour of water with an input electrical power of 30 watts [15]. According to these specifications, the energy expenditure per unit mass to nebulize the water is 188 J/g, which corresponds to an efficiency of 0.075%. Using the manufacturer's data, and the fact that the amount of cooling available from the nebulized liquid water is 2.3 kJ/g, this would correspond to a coefficient of performance (defined as the ratio of cooling power to the work input rate to the cooling system) for this cooling system of 12.8. Thus, for a 1kW PEM fuel cell stack operating at 60% conversion efficiency, a hypothetical nebulizer ultrahumidification system would require 52 watts to operate, representing a 5.5% parasitic loss, and giving a net power of 948 watts. By comparison, the 2kW air-cooled PEM fuel cell system discussed in section 3.1.2 had a cooling system parasitic loss of 70 W, which is only 3.5 % of net power. **Therefore, unless significant energy conversion efficiency gains can be realized, an ultrasonic nebulizer ultrahumidification system would not be particularly attractive to use as part of an evaporative cooling scheme for a PEM fuel cell system.**

It is the author's speculation that the simplest and most reliable way to create an evaporative cooling system for the PEM fuel cell is to use a set of swirl spray nozzle injectors machined into the bipolar plate anode gas header for each cell. This appears to be the surest method that would be capable of delivering the relatively large mass flow of finely suspended liquid water droplets required to feed evaporative cooling. In addition, the cathode gas should probably not be humidified at all, and should consist of room temperature air so that the PEM cells can benefit from both evaporative cooling and internal advection cooling due to the larger ΔT between cathode gas temperature and cell temperature. Because the membrane is so thin, it is unlikely that the cathode would

dry out if the anode side were able to receive the deluge of liquid water that is required for evaporative cooling to work in the first place.

Further data on the thermal performance of the various cases is located in Appendix C. Each of these figures in Appendix C is plot of the fuel cell temperature as a function of time. In each figure, there are two curves. One curve is that of a case using the nebulizer, while one case does not. Both cases were conducted with the same humidification chamber temperatures, thus permitting a graphical comparison of the relative performance of each case. In general, one will note that the case in which the nebulizer was used experienced a slower rate of temperature increase than the case without the use of the nebulizer. This is mostly due to the increased electrical performance for the nebulizer case, so that less waste thermal energy was being dissipated. One should also note that the sudden increase in cell temperature for the cases with the nebulizer in use (near the end of the plot) was due to the heater being turned on, thereby dramatically increasing the rate of waste thermal energy dissipation.

5.2 Electrical performance

While the use of ultrasonic nebulization delivery of water into the anode gas stream did not result in any meaningful evaporative cooling in this investigation, it did result in considerable improvement of the electrical performance of the PEM fuel cell. Figure 27 illustrates the voltage as a function of time for the best (65/65), and worst (55/55) cases with and without the use of the nebulizer. As one can see, the difference in electrical performance is noticeable, especially when comparing the 55/55 cases operated with the nebulizer to those operated without the nebulizer. The different time scales associated with the drop off in voltage is due to two causes. One, for all of the cases where the nebulizer was not used, the fuel cell eventually exceeded the maximum safe operation temperature (70 °C) if no user intervention occurred. For all cases where the nebulizer was used, the cell would not exceed 70 °C on its own and so the heater was turned on after the author was satisfied that the fuel cell had reached steady state operation (i.e. that the average cell temperature was constant); the time at which the heater was turned on was therefore not constant between the various cases.

The improvement in electrical performance is further elucidated in Figures 28a through 30b. Each pair of figures (a and b) shows the measured cell voltage as a function of time for the 65/65, 65/55, and 55/55 cases (with and without nebulizer) and the ratio of these voltages (ratio of voltage for case with nebulizer to voltage for case without nebulizer). As one can see, the ratio is nearly always above 1; the average value for the ratio is 1.07, 1.16, 1.12 for the cases of 65/65, 65/55, and 55/55 respectively. The reader may notice a small gap in the data for 55/55 case not using the nebulizer –this is due to an open circuit condition during that portion of the experiment. The reader will notice that the cases using the nebulizer lasted longer (experiment time was longer), were more stable, and for the most part, gave a higher output voltage. This increased output voltage is best seen in Figures 28b, 29b, and 30b showing the plot of the ratio of the measured voltages. As one can see, the ratio remains above 1 nearly all of the time, and if one were to integrate the area of the curve above 1.0, the area would prove to be positive,

indicating that the nebulizer does indeed lead to a higher average cell output voltage. The ratio of voltages is most dramatic for the 65/55 and 55/55 cases, showing a rather large ratio towards the end of the curve, which is due to the rapid decline of the cell voltage for the case without the use of the nebulizer as it overheats.

The reason the heater was used for the cases where the nebulizer was in use was to determine how robust the technique of ultrasonic nebulization as both a water and thermal management technique. Obviously, the conclusion from the last section is that the technique of ultrasonic nebulization of water into the anode feed gas is not robust as a cooling method**. However, the technique of ultrasonic nebulization of water into the anode feed gas is indeed a *very robust* method of ensuring adequate hydration of the PEM fuel cell, even for very high cell temperatures. This is evidenced by the fact that the average cell voltage does not drop off precipitously at high cell temperatures with the use of the nebulizer, whereas without the use of the nebulizer, the voltage does drop off rapidly as the cell overheats (see figure 31 which displays the best and worst cases of cell voltage as a function of temperature).**

The disadvantage of the use of ultrasonic nebulization as an ultrahumidification technique is the very large expenditure of energy to atomize the water, owing to the extremely poor mechanical efficiency of the atomization process (section 3.3). That is, in order to realize a conversion efficiency (voltage) gain at the fuel cell, one has to expend energy to nebulize the water, and therefore the net conversion efficiency of the overall fuel cell system may or may not benefit from the use of the ultrasonic nebulizer ultrahumidification system. The nebulizer as used in this investigation produced a substantial net loss (~90%) in overall system conversion efficiency. However, as has been mentioned in the previous subsection, the nebulizer used in this investigation could be used to supply more than one fuel cell at a time, which would dramatically reduce the energy expenditure per unit mass of water. Using the manufacturer's data to calculate the energy expenditure per unit mass of water (see reference 15), for a PEM fuel cell operating at 0.8 A/cm^2 and using the same liquid water mass flow rate per unit area that

was used in this investigation, only a 8.5 mV improvement in average cell voltage would be required to reach break-even. **Because improvements of average cell voltage on the order of 30 to 50 mV were observed in this investigation, the author believes that a well designed ultrasonic nebulization ultrahumidification system could be used to improve the overall conversion efficiency of a PEM fuel cell system. However, this gain in overall conversion efficiency would only be possible if the specific energy expenditure (energy expenditure per unit mass of water) could be made to coincide with the advertised manufacturer's specifications.**

An interesting observation is that the voltage "noise" seems to improve with an improvement in electrical performance, and indeed this is the case. Figure 32 qualitatively demonstrates this trend with the cases of 55/55, 65/60, and 65/65 (all were cases using the nebulizer). As one can see, the top curve has the least amount of noise, the middle curve a moderate amount of "noise", whereas the bottom curve has a significant amount of "noise". Table 3 gives a ranking of the various cases (with nebulizer) for average cell voltage, absolute noise amplitude, and relative noise amplitude. That is, the table lists the cases in descending order of voltage, and in ascending order of noise amplitude. As the reader can see, the ranking order is virtually identical between the categories of voltage and noise, as only the mid-range cases of 50/65 and 65/55 are transposed between the noise and cell voltage rankings. This "noise" is not EMI (electromagnetic interference), as the period of oscillation of the noise is on the order of tens to hundreds of seconds, and because the author specifically went to great lengths to minimize the influence of EMI on the measurements (see Appendix D for details). This "noise" is believed by the author to be the manifestation of an overvoltage cycling, much like that seen in cases CO poisoning of anode catalyst, but smaller in magnitude [16]. The author believes that the overvoltage is caused by a slight lack of sufficient membrane hydration (that is, it is an ohmic overvoltage), which would account for the improvement in both noise and electrical performance with increasing humidification. Previous work has shown that the majority of the electrical resistance of the ionomer membrane is caused by insufficient hydration in a narrow zone immediately

adjacent to the anode electrocatalyst site, and that this zone is starved for water primarily because the electroosmotic drag of water outstrips water delivery by back diffusion and water adsorption at the anode [17]. The concept of a cycling overvoltage can be explained as an unsteady concentration of water/hydronium ions within the membrane. While the water concentration is relatively high, the cell voltage is high due to lower ohmic losses, whereas while the water concentration is lower, the cell voltage is low. Thus, the situation is somewhat analogous to a car that surges due to insufficient fuel pressure or which has carburetor float setting that is too low, leading to a cycling between starvation and normal operation**. It is therefore suggested that the cycling amplitude could be used to estimate the water content of the Nafion™ membrane.**

If the reader is interested, a complete set of plots of the cell voltage versus time for all cases is included in Appendix C. Each figure in Appendix C shows each humidification temperature case in pairs comparing the case with the use of the nebulizer and the case without the use of the nebulizer.

5.3 Results summary

- No calculated value for evaporative cooling could be found for the cases that did not use the nebulizer and were assumed to be zero.
- The calculated value for evaporative cooling for the nebulizer-in-use cases of 65/65, 65/60, 60/65 were found to be zero.
- The best case for calculated evaporative cooling occurred for the case of 55/55, which had a calculated value of 2.0 watts. This value represents only 7% of the total waste thermal energy removal rate.
- The ultrasonic nebulizer required 19.3 Watts to operate, giving a specific energy consumption of 10.7 kJ/g.
- The specific energy consumption possible with an ultrasonic fountain nebulizer according to the advertised specifications of a major manufacturer (TDK Inc.) is 188 J/g.

- All cases using ultrahumidification gave a higher average fuel cell output voltage than the corresponding conventional case, and on average the gain in voltage was on the order of 30-50 mV (or 7-16%).
- All cases using ultrahumidification showed less output voltage oscillation amplitude ("noise") than the corresponding conventional case.
- The average cell voltage does not drop off precipitously at high cell temperatures with the use of the nebulizer, whereas without the use of the nebulizer, the voltage does drop off rapidly as the cell overheats.
- The average output voltage increases and voltage oscillation amplitude decreases with an increase in humidification temperature for all cases.

6. CONCLUSIONS

- **Evaporative cooling was therefore either a very minor or nonexistent effect in all cases studied in this investigation.**
- The evaporative cooling rate encountered in this investigation was hindered by an insufficient rate of delivery of liquid water to the fuel cell.
- The limiting factor in liquid water delivery appears to be the water particle density.
- This limiting factor in liquid water particle density may not be due to an inherent limitation in the ultrasonic nebulizer – it may be a constraint imposed by the anode gas delivery system.
- This investigation was unable to exhaustively prove whether or not evaporative cooling is feasible with the use of ultrasonic nebulization of water into the anode gas stream.
- However, because of the limitation of water particle density in the anode gas stream encountered, and because of the high energy consumption needed to nebulize the water, **this investigation does cast considerable doubt on this method being an easily implemented, robust method of providing evaporative cooling.**
- **Ultrasonic nebulization of water into the anode gas stream does provide very significant electrical performance benefits, and because of the increase in both performance and fault tolerance (excessive cell temperature), this is a technique which should be further investigated for use in commercial PEM fuel cell systems.**
- **A well designed ultrasonic nebulization ultrahumidification system could be used to improve the overall conversion efficiency of a PEM fuel cell system.**
- There is very good evidence to suggest that a one-to-one, inverse functional relationship exists between the amplitude of the cycling voltage and the water content of the Nafion™ membrane.

- The fuel cell voltage cycling is likely due to an unsteady water concentration within the membrane.

7. RECOMMENDATIONS

- Further investigation needs to be performed to examine the root cause of the limitation in water particle density in the anode gas stream. This investigation should examine how the parameters of mean saltation time (as a function of velocity/Reynolds number), critical minimum constriction hydraulic diameter, etc. affect the design of an ultrasonic nebulizer-based evaporative cooling system for a PEM fuel cell.

- Further investigation needs to be conducted to determine the functional relationship between the amplitude of PEM fuel cell cycling voltage and the water content of the Nafion™ membrane used in the Membrane Electrode Assembly. This would prove to be a very valuable diagnostic tool for assessing the "health" of a PEM fuel cell in operation.

- Evaporative cooling would most likely be easiest to accomplish by using internal injection of water at the anode bipolar plate inlet header with micronozzles machined into the bipolar plate. The only disadvantage of this system is that it would have a relatively narrow range of "efficient" operation, unless duplex (multistage) swirl nozzles were used, a difficult task given the small size of the anode gas header. The amount of pump power needed to run this cooling system would probably be comparable to that used already for the closed-loop cooling systems, but the PEM fuel cell system using this strategy would likely have higher energy conversion efficiency, and would be more fault tolerant.

REFERENCES

[1] P. Costamagna, S. Srinivasan, J. Power Sources 102 (2001) 242-252.

[2] G. Hoogers, Fuel Cell Technology Handbook, CRC Press, Boca Raton, FL, 2003.

[3] A.J. Appleby, F.R. Foulkes, Fuel Cell Handbook, Krieger Publishing Company, Malabar, FL, 1993.

[4] J.B. Heywood, Internal Combustion Engine Fundamentals, McGraw Hill, New York, 1988.

[5] T. Zawodzinski Jr., T.E. Springer, J. Davey, R. Jestel, C. Lopez, J. Valerio, S. Gottesfeld, J. Electrochem. Soc. 140 (1993) 1981.

[6] C. Wang, A.J.Appleby, J.Electrochem Soc. 150 (2003) A493-A498.

[7] J. Larminie, A. Dicks, Fuel Cell Systems Explained, 2nd Edition, John Wiley and Sons Publishing, Chichester, England, 2003.

[8] D.L. Wood III, J.S. Yi, T.V. Nguyen, Electrochemica Acta 24 (1998) 3795-3809.

[9] M.J. Moran, H.N. Shapiro, Fundamentals of Engineering Thermodynamics, 5th Edition, John Wiley and Sons Publishing, New York, NY, 2004.

[10] L. Bayvel, Z. Orzechowski, Liquid Atomization, Taylor and Francis, Washington, DC, 1993.

[11] H. Liu, Science and Engineering of Droplets-Fundamentals and Applications, William Andrew Publishing, LLC, Norwich, NY, 2000.

[12] W.C. Hinds, Aerosol Technology-Properties, Behavior, and Measurement of Airborne Particles, John Wiley and Sons Publishing, New York, 1982.

[13] L.D. Rozenberg, Physical Principles of Ultrasonic Technology, Vol.2, Plenum Press, New York, 1973.

[14] B.R. Munson, T.H. Okiishi, D.F. Young, Fundamentals of Fluid Mechanics, 4th Ed., John Wiley and Sons Inc., New York, NY 2002.

[15] Product information on TDK Inc. NB series nebulizer modules found at TDK, Inc. (TDK Inc. is a leading Japanese electronics manufacturer) website: www.tdk.co.jp/tefe02/ef441_nb.pdf, Apr. 2004.

[16] A. Thomason, Master's Thesis, Texas A&M University, College Station, TX Dec. 2003.

[17] B. Andreaus, G.G. Scherer, Solid State Ionics 168 (2004) 311-320.

APPENDIX A

FIGURES AND TABLES REFERRED TO FROM TEXT

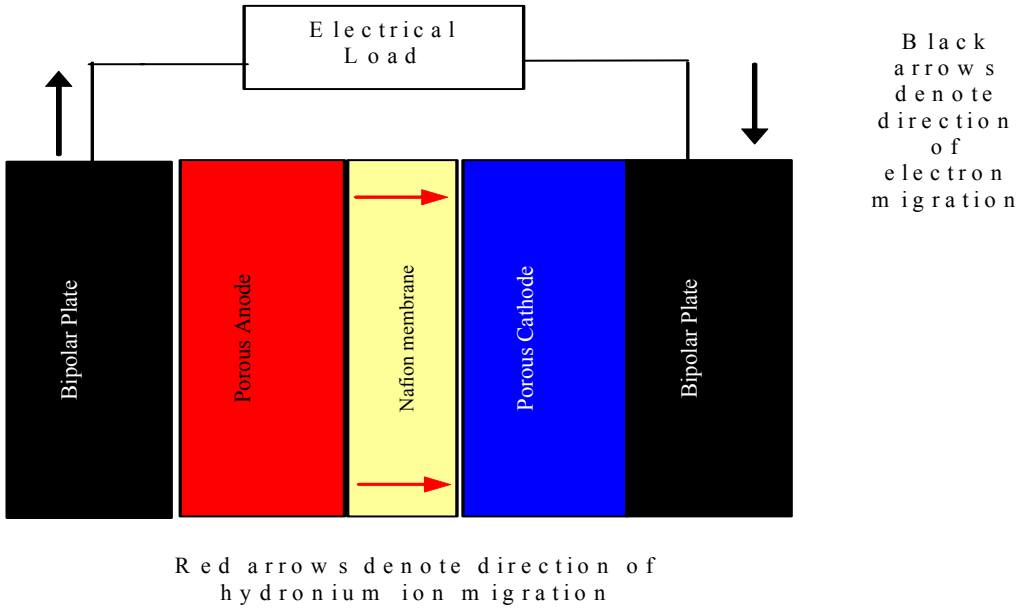

Figure 1: Illustration of basic schematic of PEM fuel cell showing direction of electron and hydronium ion travel.

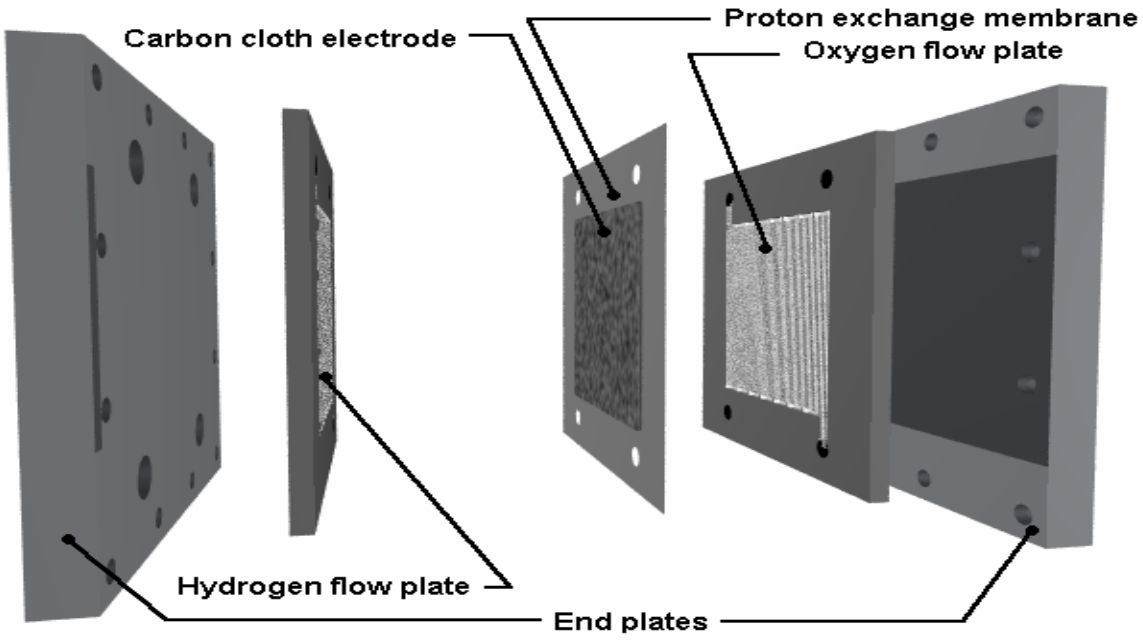

Figure 2: Illustration of internal components of single cell PEM fuel cell, showing the end plates, bipolar plates, and proton exchange membrane.

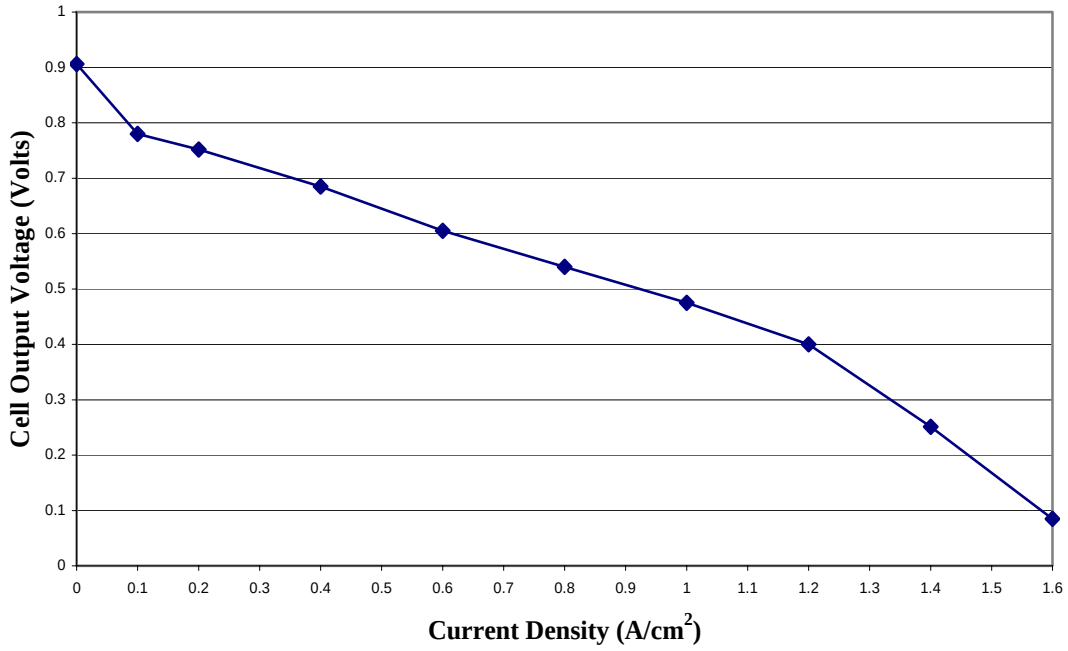

Figure 3: Polarization curve for PEM fuel cell used in this investigation (from experimental data)

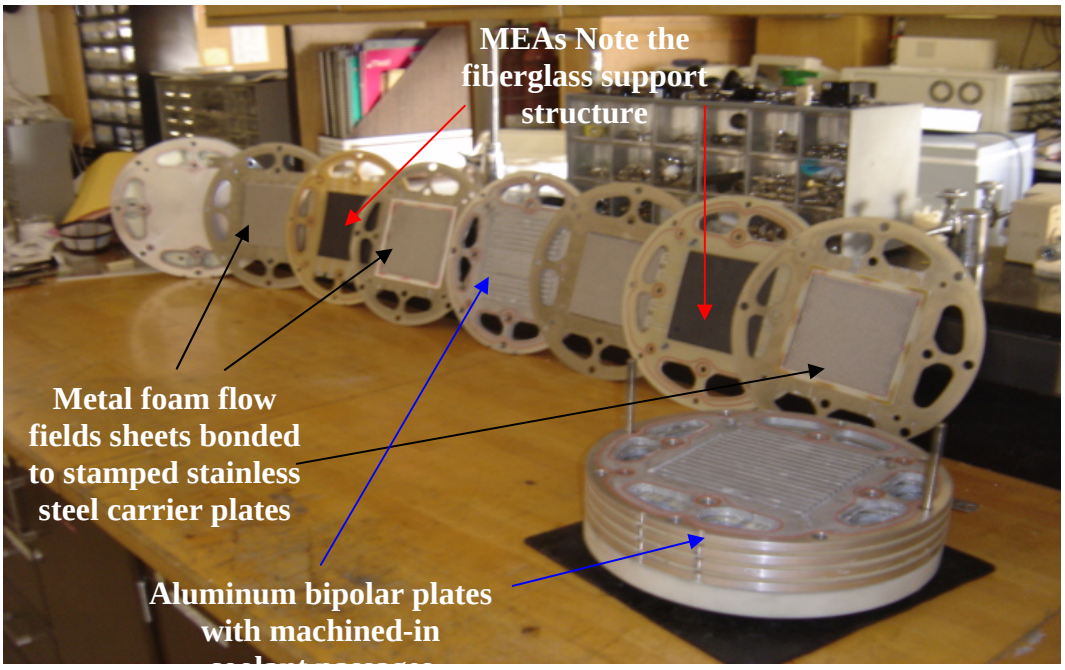

Figure 4: Photograph of commercial PEM fuel cell stack, disassembled to show repeating elements of bipolar plates, metal foam flow fields, Membrane Electrode Assemblies, and gaskets.

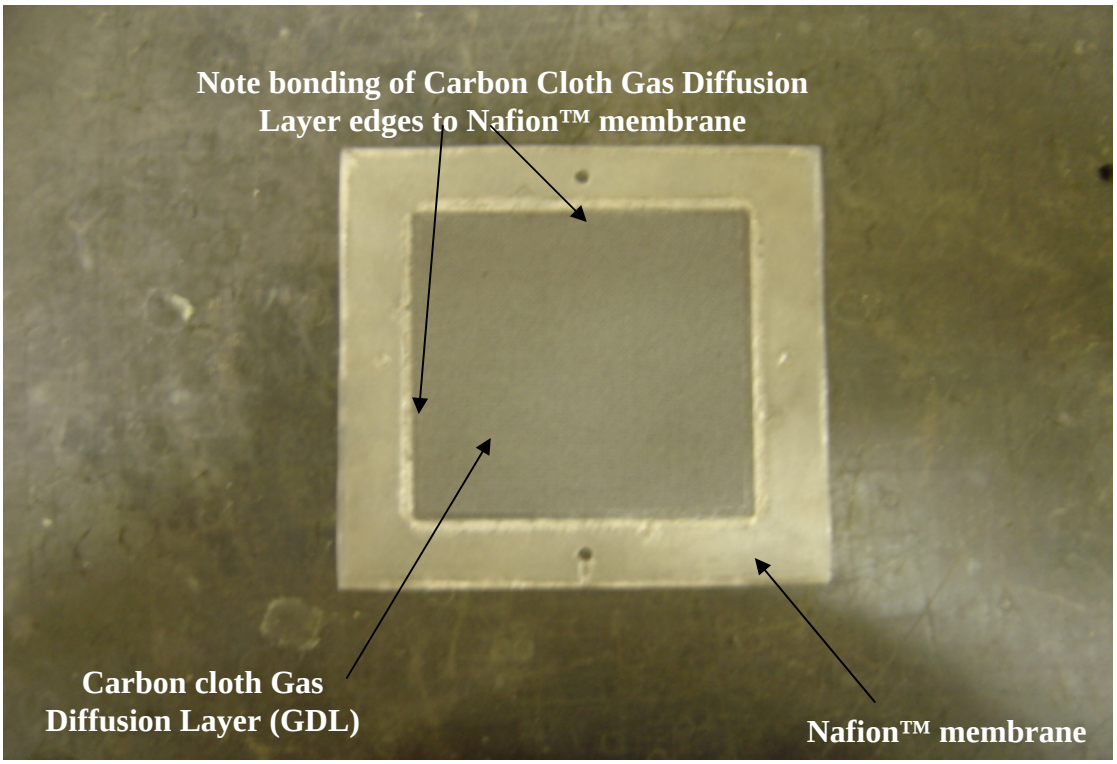

Figure 5: Photograph of 50 cm^2 3M™ Membrane Electrode Assembly used in this investigation.

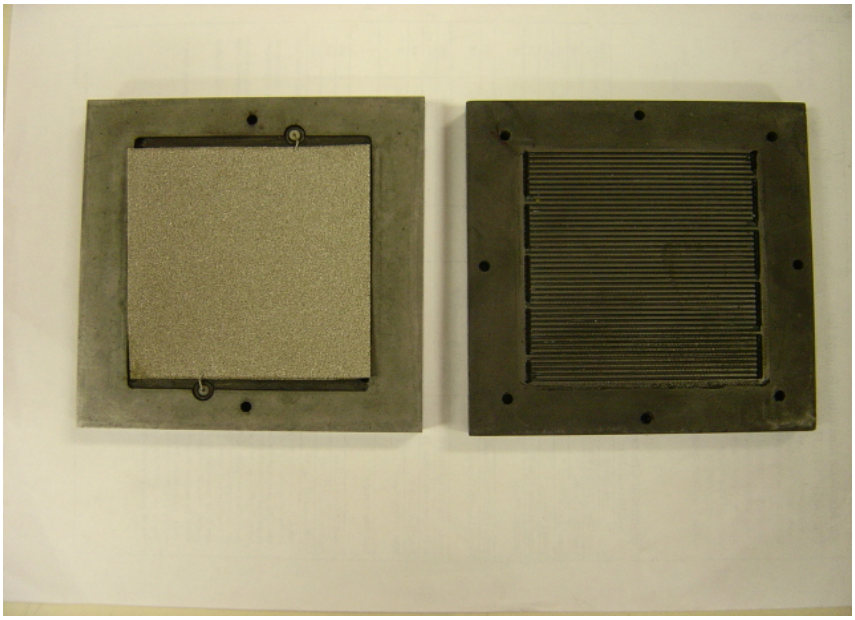

Figure 6: Photograph of metal foam flow field (left) and serpentine flow field (right). The metal foam flow field is shown installed in the recess in the graphite bipolar plate.

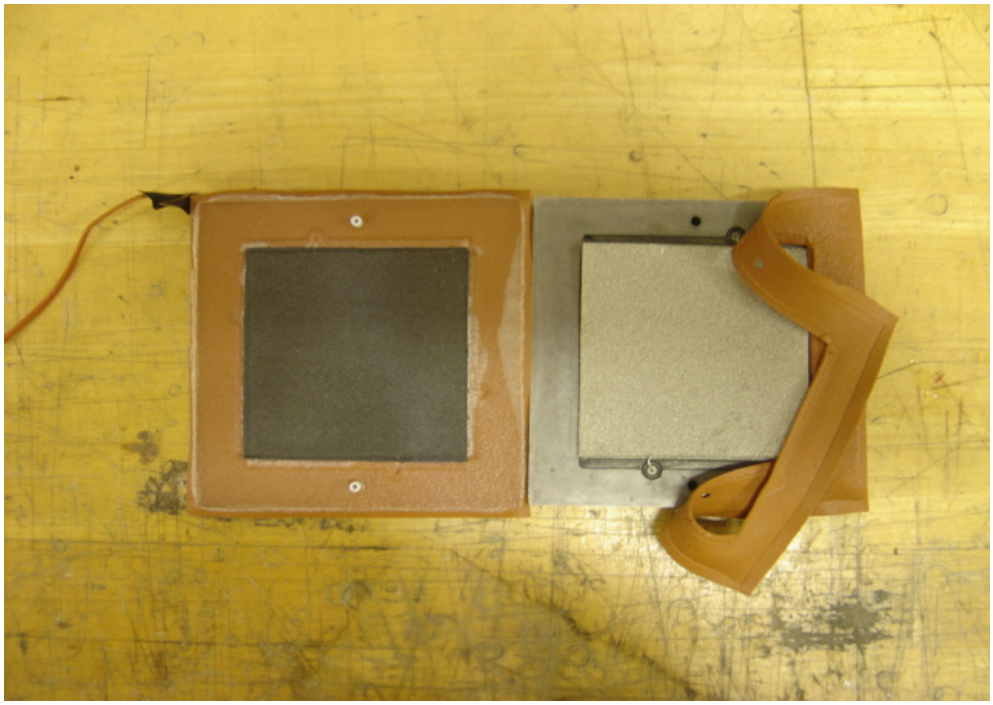

Figure 7: Photograph of showing the MEA, silicone gaskets, Nickel metal foam flow fields, and bipolar plate.

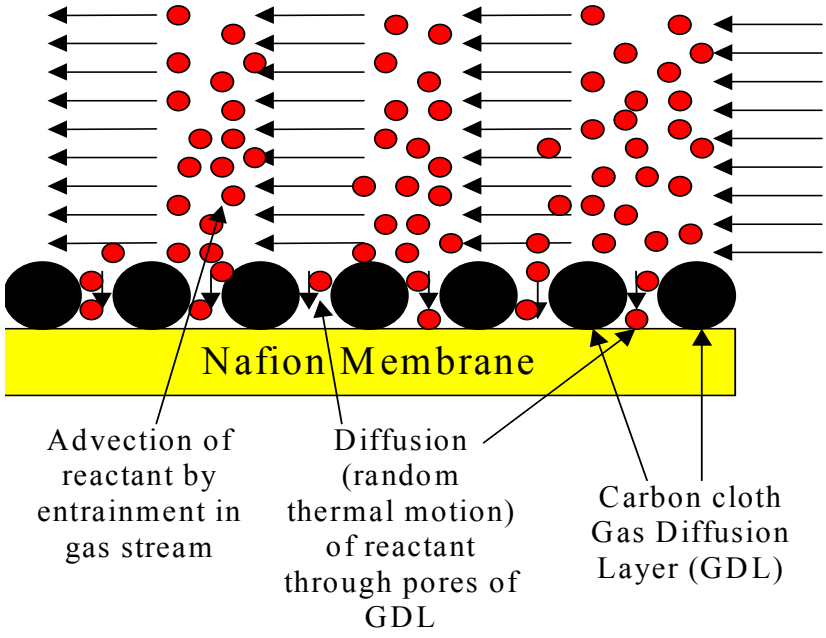

Figure 8: Illustration of processes of advection and diffusion transport within fuel cell. Note arrows depict direction of bulk reactant gas flow.

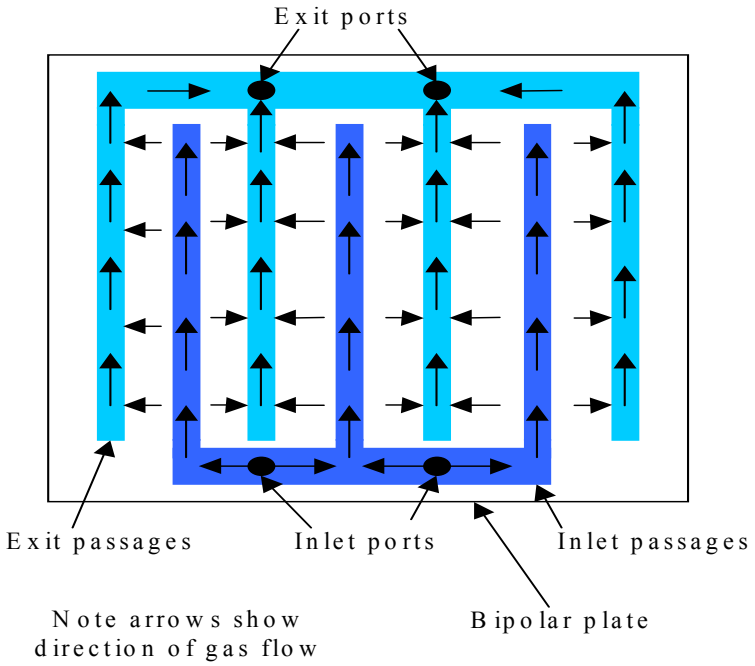

Figure 9: Illustration of interdigitated flow field concept. Reactant gas flows out through one set of passages, through the porous Gas Diffusion Layer and into the next set of passages where it leaves the cell.

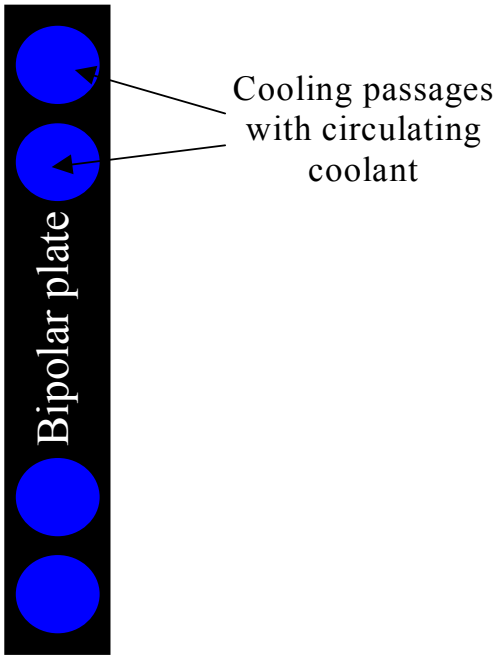

Figure 10: Illustration depicting internal coolant passages within bipolar plate.

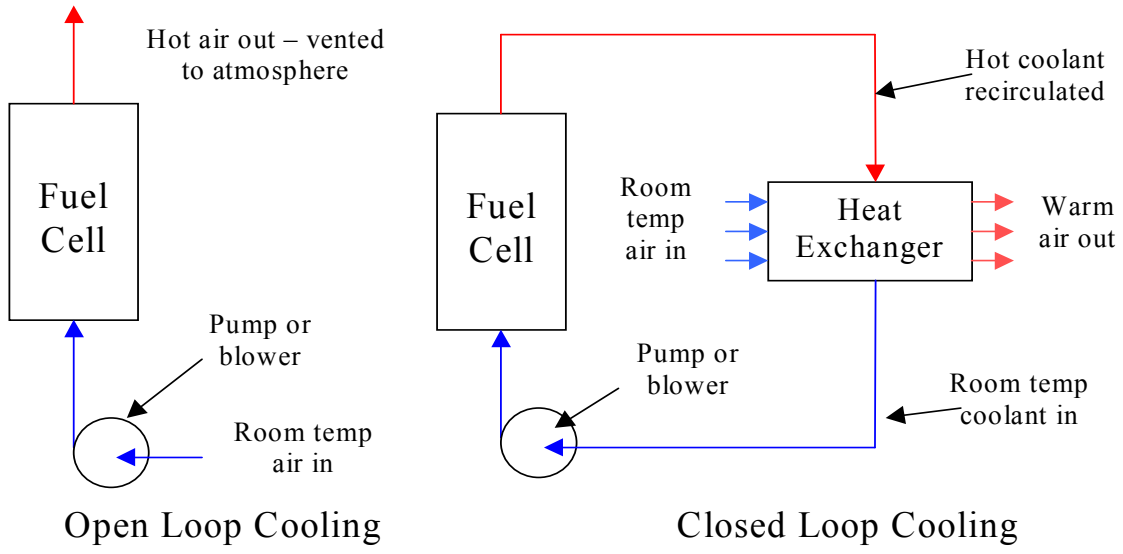

Figure 11: Illustration depicting open- and closed-loop cooling modes.

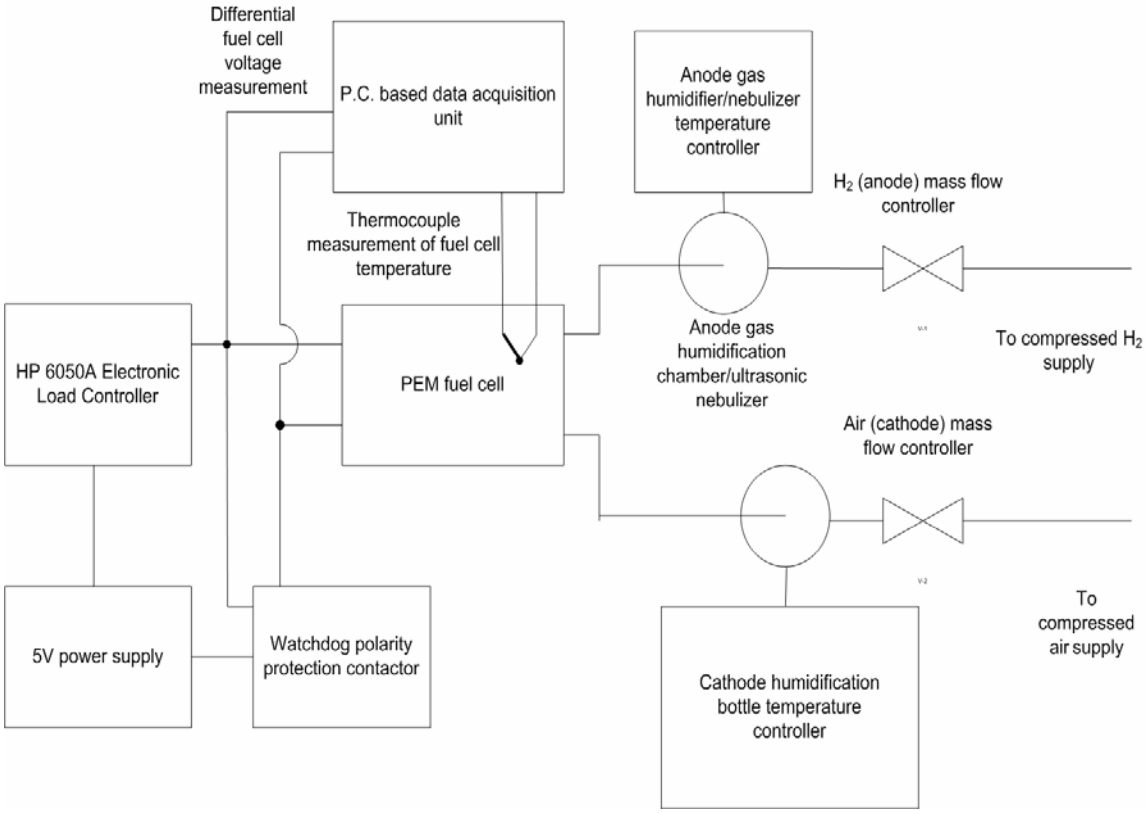

Figure 12: Schematic of experimental set up for determination of thermal and electrical performance of 50 cm^2 single cell PEM fuel cell.

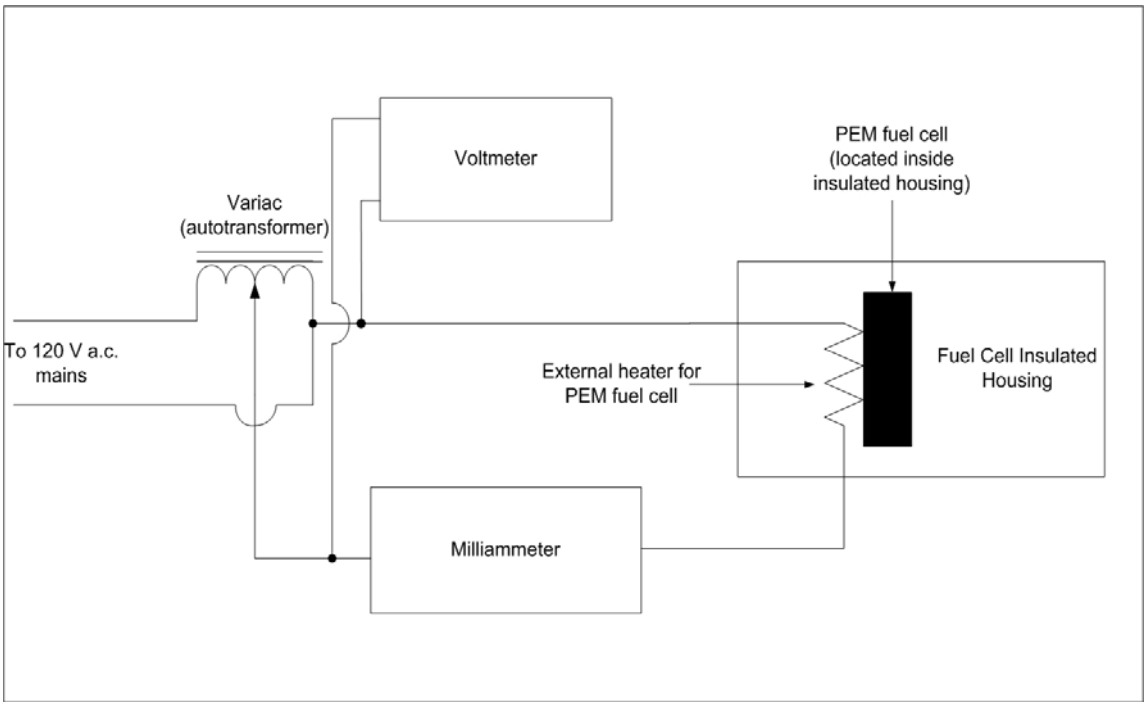

Figure 13: Schematic of experimental setup to determine rate of external and internal heat transfer for insulated 50 cm^2 PEM fuel cell.

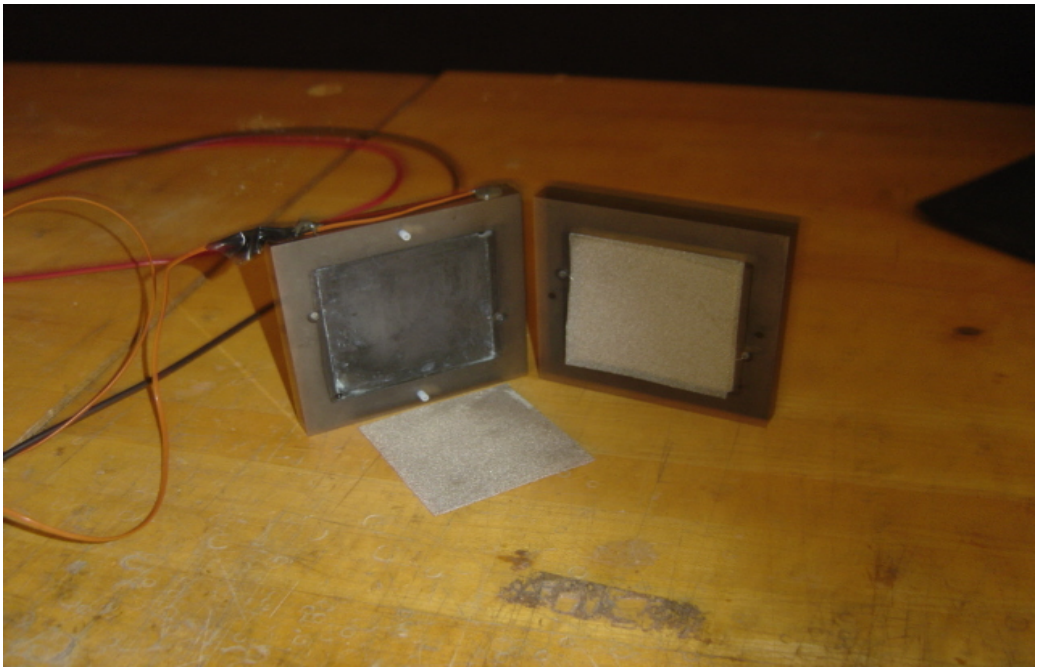

Figure 14: Photograph of bipolar plates used in investigation showing metal foam flow field installed (right) and recess for metal foam flow field (left).

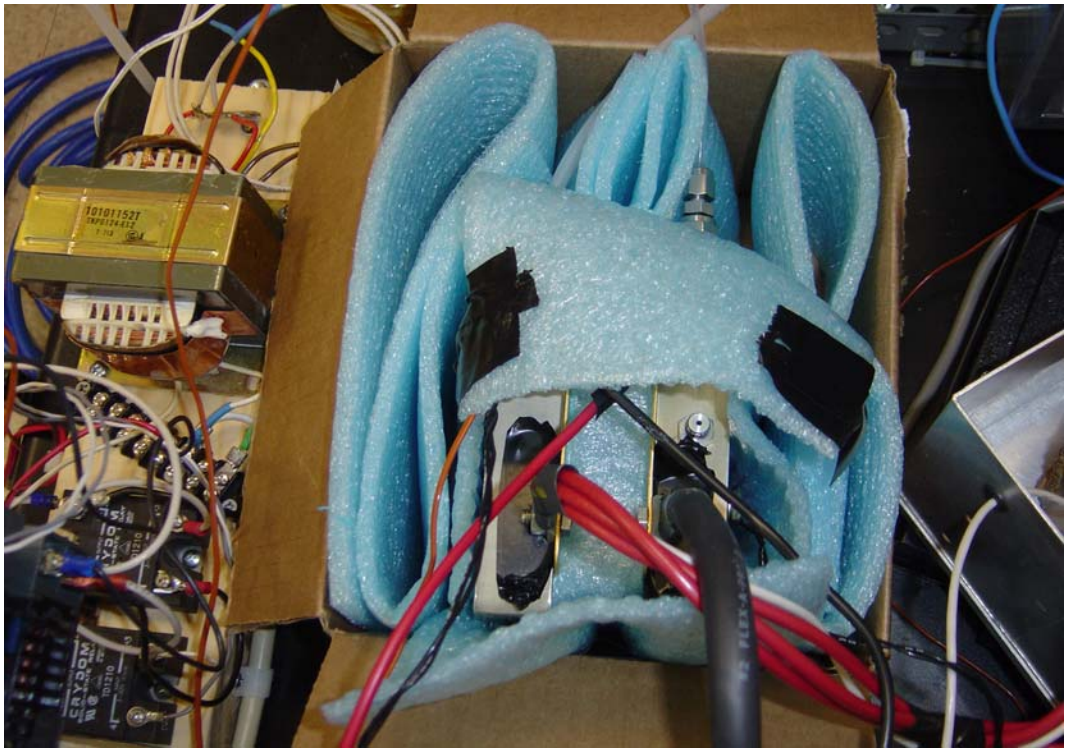

Figure 15: Top view photograph of the 50 cm2 PEM fuel cell in the insulated box used for this investigation.

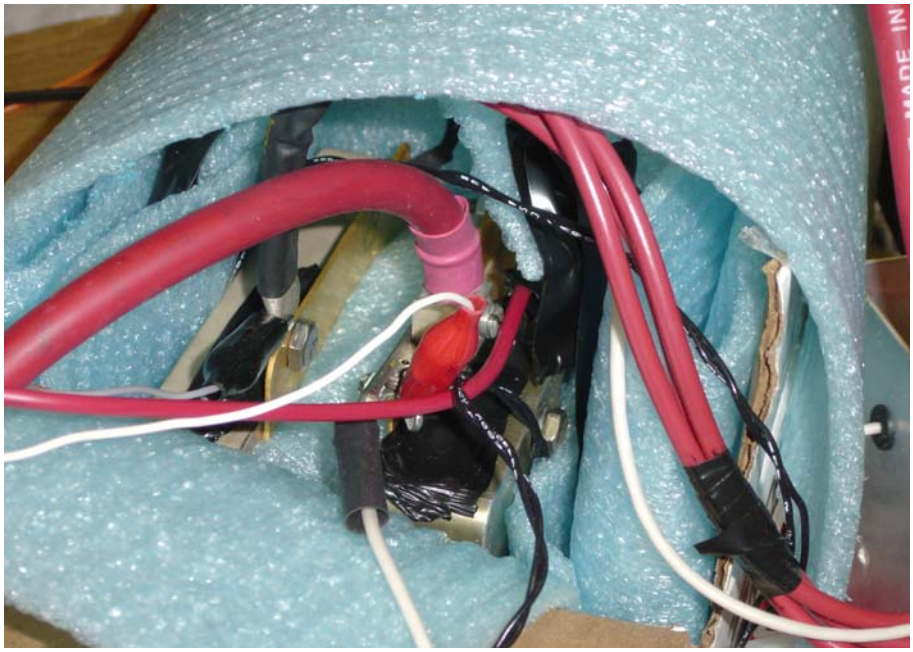

Figure 16: Close up photograph of 50 cm2 PEM fuel cell in insulated box. Note location of alligator clip leads used for cell voltage measurement.

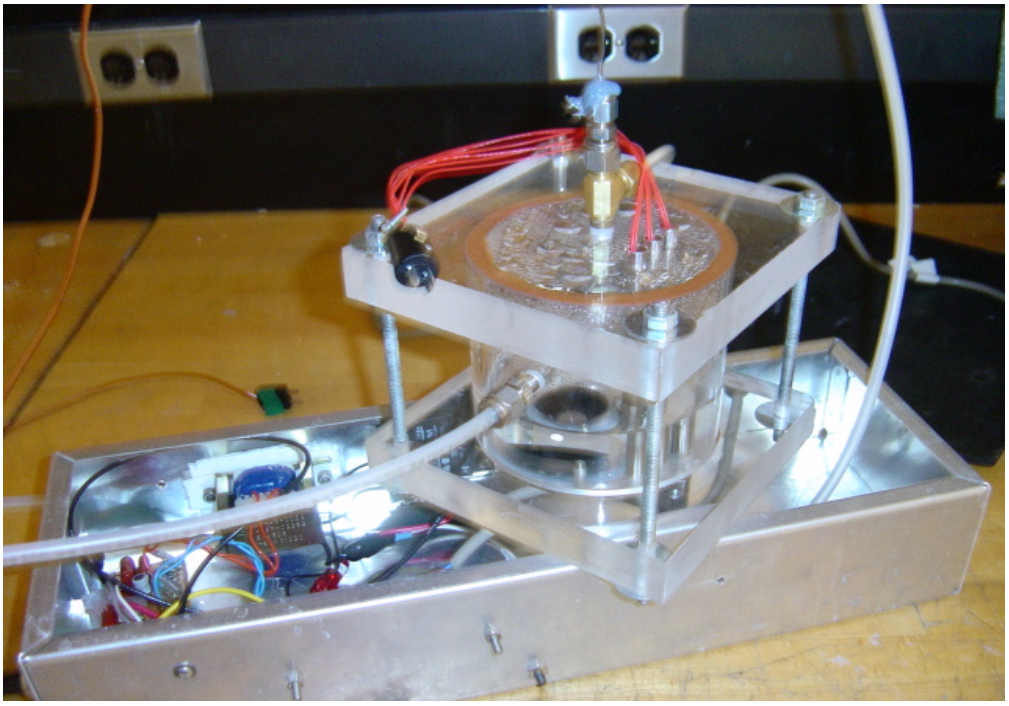

Figure 17: Side view photograph of anode gas humidification chamber/ultrasonic nebulizer used in this investigation.

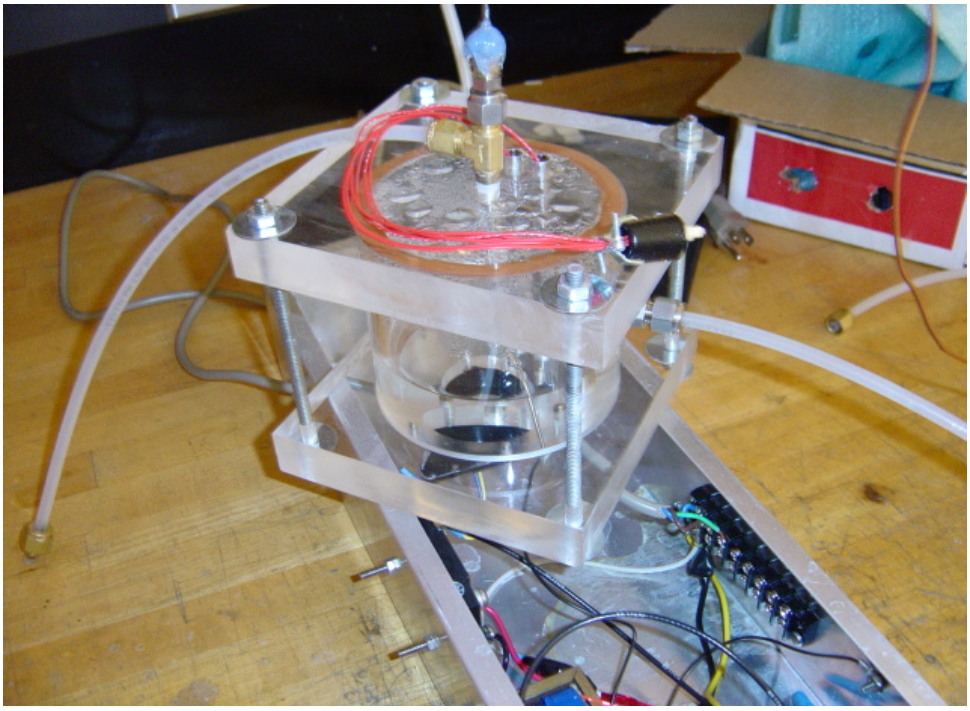

Figure 18: Front view photograph of anode gas humidification chamber/ultrasonic nebulizer used in this investigation.

Table 1: Listing of experimental conditions used in primary experiments conducted to determine thermal and electrical performance of PEM fuel cell with and without use of ultrasonic nebulization of water into anode gas.

Anode Humidification Temperature (Celsius)	Cathode Humidification Temperature (Celsius)	Use of Nebulizer (X denotes use of nebulizer for given experiment)	H_2 Mass Flow Rate	Air Mass Flow Rate
50	65	X	0.86	1.63
50	65		0.86	1.63
55	55	X	0.86	1.63
55	55		0.86	1.63
60	60	X	0.86	1.63
60	60		0.86	1.63
60	65	X	0.86	1.63
60	65		0.86	1.63
65	55	X	0.86	1.63
65	55		0.86	1.63
65	60	X	0.86	1.63
65	60		0.86	1.63
65	65	X	0.86	1.63
65	65		0.86	1.63

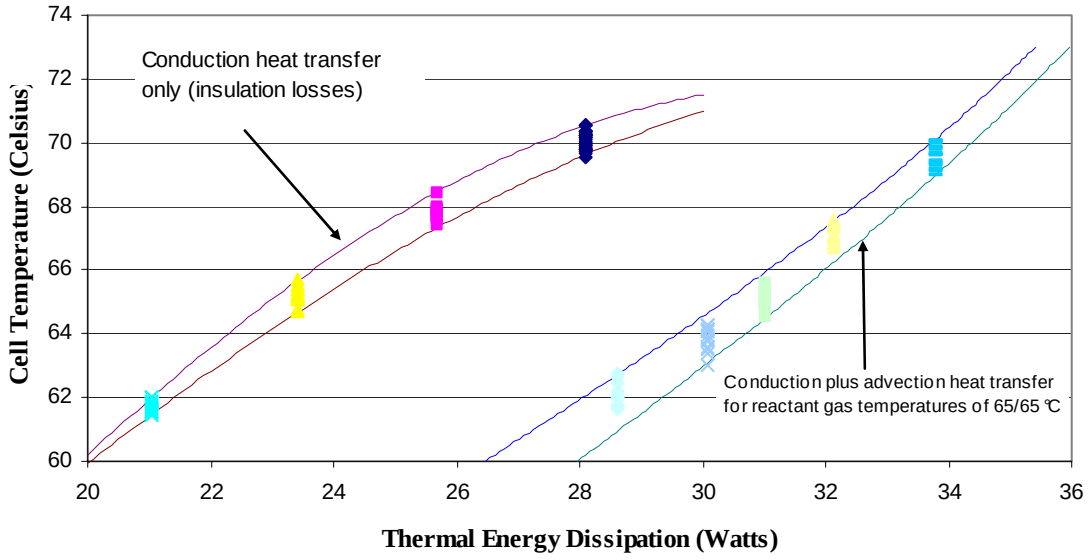

Figure 19: Plot of measured cell temperature as a function of external heater power for case with insulation loss only (left) and for case with reactant gas flowing through fuel cell (right). The fuel cell was not operated (no current), thus the waste heat in this instance was generated exclusively by the electric heater.

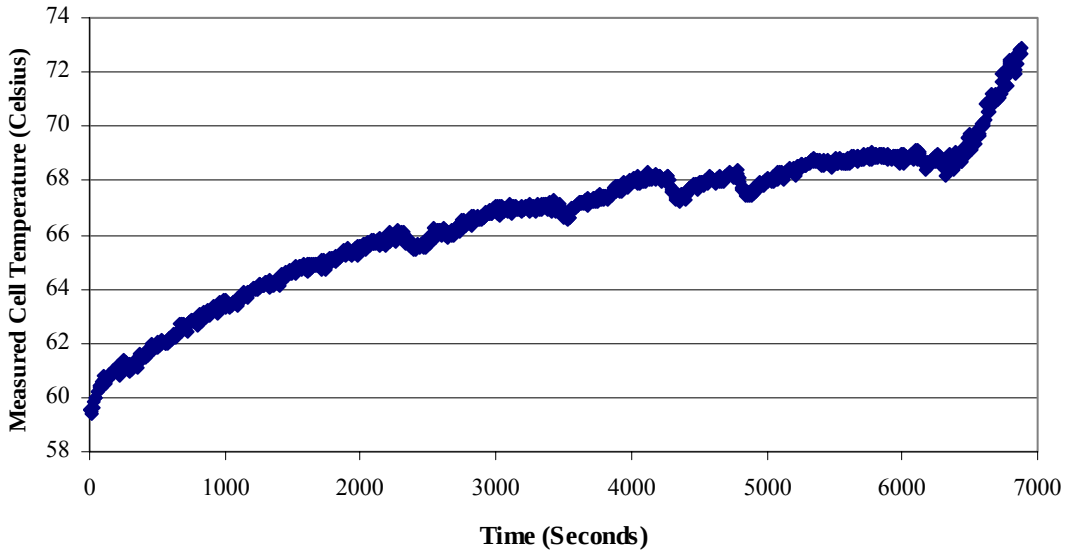

Figure 20: Plot of cell temperature as a function of time for 60/65 case without nebulizer in use. Note that the temperature constantly increases, never reaching an equilibrium point. Also note the sharp increase in temperature near the end of the plot.

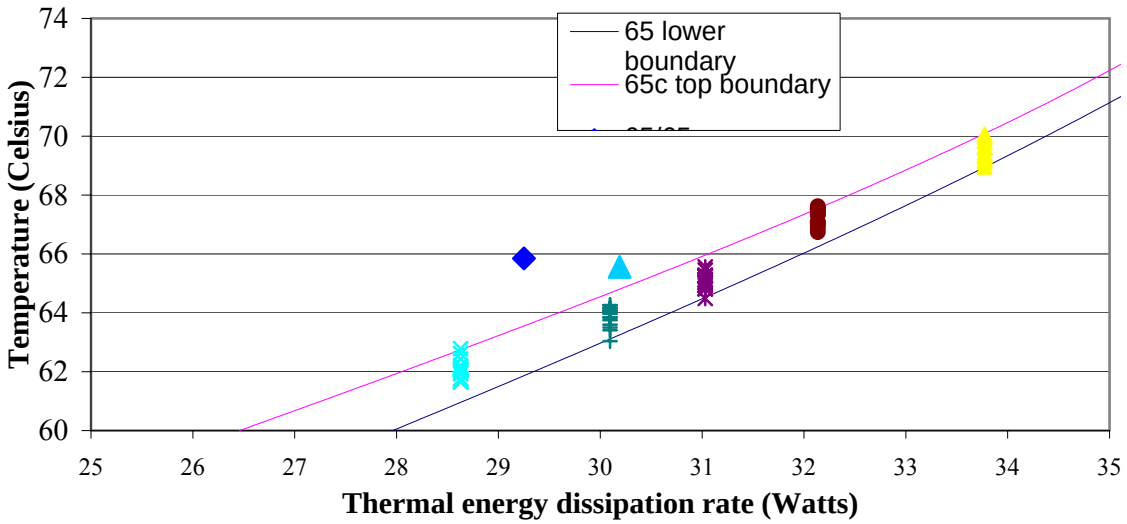

Figure 21: Plot of cell temperature as a function of thermal energy dissipation for the fuel-cell-operation cases of 65/65, 65/60, and the heat transfer experiment case of 65/65 C. The two lines shown are the calculated best fit curves for the boundary/extremum data generated from the 65/65 C heat transfer experiment data. The data inside the lines is that from the heat transfer experiment.

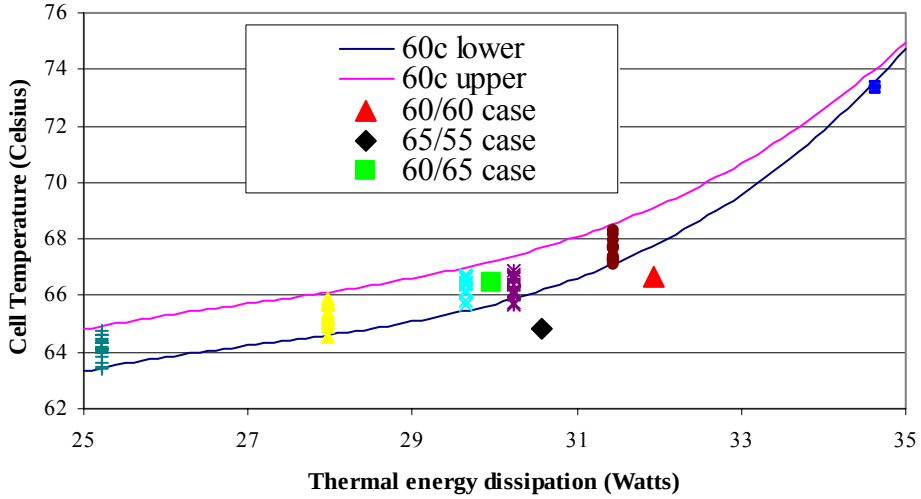

Figure 22: Plot of cell temperature as a function of thermal energy dissipation for the fuel-cell-operation cases of 60/60, 65/55, 60/65, and the heat transfer experiment case of 60/60 C. The two lines shown are the calculated best fit curves for the boundary/extremum data generated from the 60/60 C heat transfer experiment data. The data inside the lines is that from the heat transfer experiment.

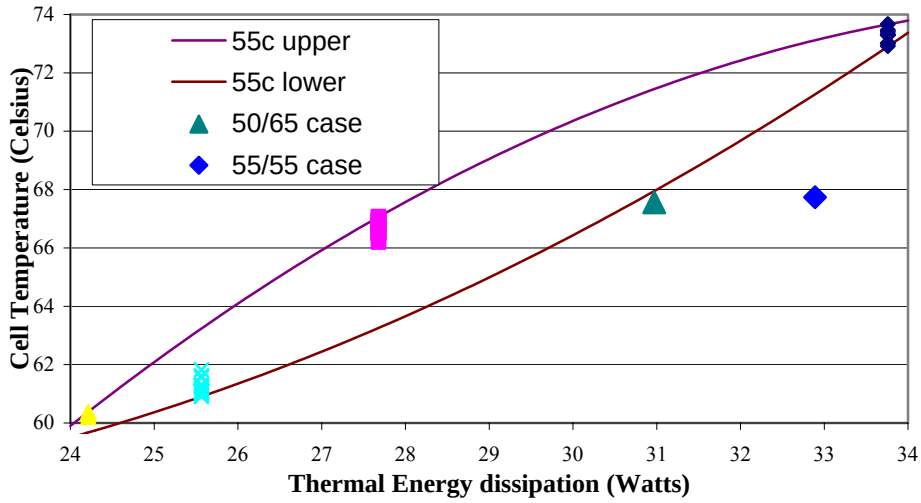

Figure 23: Plot of cell temperature as a function of thermal energy dissipation for the fuel-cell-operation cases of 60/60, 65/55, 60/65, and the heat transfer experiment case of 55/55 C. The two lines shown are the calculated best fit curves for the boundary/extremum data generated from the 55/55 C heat transfer experiment data. The data inside the lines is that from the heat transfer experiment.

Table 2: Listing of calculated rates of evaporative cooling for cases using nebulizer.

Humidification case (nebulizer used in all cases)	Calculated Evaporative Cooling Rate (Watts)
65/65	0
65/60	0
65/55	2.0
60/65	0
60/60	0.9
55/55	2.0
50/65	0.2

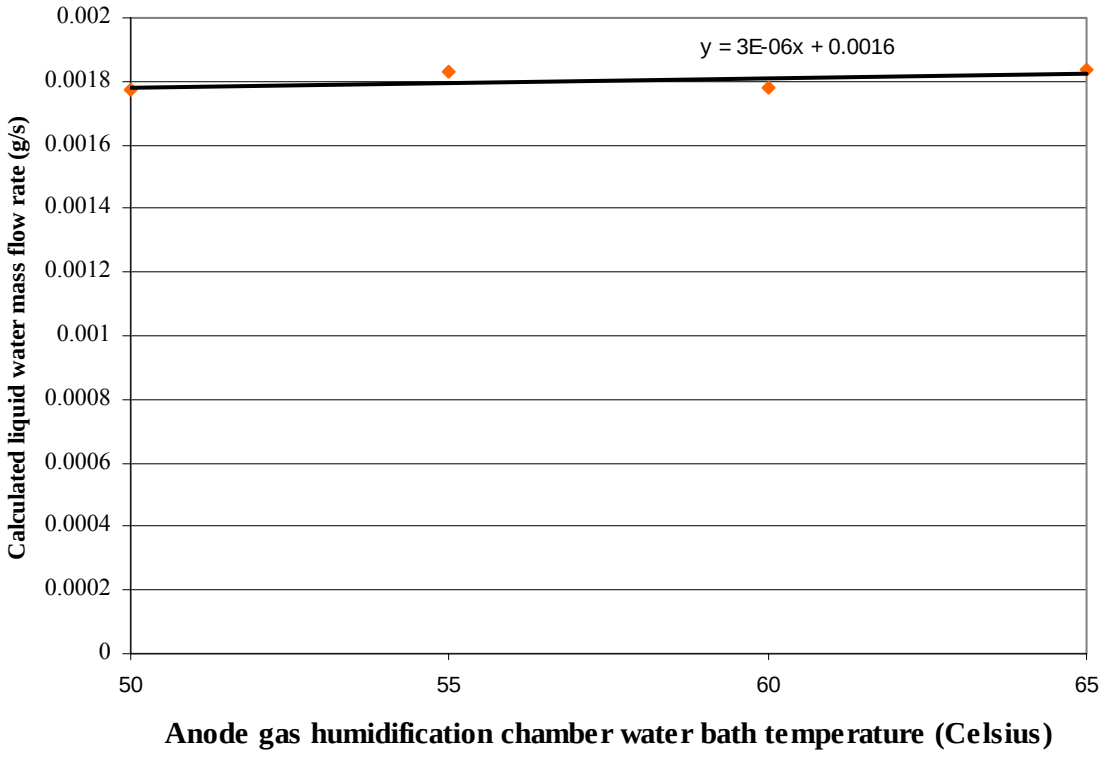

Figure 24: Calculated liquid water output mass flow rate (g/s) for anode humidification chamber while using ultrasonic nebulizer. Note trend line and equation of trendline on plot, showing extremely low slope. The calculated liquid water mass flow rate is therefore found to be have a weak dependence on temperature.

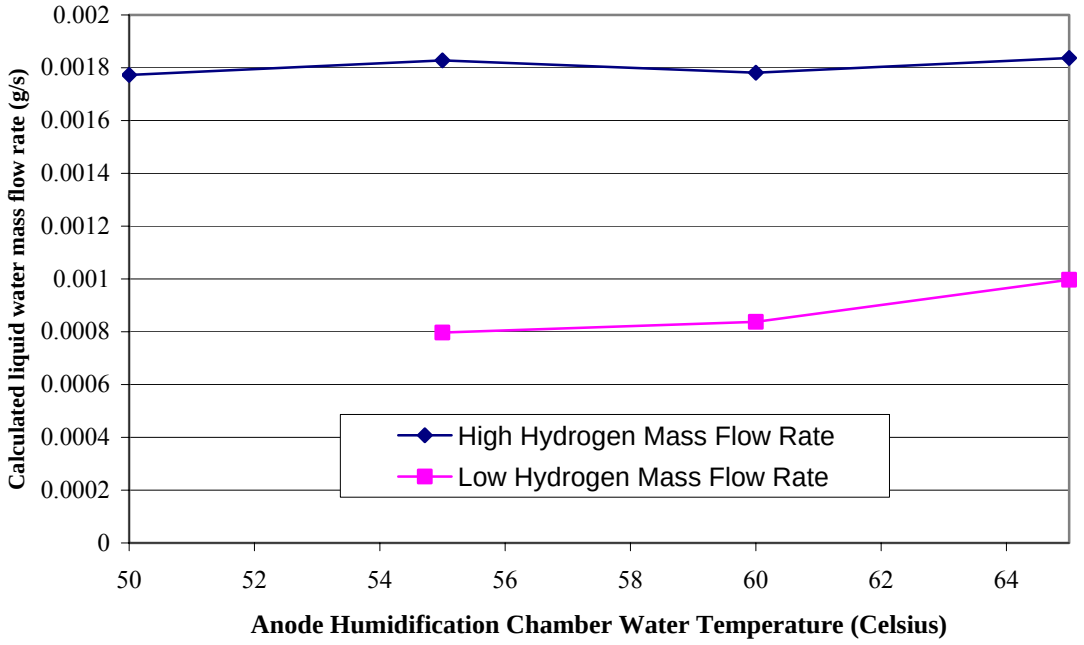

Figure 25: Plot of calculated liquid water mass flow rates as a function of temperature for high and low hydrogen mass flow rate cases.

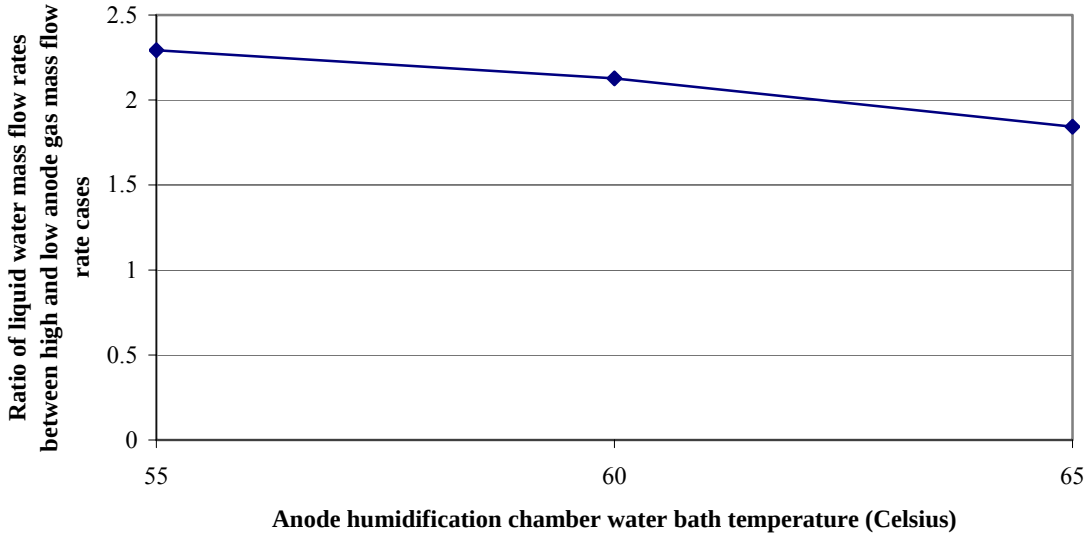

Figure 26: Plot of the ratio of liquid water mass flow rates between high and low hydrogen mass flow rate cases as a function of temperature.

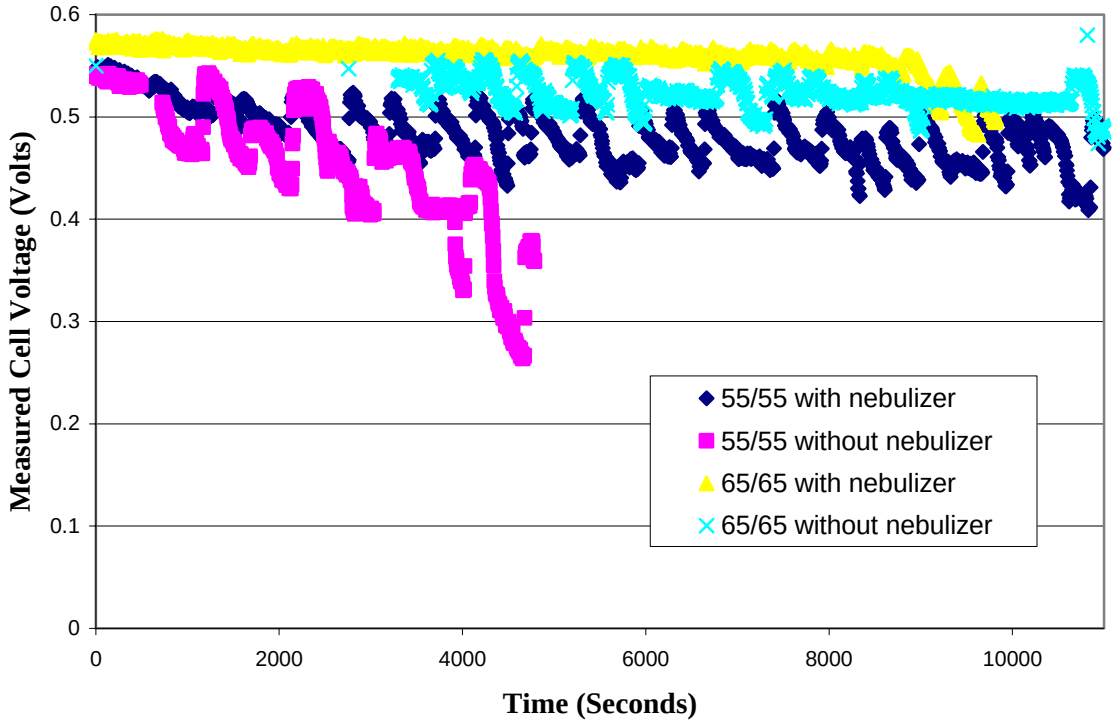

Figure 27: Plot of measured cell voltage as a function of time for the cases of 55/55 and 65/65, with and without the use of the nebulizer.

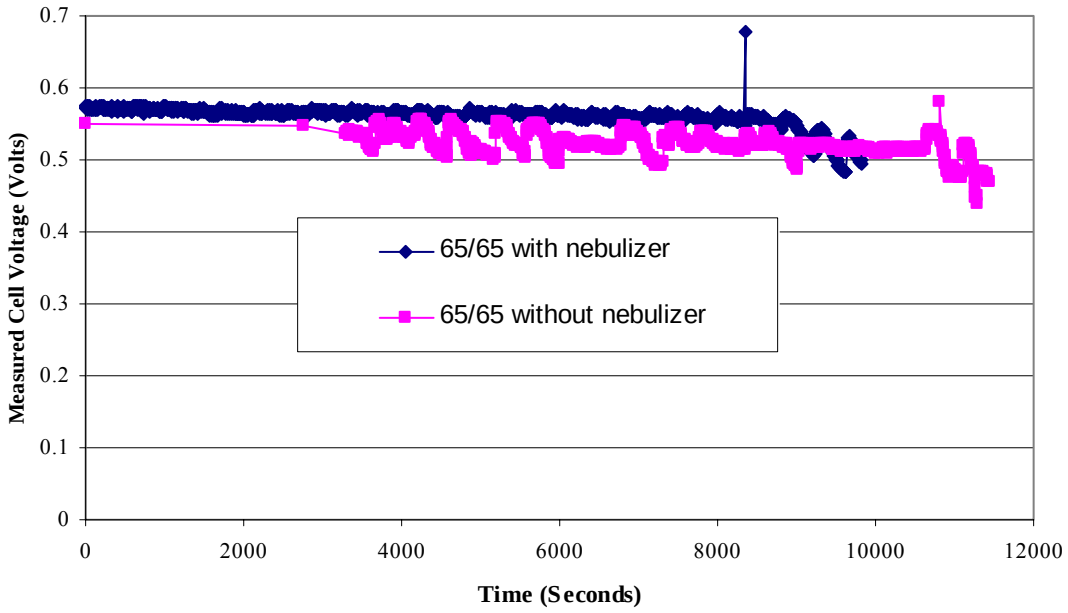

Figure 28a: Plot of voltage as a function of time for 65/65 humidification cases with and without use of nebulizer.

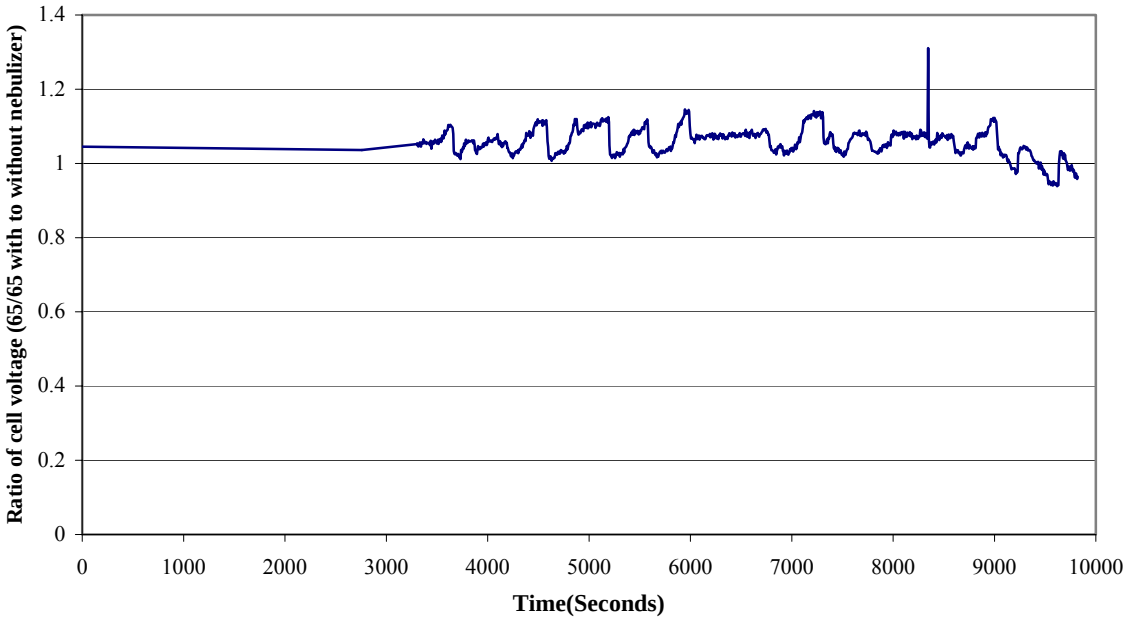

Figure 28b: Plot of ratio of voltage as a function of time for 65/65 case with use of nebulizer to the 65/65 case without use of nebulizer.

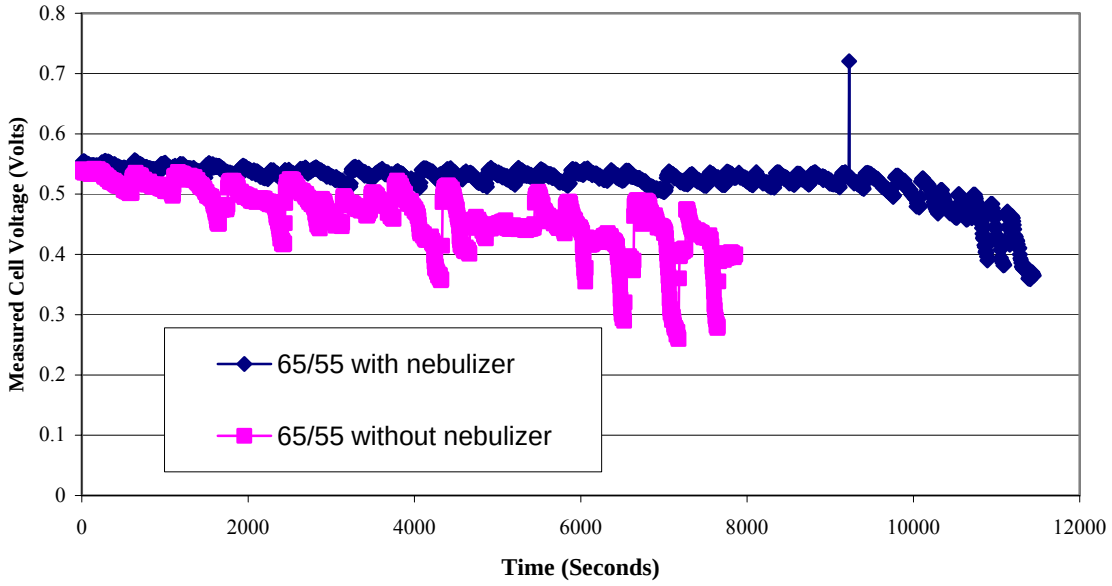

Figure 29a: Plot of voltage as a function of time for 65/55 humidification cases with and without use of nebulizer.

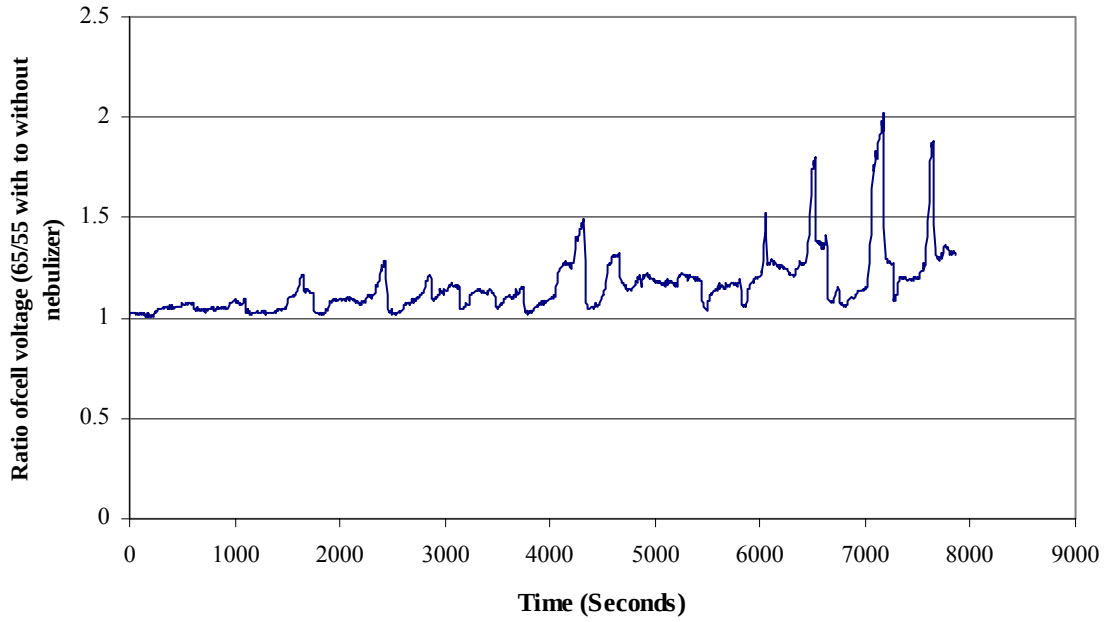

Figure 29b: Plot of ratio of voltage as a function of time for 65/55 case with use of nebulizer to the case without use of nebulizer.

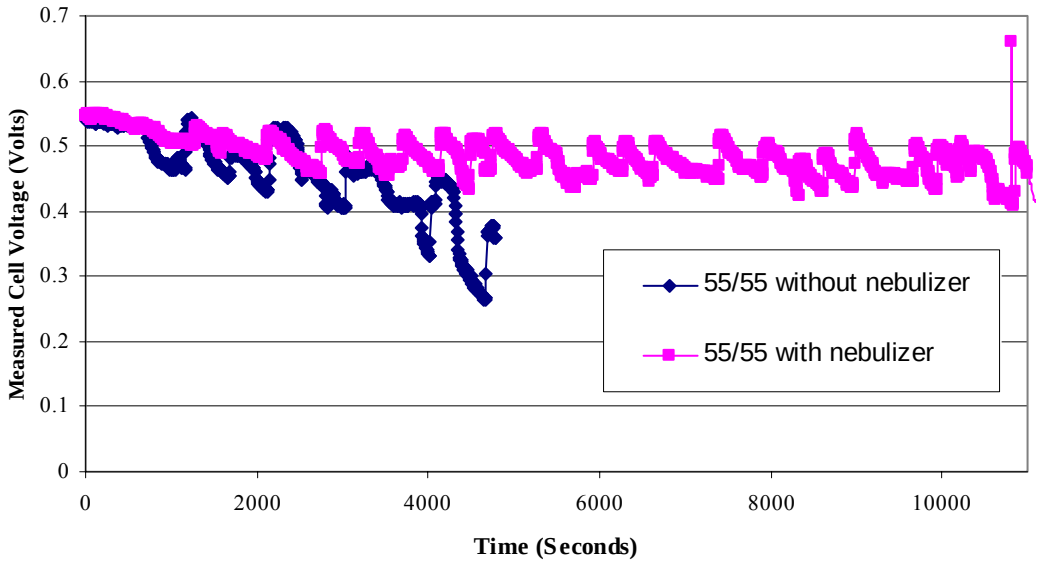

Figure 30a: Plot of voltage as a function of time for 55/55 humidification cases with and without use of nebulizer.

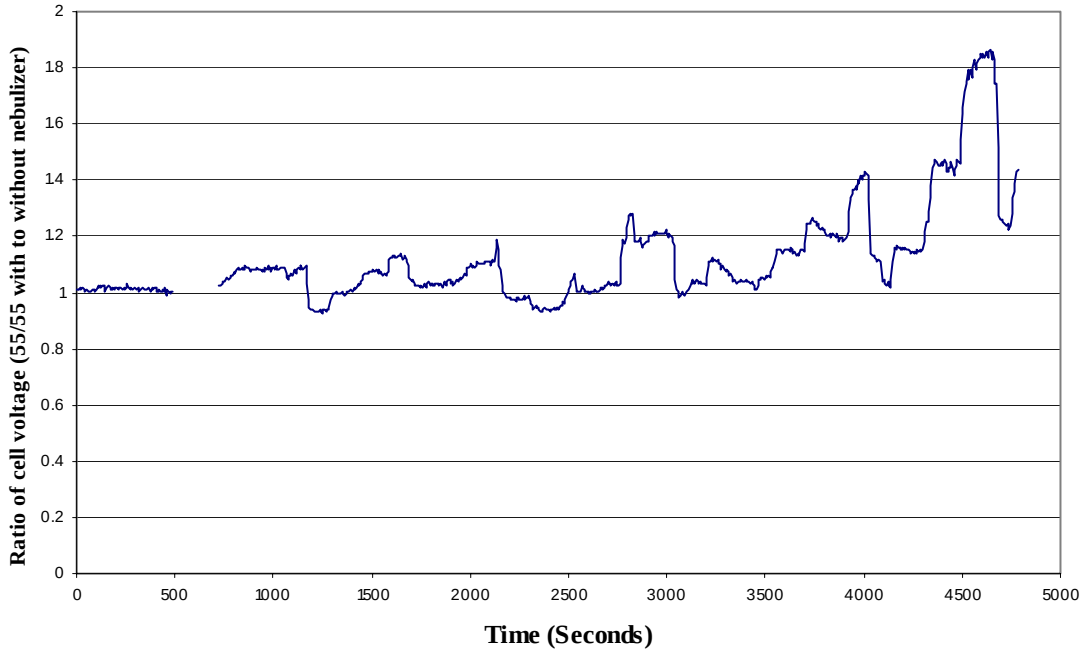

Figure 30b: Plot of ratio of voltage as a function of time for 65/55 case with use of nebulizer to the case without use of nebulizer.

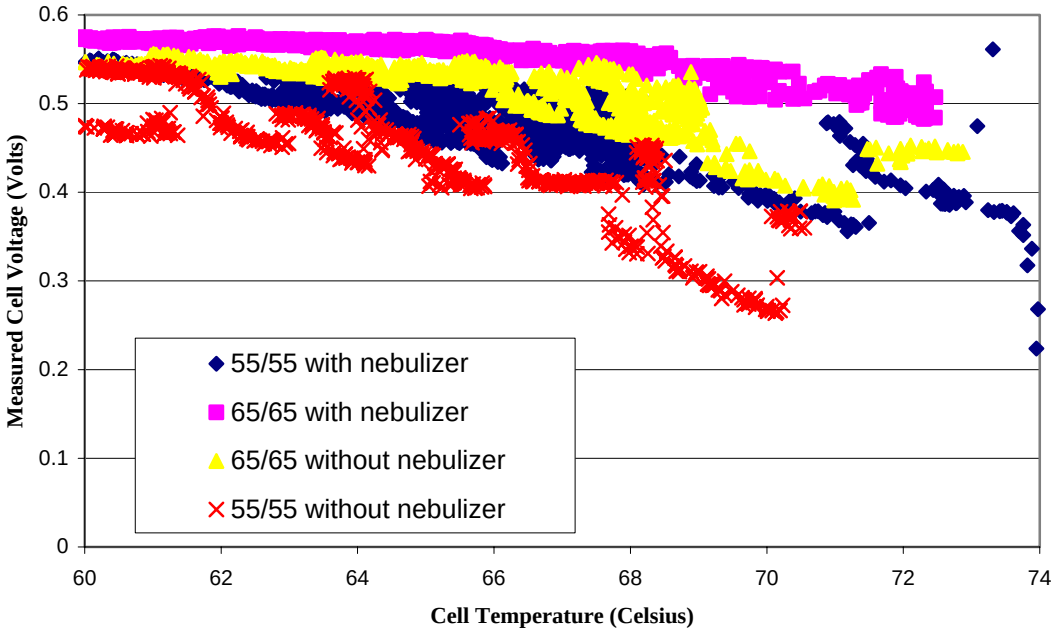

Figure 31: Plot of measured fuel cell voltage as a function of cell temperature for cases: 65/65 with nebulizer (pink), 65/65 without nebulizer (yellow), 55/55 with nebulizer (blue), and 55/55 without nebulizer (red).

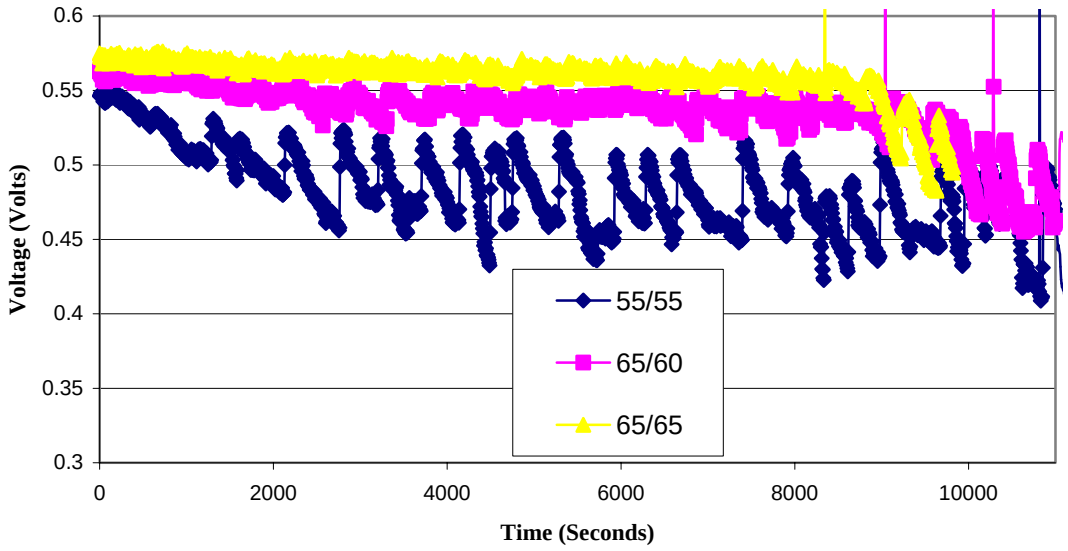

Figure 32: Plot of measured cell voltage as a function of time for the cases of 65/65, 65/60, and 55/55 (all using nebulizer).

Table 3: Comparison of rankings of average cell output electrical power, relative cycling noise amplitude (at 1 standard deviation), and absolute cycling noise amplitude (at 1 standard deviation).

Humidification case	Average Cell Output Electrical Power (Watts)	Humidification case	Relative noise amplitude (1 standard deviation)	Humidification case	Absolute noise amplitude (volts-1 standard deviation)
65/65	22.34738	65/65	0.0070105	65/65	0.0039167
60/65	21.63726	60/65	0.0113004	60/65	0.0061127
65/60	21.40698	65/60	0.0119788	65/60	0.0064108
65/55	21.01595	50/65	0.0133561	50/65	0.0068885
50/65	20.63012	65/55	0.0136007	65/55	0.0071458
60/60	19.66238	60/60	0.0280377	60/60	0.0137822
55/55	18.70508	55/55	0.0457674	55/55	0.0214021

APPENDIX B

ADDITIONAL INFORMATION REGARDING EXPERIMENTAL APPARATUS

Auxiliaries

Cathode humidification bottle

The design of the cathode humidification system could not be simpler: it consists of an externally heated stainless steel bottle filled with water and fitted with a dip tube, thermocouple well, and outlet port. The cathode gas (air) is bubbled through the water and then is allowed to vent out of the top of the bottle through the exit port. The external heater is an Omega SRFG silicone rubber heater wrapped about the circumference of the bottle. The heater is then wrapped on the exterior by fiberglass insulation and taped with aluminum-backed duct tape.

Back bias watchdog contactor

The back bias relay is a vital part of the fuel cell electrical system as it prevents the very destructive condition of reverse cell bias. Essentially, to reverse bias a fuel cell is to impose a voltage across the terminals of the fuel cell which is greater than the forward voltage of the fuel cell itself. This reverse bias is created when enough current moves through the internal resistance of the fuel cell to cause an I*R voltage drop that overwhelms the forward voltage of the cell. This condition can be manifested in one of two ways – overcurrenting the fuel cell (external short), or by starving the fuel cell of one or both reactants. In either case, the backwards bias causes the cell to operate as an electrolysis cell, electrolyzing water at the former cathode (releasing oxygen) and pumping hydrogen electroosmotically back to the former anode. This electrolysis can quickly deplete the membrane of water, thereby greatly decreasing its ionic conductivity. Furthermore, this electrolysis action at the former cathode can cause rapid corrosion of the metal foam flow field, and the resulting release of metal ions into the membrane will eventually cause failure. Because a very low impedance d.c. power supply is in series with the fuel cell, it is very easy to accidentally cause this condition, and it must be prevented. The solution is to implement a device which will immediately open the

connection between the fuel cell and the external electric circuit once this condition occurs, which the author has dubbed a “back bias watchdog”.

The back bias contactor consists of a ganged 3 phase motor starter relay, relay coil driver, voltage comparator, monostable multivibrator (one shot) and interface electronics. A high input impedance comparator measures the voltage differential between the anode and cathode, while loading the fuel cell itself a negligible amount (the d.c. input impedance is on the order of 10^{12} ohms). The single ended (bipolar power supply not used) comparator has a large amount of common mode signal rejection (~120 dB), meaning that the fuel cell voltage input is treated in an almost ideal differential sense. The comparator inputs are filtered via a simple RC low pass circuit to minimize response to electrical noise (especially 60 Hz). The output of the comparator is then fed into a lm555 monostable multivibrator (one shot). The one-shot is used so as to ensure that the relay remains open for a long enough period (~4 seconds) to eliminate any type of electromechanical resonances, and to give the load controller or power supply enough time to re-equilibrate should the disturbance have been due to a power-line transient. The one-shot output is then used to drive a 2n2222 common emitter amplifier which provides base current control for the TIP–122 relay coil drive bipolar power transistor. The 12-volt relay coil is snubbered via a freewheeling 1N4002-silicon power diode. Two “wall wart” unregulated 9v full-bridge rectified power supplies were used for d.c. power. These unregulated supplies were used in conjunction with a large electrolytic capacitor (5000 μF) for ripple control and a large tantalum capacitor (20 μF) for high frequency line noise control.

The back bias watchdog gave very satisfactory performance, and was used by more than one investigator due to its excellent ability to protect the fuel cell. The only consideration with this design was that it was at times too sensitive to line noise, and that the comparator gave strange behavior when the backwards bias was more than 1 volt reverse potential. The latter concern was not a major issue, as long before the fuel cell could experience such a large backwards bias, the relay contacts would be broken, and,

because of the length of the monostable pulse, the fuel cell would have more than ample time to recover to a normal forward voltage.

Omega CN9000A PID temperature controller

Two Omega temperature controllers were used to control the temperature of the water in the reactant gas humidification units – one for the anode, and one for the cathode. The controllers are a digital PID design, and have built-in software which automatically tunes the proportional, integral, and derivative gains so as to minimize overshoot and yet maintain control stability. Once the controllers have been operated in auto-tune mode, the only user input needed was the programming of the temperature set-point, which is achieved very easily.

Unfortunately, the controllers were set up to use type-J thermocouples instead of type-T, and so the water bath temperature uncertainty was higher as a result of this. The resolution of the control set-point is only 1 °C, which is smaller than the 2.2 °C uncertainty associated with using the inferior type-J thermocouples.

The output of the temperature controllers was a 0-5 volt TTL digital signal, which was used to trigger an optically-coupled solid-state relay (Crydom TD1210) so as to control the electric heaters. The external Crydom relay was used as the switching element for two reasons. One, the Crydom relay has a much larger wattage rating (1200 watt) than the rather meager electromechanical relay contained within the Omega controller (240 watt). And secondly, the Crydom relay was used because, unlike the electromechanical relay, it is zero-voltage switching. The zero voltage switching feature means that it will not turn on or off until the line voltage has moved very close to zero, minimizing electrical noise and maximizing switching device (triac) lifetime.

MKS 1159b reactant gas mass flow controller

The mass flow rate of the reactant gases was controlled through the use of MKS gas mass flow controllers. The use of these mass flow controllers allowed the operator to conduct experiments without constant supervision, as the alternative approach to

controlling mass flow control would entail using a needle valve and accurately measuring the pressure drop and adjusting the needle valve as needed to compensate for changes in line/tank pressure and temperature. Not only did these mass flow controllers make it easier to conduct the experiments, it ensured the accuracy of the mass flow rate of the reactant gases, as the maximum error associated with the use of the mass flow controllers is 1.5% of full scale. This maximum error is 0.045 and 0.15 standard liters per minute (slm) for the hydrogen and air streams, respectively.

The basic operation of these closed loop PID mass flow controllers is relatively simple. In the mass flow controllers, gas passes through a mass flow sensor section and then out through a solenoid-actuated needle valve. The operator applies a 0-5 volt analog signal for the mass flow setpoint. The controller measures the massflow rate at the sensor tube, computes the error with the use of an op-amp, and adjusts the needle valve accordingly.

The mass flow sensing section consists of a sensor tube and parallel shunt tube. The shunt tube is selectable depending on the range requested by the electronic setpoint. That is, there are several shunt tubes that can be selected to be used in parallel with the sensing tube, and the particular shunt tube is selected based upon the range demanded by the setpoint signal. The shunt tube is selected by a solenoid actuator. The sensor tube used with the MKS mass flow controller operates much like that used in modern fuel injected automobiles. An RTD is wrapped on a ceramic tube next to an electric heater, and this RTD/heater tube assembly is placed upstream of a RTD (Resistive Temperature Device), and the heater power is adjusted to provide a constant differential temperature reading between the upstream and downstream RTDs. The large length to diameter ratio (>100:1) of the sensor and shunt tubes ensures fully developed laminar flow within the sensor and shunt tubes, and therefore ensures that the relationship between the heater power and mass flow rate is linear.

Staco 3PN1010 1.4 kVa variable autotransformer (variac)

The Staco variac was used to precisely control the voltage applied to the fuel cell electric pad heater. The variac was a standard ring-shaped, ferrosilicon core autotransformer with graphite winding wiper.

Solid-state variable duty cycle electric heater controller

The solid state variable duty cycle electric heater controller was also used to control the *average* electric power applied to the fuel cell pad heater. The duty cycle of the electric heater was controlled by use of a 555 astable multivibrator oscillator driving a solid-state relay. The duty cycle of oscillation was varied by use of a vernier 10-turn wirewound precision potentiometer.

This controller was used during the experiments to determine the stability of the evaporative cooling method. This controller was not used during the experiments to determine the steady state heat loss experiments because of the relative difficulty of accurately confirming the average heater power with the oscilloscope – it simply was much easier to use the variac, a voltmeter, and a milliammeter to accomplish this task.

Lambda 5Volt-100 amp switching power supply

The Lambda (Lambda is now part of Invensys Inc. San Diego, CA) power supply was used to generate the necessary minimum “stack” voltage required for the HP load controller to function properly. A power supply with a lower output voltage could have been used, but it is extremely difficult to locate low noise regulated d.c. power supplies with a 100 amp rating below 5 volts.

Desiccant water collector

In the course of this investigation, it became apparent that there existed a need to measure the actual water mass flow output rate from the nebulizer/humidifier. A simple, inexpensive method for obtaining the *average* mass flow rate is to collect and measure the mass of water collected in a sorptive trap during a given time interval.

The design criteria for the sorptive trap was that it needed to have a consistently high collection efficiency, be inexpensive to build, and that the dry mass be no greater than 190 grams. Several prototypes were built, using saltation, condensation, freezing, or desiccation as the sorption mechanism. The final design which emerged as the most reliable, consistent, and easy to use was a design which used a saltation first stage and desiccating second stage.

The device actually used consists of a short length of ½" i.d. pvc tubing glued into a flat-bottomed pv.c. cap. At the bottom of the cap a hole was drilled and tapped to fit a Swagelock™ adapter to so as to allow connection to the gas delivery tubing. The bottom of the collector was stuffed with a cotton ball plug – the saltation collector. The remaining space to the top of the tube was filled with Drierite (calcium sulphate) desiccant. The top of the collector tube was covered with a section of polyethylene bag with an array of small holes poked through. This section of polyethylene bag was held in place by a rubber band.

Instrumentation

GW GDM 8145 digital multimeters

The GW (Goodwill Instrument, Inc.) multimeters used in this investigation were used as either voltmeters or milliammeters. When used as voltmeters, the instrument displayed 5 significant figures, and when used as milliammeters, displayed 4 significant figures.

HP 6050A digital electronic load controller

The HP 6050A electronic load controller was used as a stable, programmable constant current load for the PEM fuel cell.

The HP 6053 can be programmed to operate in constant voltage, constant current, or constant resistance mode. For this investigation, the load controller was used

in the constant current mode. The programming resolution of the current is 0.01 amps, giving 4 significant figures when used in this investigation (10-40 amps).

The load controller requires a minimum of 3.0 volts at the terminals in order to function as a constant current load regulator. Because the fuel cell only produces a fraction of a volt (~.6 v) during operation, it is necessary to connect a floating power supply or battery in series with the fuel cell to create the necessary "stack" voltage. The Lambda 5V switching power supply was used for this purpose.

Type-T and type-J thermocouples

Thermocouples were selected for use as temperature sensing transducers for this investigation because of their relatively good accuracy, low cost, ease of use, and corrosion resistance. A type-T thermocouple was used to monitor the fuel cell temperature, and two type-J thermocouples were used to monitor the temperatures of the water in the anode and cathode gas humidification chambers.

In case the reader is not familiar with thermocouples, a good reference can be found at the www.omega.com website. Thermocouples work by taking advantage of the Seebeck effect, in which a junction of dissimilar conductors produces an electric potential proportional to the temperature difference between the junction and the free end of the conductors. The Seebeck effect is due to the difference in majority charge carrier mobility in the two different conductors at a given temperature. Since nearly all thermocouples are composed of metals, the majority charge carrier for this discussion is the electron. Essentially what occurs is that electrons in the more mobile conductor are able to diffuse into the lower-mobility conductor faster than they can back diffuse, thereby giving the lower mobility conductor a net negative charge near the junction, and giving the higher mobility conductor a net positive charge near the junction, and thereby generating an electric field within the conductors. Because electron mobility is a function of temperature, this potential so generated can be used to uniquely determine the temperature at the junction itself when referenced to the voltage produced at a standard temperature. This standard reference temperature is usually 0 °C, and is known

as the cold junction temperature. In this investigation, the hardware used for data acquisition had built-in semiconductor cold-junction references, making temperature measurement with the thermocouples very simple.

The thermoelectric potential produced by the Seebeck effect in metallic conductor is on the order of 10's of millivolts. While this signal voltage is rather low, thermocouples have the advantage of having extremely low impedance, and so the signal to noise ratio is still rather large even in a relatively noisy environment. The signal to noise ratio for thermocouples can be reduced further by filtering high-frequency noise out by use of analog filters (usually simple RC filters). The low voltage produced by the thermocouple is usually amplified by an op-amp, and this filtering can be built into the op-amp circuit itself.

The uncertainty of thermocouple junctions varies with the temperature range used, and the thermocouple type. For the temperature range used in this investigation (approximately 20-80 °C), type-T thermocouples have the lowest uncertainty of all types at +/- 1.0 °C. However, it was necessary to use type-J thermocouples for the anode and cathode humidification chambers, as the temperature controller units were set-up to use them. For the type J thermocouples, the uncertainty is a rather large +/- 2.2 °C.

Fisher electronic timer

The Fisher electronic timer is a very simple programmable digital timer. The timer displayed the countdown time left, and once the countdown had completed, it sounded a piezo beeper alarm for approximately 10 seconds. The resolution was only 1 second. This low resolution was fine as the total length of time of the experiment was ~15 minutes (900 seconds), giving a very manageable 1.1% uncertainty.

Fisher XA-200DS digital analytical electronic balance

The digital electronic balance was used to measure the mass of the desiccator collector before and after a timed collection trial, thereby providing an average water mass flow value.

The digital electronic balance has a range of 0-200 grams, with a resolution of 0.0001 grams. Because this balance is so sensitive, the weighing chamber is covered with sliding glass doors. These glass doors are used to block any air currents which could influence the measured value but allow easy sample access. The balance also had adjustable feet and a bubble level to ensure that it was level (i.e. parallel with floor). Another useful feature of this balance is that it had a tare feature, so that the mass difference of the desiccator collector before and after the timed trial could be measured directly.

The sensing element used in the electronic balance is a strain gauge based load cell. The electronics associated with the electronic balance are a power supply, temperature compensated strain gauge element, Wheatstone bridge amplifier, and voltmeter. Should the reader be interested, more information is available from the manual.

Electronic micromanometer

The electronic micromanometer was used to measure the chamber pressure in the anode gas humidification chamber/nebulizer. Because the pressure drop between the fuel cell anode inlet and anode humidification chamber is so low (measured at 0.01 lb_f/in^2 for the maximum flow used in this investigation), this was pressure was treated as the fuel cell anode backpressure. The electronic micromanometer had a resolution of 0.01 lb_f/in^2, and typical values for backpressure varied from 0.08 to 0.22 lb_f/in^2 depending on mass flow rate and amount of suspended water present in the hydrogen gas stream.

The electronic micromanometer was not actually a manometer – it used a strain-gauge based diaphragm pressure sensor as opposed to a manometer tube and level sensing device.

This device was not used to collect data; instead, it was used to provide a means of double checking the health of the gas delivery system to the fuel cell. A low backpressure reading indicated that a leak had occurred, and a high reading indicated

that either excess water build-up had occurred in the anode compartment, or that the MEA had collapsed due to poor fuel cell assembly technique or over temperature.

Tectronix 2430A digital storage oscilloscope

The Tectronix oscilloscope was used to confirm the duty cycle of the fuel cell heater, so as to accurately determine the actual average heater power applied to the fuel cell assembly. The Tectronix scope was a 20 MHz, two channel scope with the very useful feature that it could store ~1 Megasamples in acquisition mode.

Empro HA-50-100 50 amp current measuring shunt

An Empro 50 amp shunt was used to confirm that the programmed current value was indeed the current flowing through the fuel cell during operation. The shunt (more correctly, resistor) had a sensitivity of 2mV/A. This shunt was used in conjunction with one of the GW digital multimeters to measure the voltage drop and hence the current.

APPENDIX C

ADDITIONAL FIGURES

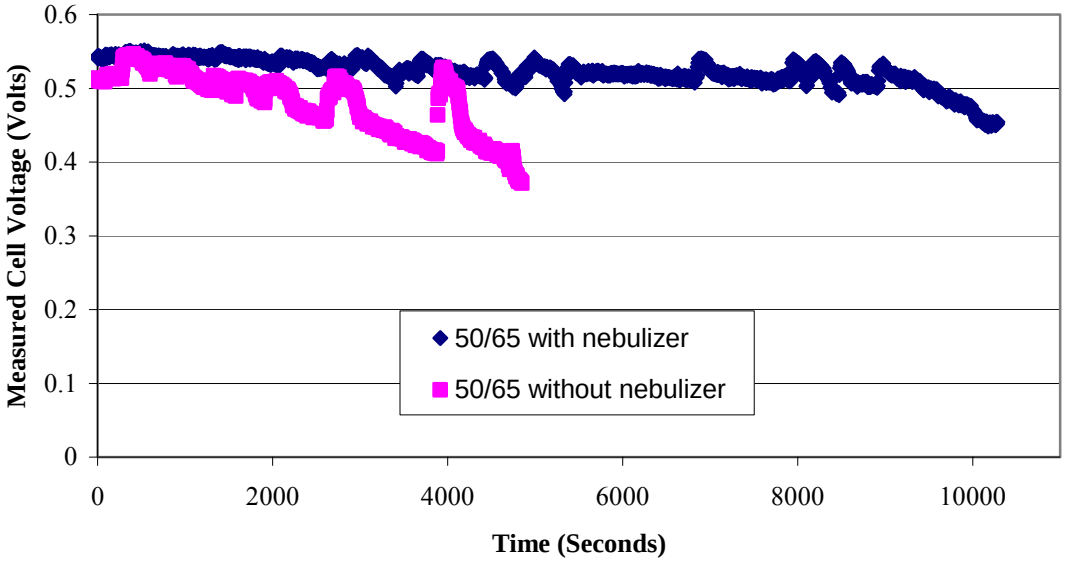

Figure C1a: Plot of measured cell voltage as a function of time for 50/65 humidification case.

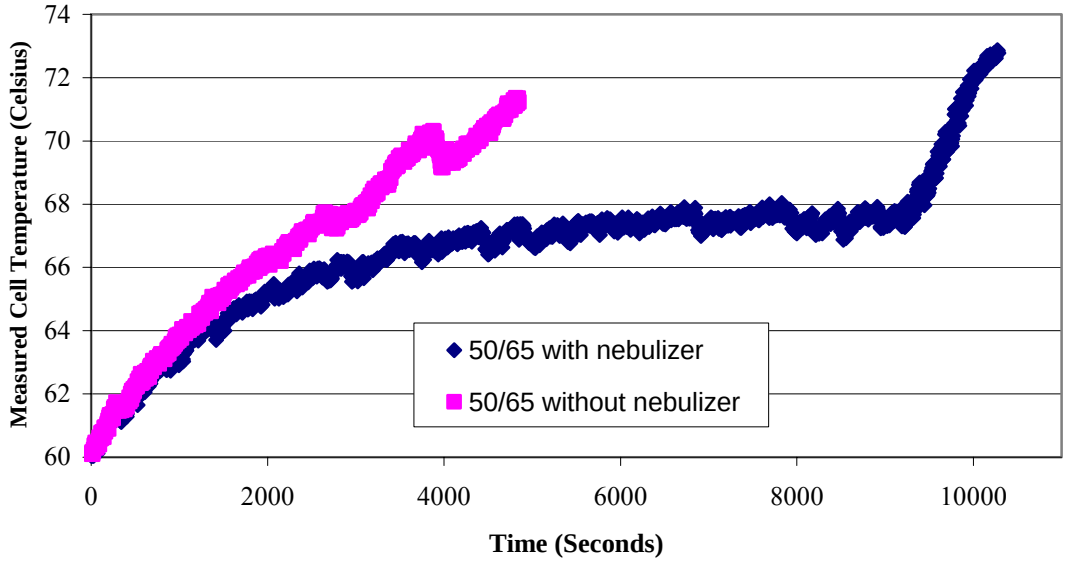

Figure C1b: Plot of measured cell temperature as a function of time for 50/65 humidification case.

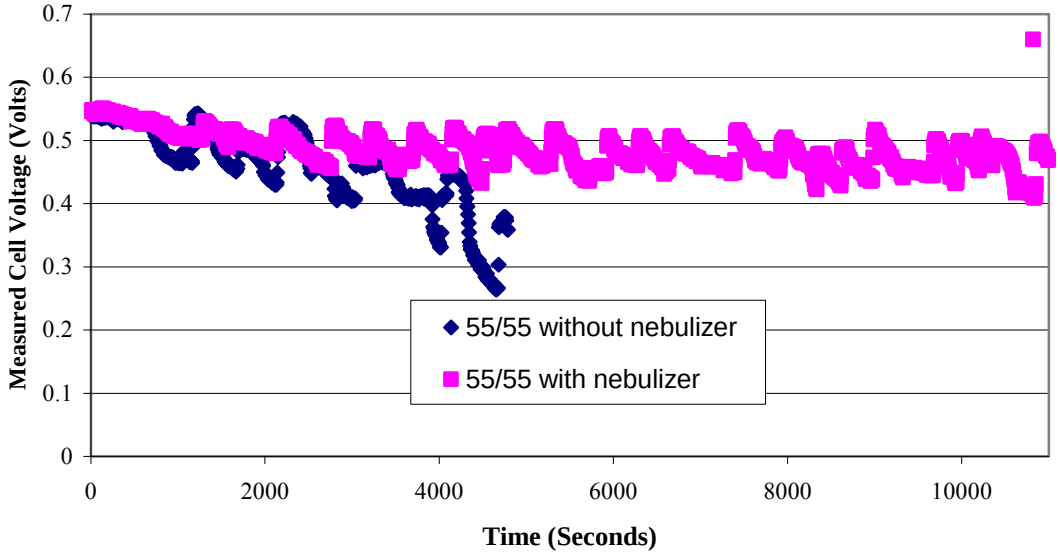

Figure C2a: Plot of measured cell voltage as a function of time for 55/55 humidification case.

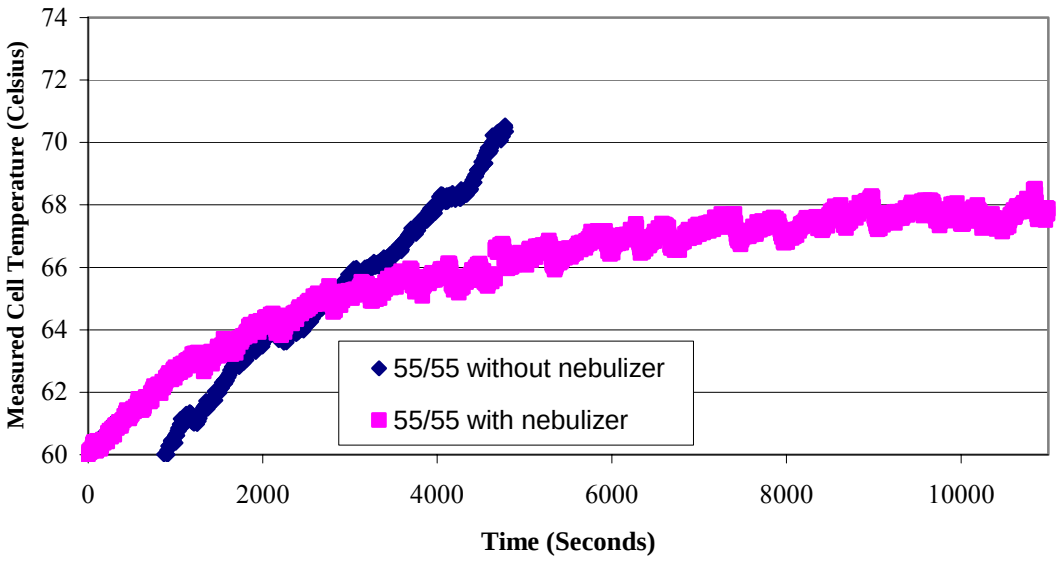

Figure C2b: Plot of measured cell temperature as a function of time for 55/55 humidification case.

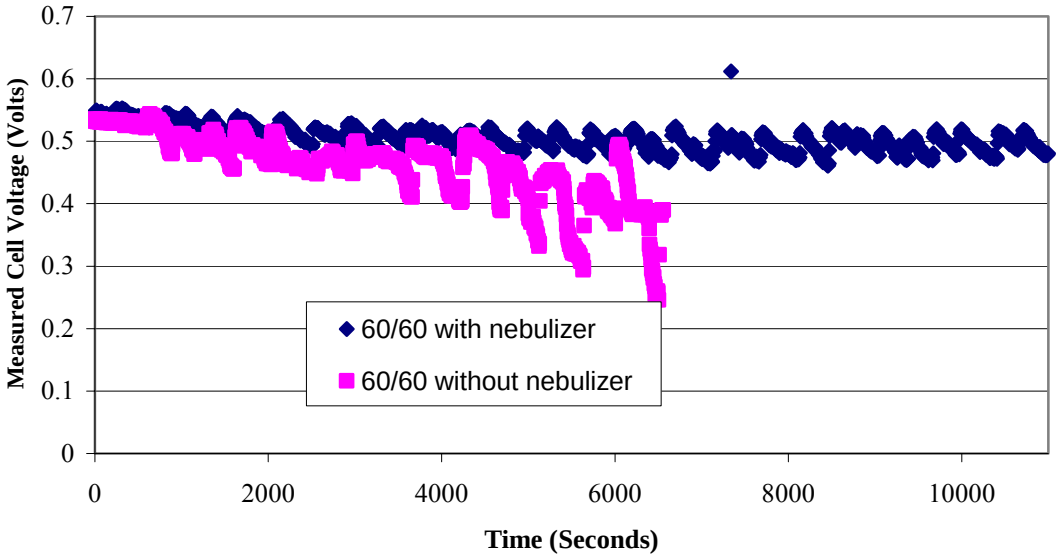

Figure C3a: Plot of measured cell voltage as a function of time for 60/60 humidification case.

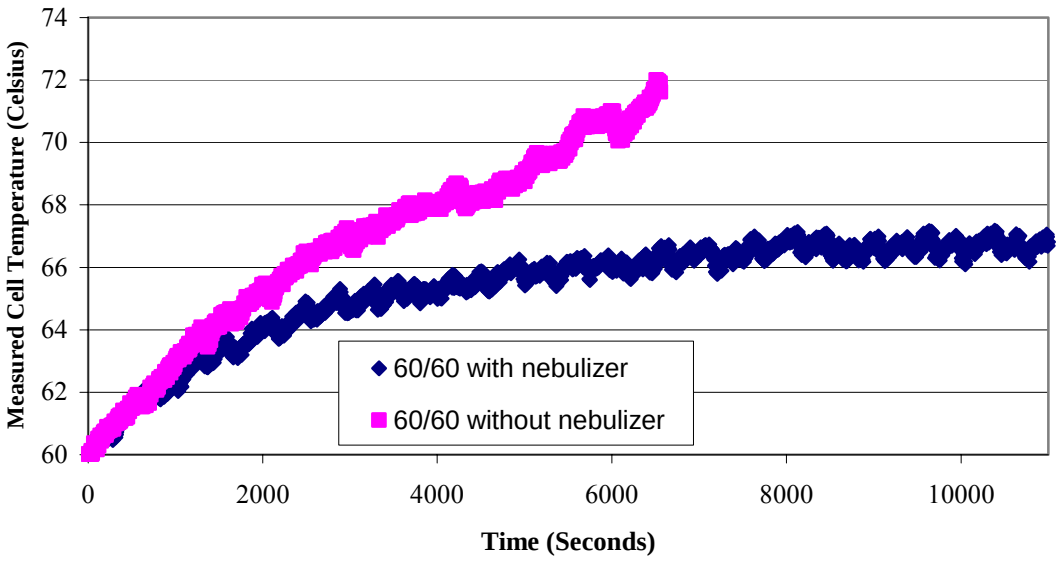

Figure C3b: Plot of measured cell temperature as a function of time for 60/60 humidification case.

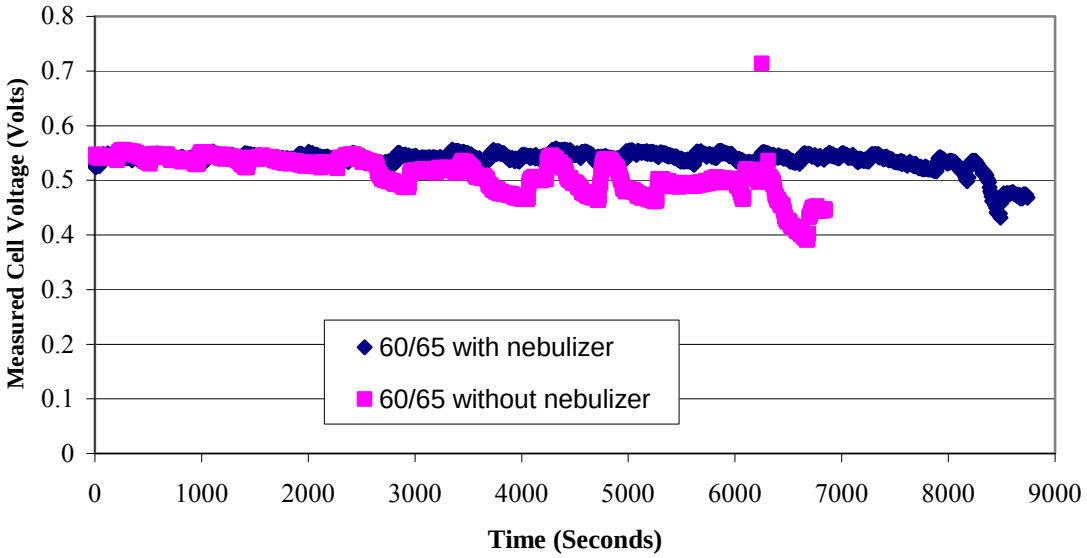

Figure C4a: Plot of measured cell voltage as a function of time for 60/65 humidification case.

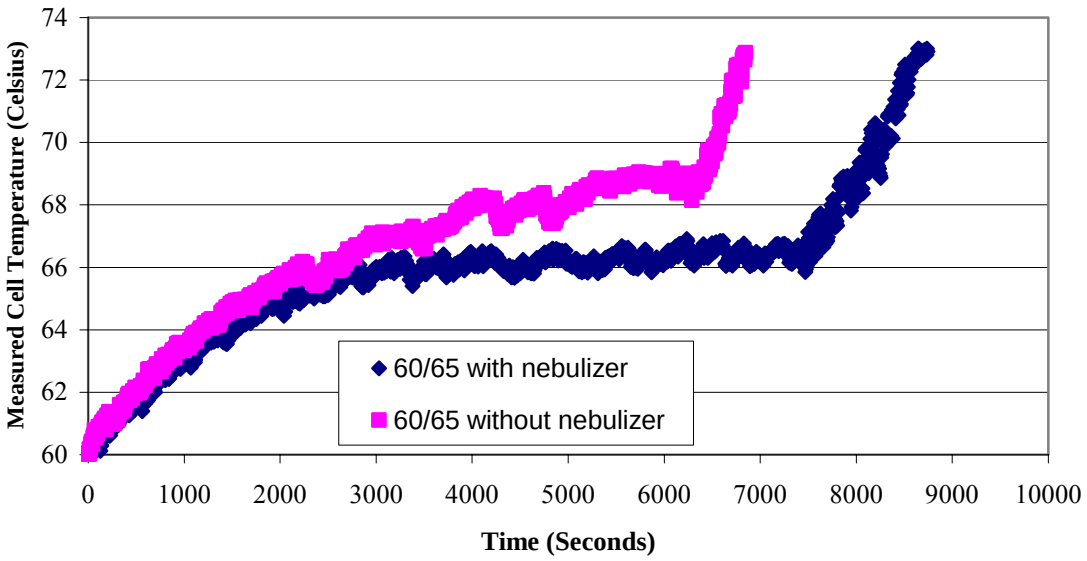

Figure C4b: Plot of measured cell temperature as a function of time for 60/65 humidification case.

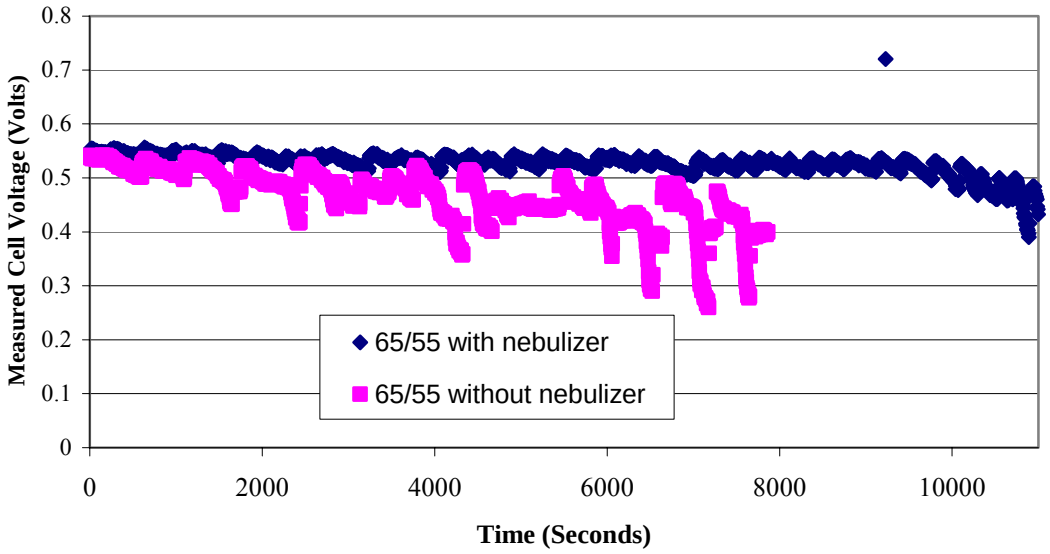

Figure C5a: Plot of measured cell voltage as a function of time for 65/55 humidification case.

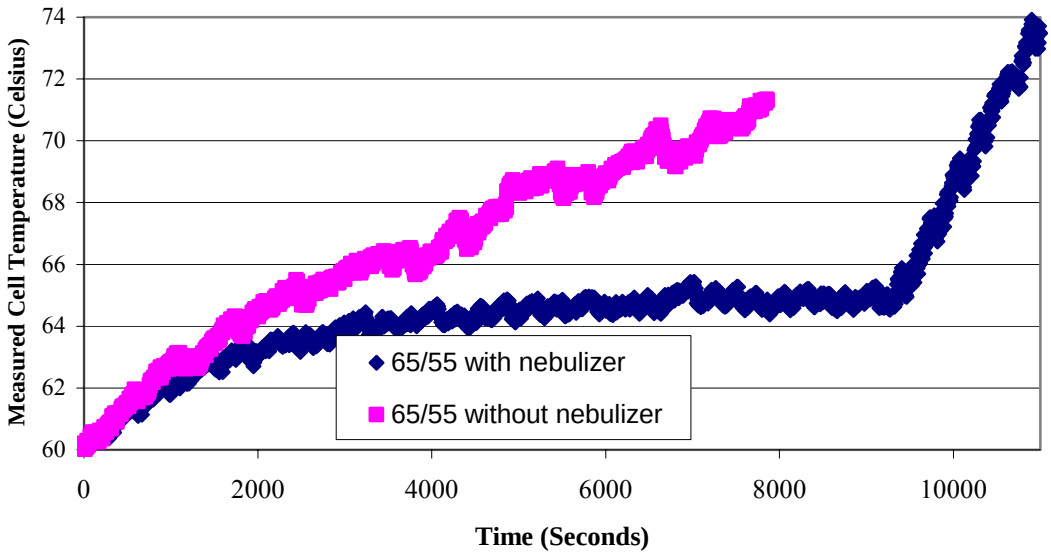

Figure C5b: Plot of measured cell temperature as a function of time for 65/55 humidification case.

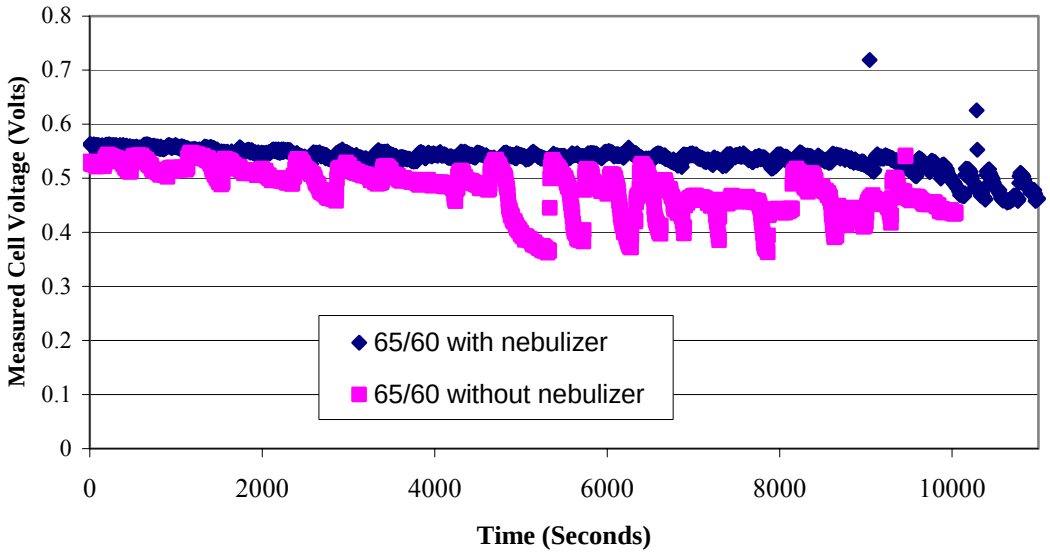

Figure C6a: Plot of measured cell voltage as a function of time for 65/60 humidification case.

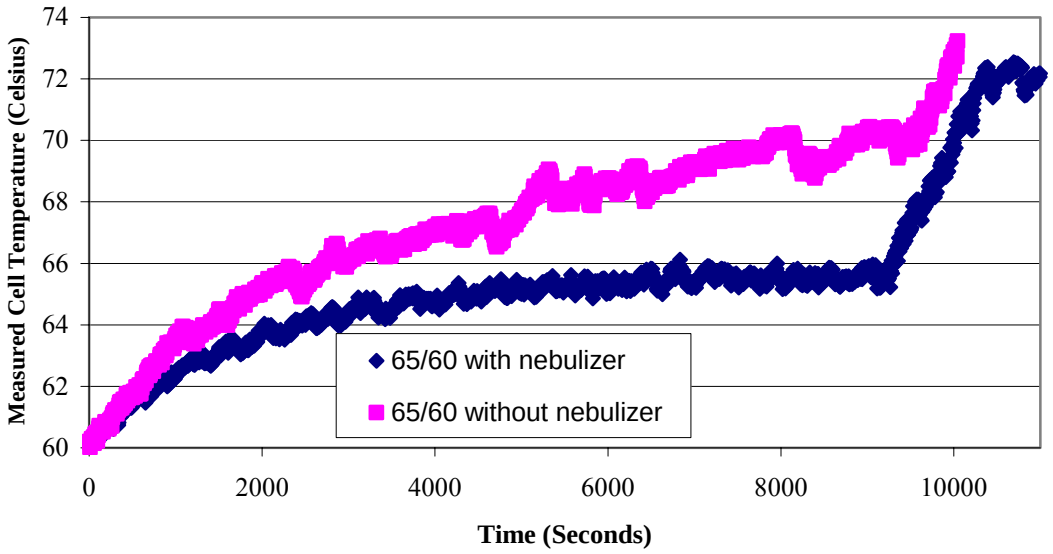

Figure C6b: Plot of measured cell temperature as a function of time for 65/60 humidification case.

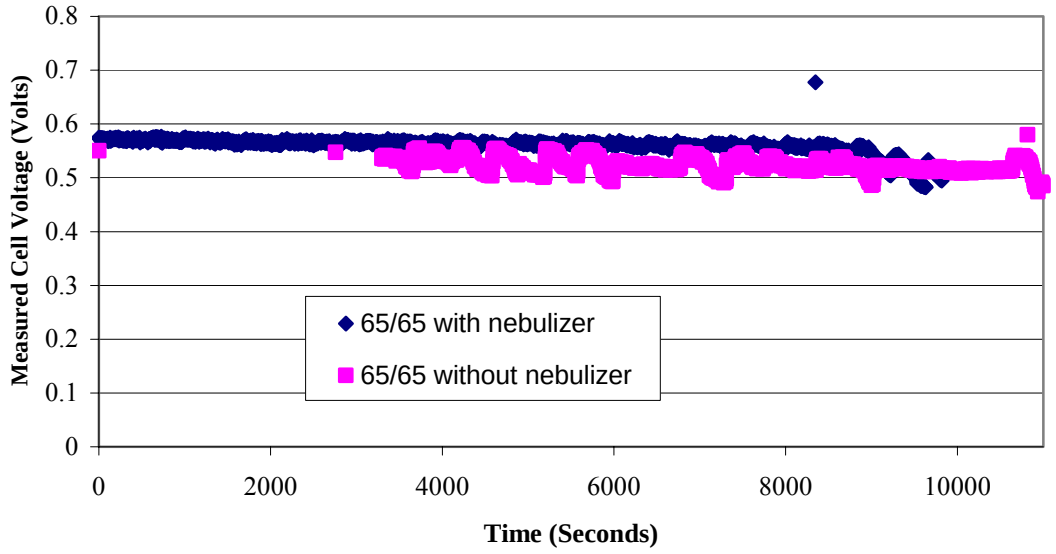

Figure C7a: Plot of measured cell voltage as a function of time for 65/65 humidification case.

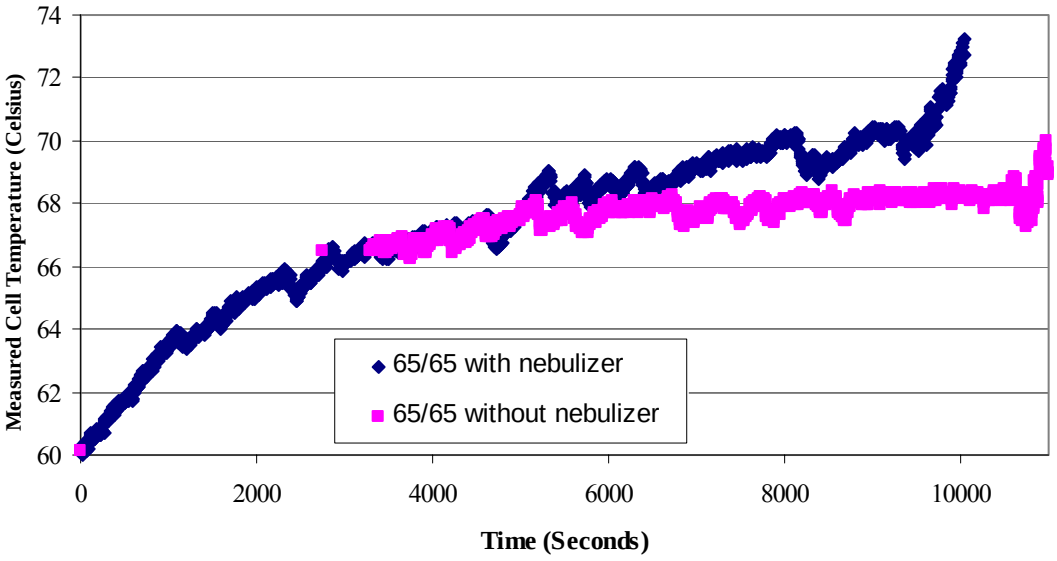

Figure C7b: Plot of measured cell temperature as a function of time for 65/65 humidification case.

VITA

Loren Erik Snyder was born in Houston, Texas, in 1977. His childhood was spent in Houston; Denver, Colorado; and Little Rock, Arkansas. His childhood accomplishments include nearly burning his house down (Calcium Hypochlorite/Sulfur/Naphtha rocket propellant mixture spontaneously combusted explosively), chasing a dog until it attacked him and his sister, eating honey from a bee hive soaked in Tox II insecticide, and winning first place in the 12th grade science fair only to be disqualified later in the afternoon.

In May of 2000, Erik graduated from Colorado State University with a Bachelor of Science in Mechanical Engineering. He then worked for a year as a manufacturing engineer for Mueller Industries in Wynne, Arkansas. After becoming bored with the corporate world, he then worked for 6 months as a freelance electronics contractor for the Arkansas Museum of Discovery in Little Rock, Arkansas, while applying to various graduate schools. He then moved to College Station, Texas to pursue a Master of Science in Mechanical Engineering, which he received in December 2004.

His work experience includes working as a research assistant for Dr. Steven Flock with the Laser Surgery Research Group at the Arkansas Cancer Research Center in Little Rock, Arkansas; working as an undergraduate research assistant for Dr. Ellen R. Fisher with the Colorado State University Chemistry Department in Fort Collins, Colorado; working as a summer engineering intern at the Baldor Electric Company in Fort Smith, Arkansas; and working as a graduate research assistant for Dr. A.J. Appleby at the Center for Electrochemical Systems and Hydrogen Research at Texas A&M University in College Station, Texas.

The permanent address at which Loren Erik Snyder can be reached is 441 Midland Ave., Little Rock, AR 72205.